

TRAJECTORY PLANNING FOR A QUADRUPED ROBOT

PLANIFICATION DE TRAJECTOIRES POUR UN ROBOT MARCHEUR QUADRUPÈDE

A Thesis Submitted
to the Division of Graduate Studies of the Royal Military College of Canada
by

Sarah Carroll McRae
Second Lieutenant

In Partial Fulfillment of the Requirements for the Degree of
Master of Applied Science in Mechanical Engineering

April, 2008

© This thesis may be used within the Department of National Defence but copyright for open publication remains the property of the author.



Library and
Archives Canada

Published Heritage
Branch

395 Wellington Street
Ottawa ON K1A 0N4
Canada

Bibliothèque et
Archives Canada

Direction du
Patrimoine de l'édition

395, rue Wellington
Ottawa ON K1A 0N4
Canada

Your file *Votre référence*

ISBN: 978-0-494-42144-4

Our file *Notre référence*

ISBN: 978-0-494-42144-4

NOTICE:

The author has granted a non-exclusive license allowing Library and Archives Canada to reproduce, publish, archive, preserve, conserve, communicate to the public by telecommunication or on the Internet, loan, distribute and sell theses worldwide, for commercial or non-commercial purposes, in microform, paper, electronic and/or any other formats.

The author retains copyright ownership and moral rights in this thesis. Neither the thesis nor substantial extracts from it may be printed or otherwise reproduced without the author's permission.

In compliance with the Canadian Privacy Act some supporting forms may have been removed from this thesis.

While these forms may be included in the document page count, their removal does not represent any loss of content from the thesis.

AVIS:

L'auteur a accordé une licence non exclusive permettant à la Bibliothèque et Archives Canada de reproduire, publier, archiver, sauvegarder, conserver, transmettre au public par télécommunication ou par l'Internet, prêter, distribuer et vendre des thèses partout dans le monde, à des fins commerciales ou autres, sur support microforme, papier, électronique et/ou autres formats.

L'auteur conserve la propriété du droit d'auteur et des droits moraux qui protège cette thèse. Ni la thèse ni des extraits substantiels de celle-ci ne doivent être imprimés ou autrement reproduits sans son autorisation.

Conformément à la loi canadienne sur la protection de la vie privée, quelques formulaires secondaires ont été enlevés de cette thèse.

Bien que ces formulaires aient inclus dans la pagination, il n'y aura aucun contenu manquant.



Canada

Acknowledgements

This thesis would not have been possible without the support of my thesis supervisor, Dr.Jnifene. I would also like to thank Capt Dan Jehan and Lt(N) Trevor Davies who provided me with continual support throughout this process.

Abstract

McRae, Sarah Carroll. M.A.Sc. Royal Military College of Canada, April, 2008. *Trajectory Planning for a Quadruped Robot*. Supervised by Dr. Amor Jnifene.

This thesis presents the development of a trajectory planner for a four legged robot. This study is the initial step toward integrating a quadruped robot into a team of wheeled robots available in the Robotics lab at the department of Mechanical Engineering at RMC. For the purposes of this thesis, the specifics of the SILO 4 robot have been used in the trajectory planner. The trajectory planner that has been developed can be implemented on any quadruped robot with the insect leg architecture.

The trajectory planner used a two phase discontinuous creeping gait in conjunction with a discontinuous spinning gait to plan the different foot and body positions to follow a desired path. Static stability was checked and maintained throughout the gaits by ensuring that the projection of the centre of gravity would always remain within the support polygon. The body and foot positions produced by the gaits were joined using appropriate trajectories and then the Inverse Kinematic Problem was solved to produce joint trajectories that would allow a quadruped to follow a desired path. The dynamics of the robot legs were also developed and the produced joint variables were then used to obtain torque requirements to allow the motors to be sized.

The trajectory planner allows a quadruped robot to closely follow a given two dimensional path by producing the required joint positions, velocities and accelerations. Appropriate gaits are used in conjunction with stability analysis, leg and body trajectories, and kinematic equations to allow for omni-directionality of locomotion, simplicity of implementation and maintenance of static stability.

Resumé

McRae, Sarah Carroll. M.Sc.A. Collège militaire royal du Canada, Avril, 2008. *Planification de Trajectoires pour un Robot Marcheur Quadrupède*. Thèse dirigée par M. Amor Jnifene, Ph.D.

Cette thèse présente le développement d'une méthode de planification de trajectoire pour un robot marcheur quadrupède à être intégré avec une équipe de robots mobiles à roues. Pour les buts de cette thèse, les données du robot SILO 4 ont été utilisées dans le planificateur de trajectoire. Cependant, le planificateur de trajectoire peut être utilisé avec n'importe quel robot quadrupède qui a l'architecture d'un insecte.

Le planificateur de trajectoire a utilisé une démarche larvante discontinue de deux phases en conjonction avec une démarche filante discontinue pour planifier les différentes positions des pieds et du corps pour suivre un chemin désiré. La stabilité statique a été vérifiée et maintenue en assurant que la projection du centre de gravité demeurait dans le polygone de support. Les positions des pieds et du corps produites par les démarches ont été jointes par des trajectoires appropriées et par la suite les équations cinématiques ont été résolues produisant les trajectoires d'articulation qui permettraient à un robot quadrupède de suivre un chemin désiré. Les équations de la dynamique d'une jambe du robot ont aussi été développées pour produire le couple nécessaire en fonction des trajectoires des articulations.

Le planificateur de trajectoire permet à un robot quadrupède de suivre un chemin de deux dimensions en produisant les positions, vitesses et accélérations d'articulations. Des démarches appropriées, utilisées en conjonction avec l'analyse de stabilité, des trajectoires des pieds et du corps et les équations cinématiques permettent une mobilité dans toutes directions, une simplicité d'implémentation et l'entretien de stabilité statique.

Table of Contents

Abstract	iv
Resumé	v
List of Tables	viii
List of Figures	ix
Nomenclature	xii
Chapter 1. Introduction	1
1.1. Thesis Motivation	1
1.2. Aim of the Thesis	2
1.3. Background	2
1.3.1. Stationary Robot Manipulators	3
1.3.2. Mobile Robots	3
1.4. The Trajectory Planner	6
1.5. Thesis Organization	7
Chapter 2. Literature Review	9
2.1. Legged Robots	9
2.2. Trajectory Planning	14
2.2.1. Gaits for Multi-Legged Robots	15
2.2.2. Methods of Defining Stability	23
2.2.3. Leg and Body Trajectories	27
Chapter 3. Kinematics of an Insect Type Leg	31
3.1. Forward Kinematic Equations	31
3.2. Inverse Kinematic Equations	34
3.3. Velocity Equations	36
3.4. Acceleration Equations	38
3.5. Singularity Analysis	39
3.6. The Leg Workspace	40
Chapter 4. Selection of Appropriate Gaits	42
4.1. Background	42
4.1.1. Gait Terminology	42
4.1.2. Gaits in General	43
4.2. A Description of the Selected Gaits	48
4.2.1. A Two Phase Discontinuous Creeping Gait	49
4.2.2. A Discontinuous Spinning Gait	59

Chapter 5. Trajectory Planning for a Quadruped Robot	65
5.1. Maintaining Static Stability	65
5.2. Leg Trajectories	67
5.3. Body Trajectories	69
5.4. Changing Between the Global and CoG Reference Frames	81
5.5. The Trajectory Planner	83
Chapter 6. Case Studies and Results	89
6.1. Results of the Trajectory Planner for the Follow of a Straight Line Path	90
6.2. Results of the Trajectory Planner for the Follow of a Circular Path .	105
6.3. Results of the Trajectory Planner when the Accuracy of the Follow is Purposely Reduced	119
6.4. An Example of a Ditch Crossing for a Quadruped Robot	123
6.5. Summary	123
Chapter 7. Conclusions and Recommendations	127
7.1. Conclusions	127
7.2. Recommendations and Future Works	129
References	131
Appendix A. Dynamics of an Insect Type Leg	139
A.1. Developing the Dynamic Equations	139
A.1.1. Determining the Kinetic Energy	140
A.1.2. Determining the Potential Energy	141
A.1.3. The Dynamic Equations	142
A.2. Sizing the Motors	144
A.2.1. Moving the Joints	145
A.2.2. Supporting the Body	145
A.2.3. Motor Torques and Angular Velocities	147

List of Tables

Table 2.1. Specifications of the SILO 4 Robot [1]	13
Table 3.1. DH Parameters	33
Table 6.1. Performance Values for a Straight Line Path at Different Heights .	104
Table 6.2. Performance Values for a Circular Path at Different Heights . .	110
Table 6.3. Performance Values for a Circular Path at Different Heights With Decreased Accuracy	119
Table A.1. Dynamic Constants of the Leg [2]	140

List of Figures

Figure 2.1.	Quadruped Robot With Simple Legs	11
Figure 2.2.	Three Degree of Freedom Leg	11
Figure 2.3.	Pantograph Leg	12
Figure 2.4.	The SILO 4 Robot [3]	13
Figure 2.5.	The Stability Margin	25
Figure 2.6.	The Longitudinal Stability Margin	26
Figure 2.7.	The SSA	26
Figure 2.8.	Examples of a Sinusoidal and a Composite Cycloid Trajectory	28
Figure 3.1.	DH Reference Frames for the Robot Leg	32
Figure 3.2.	Knee up and Knee Down Leg Configurations	36
Figure 3.3.	Singular Configurations	39
Figure 3.4.	View of Leg Workspace	40
Figure 4.1.	Gait Diagram	43
Figure 4.2.	The Quadruped Trot Gait [4]	45
Figure 4.3.	The Quadruped Gallop [4]	45
Figure 4.4.	Hexapod Wave Gait	46
Figure 4.5.	Hexapod Tripod Gait	47
Figure 4.6.	Discontinuous Creeping Gait Gait, $\beta = 7/8$	50
Figure 4.7.	Redefined Workspace	51
Figure 4.8.	Foothold Positions	52
Figure 4.9.	Gait Sequence for the Positive y Direction	53
Figure 4.10.	Joint Positions for one Creeping Gait Cycle	56
Figure 4.11.	Joint Velocities for one Creeping Gait Cycle	57
Figure 4.12.	Joint Accelerations for one Creeping Gait Cycle	58
Figure 4.13.	Discontinuous Spinning Gait Gait, $\beta = 5/6$	60
Figure 4.14.	Joint Positions for one Spinning Gait Cycle, $\psi = \pi/3$	62
Figure 4.15.	Joint Velocities for one Spinning Gait Cycle, $\psi = \pi/3$	63
Figure 4.16.	Joint Accelerations for one Spinning Gait Cycle, $\psi = \pi/3$	64
Figure 5.1.	The Support Triangle	66
Figure 5.2.	Position of Leg 1 in Transfer Phase	70
Figure 5.3.	Velocity of Leg 1 in Transfer Phase	71
Figure 5.4.	Acceleration of Leg 1 in Transfer Phase	72
Figure 5.5.	Cartesian Positions During the Body Movement Phase of the Creeping Gait	74
Figure 5.6.	Cartesian Velocities During the Body Movement Phase of the Creeping Gait	75

Figure 5.7. Cartesian Accelerations During the Body Movement Phase of the Creeping Gait	76
Figure 5.8. Joint Positions During the Body Movement Phase of the Spinning Gait	78
Figure 5.9. Joint Velocities During the Body Movement Phase of the Spinning Gait	79
Figure 5.10. Joint Accelerations During the Body Movement Phase of the Spinning Gait	80
Figure 5.11. The Angle ϕ	82
Figure 5.12. Determining the Position of the Foot with Respect to the New position of the CoG	83
Figure 5.13. The Creeping Gait	85
Figure 5.14. The Spinning Gait	87
Figure 5.15. The Trajectory Planner	88
 Figure 6.1. Straight Line Path	90
Figure 6.2. Joint Positions for a Height of Travel of 0.2 m Following a Straight Line Path	91
Figure 6.3. Joint Velocities for a Height of Travel of 0.2 m Following a Straight Line Path	92
Figure 6.4. Joint Accelerations for a Height of Travel of 0.2 m Following a Straight Line Path	93
Figure 6.5. Allowed and Desired Straight Line Paths at 0.2 m	95
Figure 6.6. Joint Positions for a Height of Travel of 0.4 m Following a Straight Line Path	96
Figure 6.7. Joint Velocities for a Height of Travel of 0.4 m Following a Straight Line Path	97
Figure 6.8. Joint Accelerations for a Height of Travel of 0.4 m Following a Straight Line Path	98
Figure 6.9. Allowed and Desired Straight Line Paths at 0.4 m	99
Figure 6.10. Joint Positions for a Height of Travel of 0.6 m Following a Straight Line Path	100
Figure 6.11. Joint Velocities for a Height of Travel of 0.6 m Following a Straight Line Path	101
Figure 6.12. Joint Accelerations for a Height of Travel of 0.6 m Following a Straight Line Path	102
Figure 6.13. Allowed and Desired Straight Line Paths at 0.6 m	103
Figure 6.14. Circular Path	105
Figure 6.15. Joint Positions for a Height of Travel of 0.2 m Following a Circular Path	106
Figure 6.16. Joint Velocities for a Height of Travel of 0.2 m Following a Circular Path	107
Figure 6.17. Joint Accelerations for a Height of Travel of 0.2 m Following a Circular Path	108
Figure 6.18. Allowed and Desired Circular Paths at 0.2 m	109

Figure 6.19. Joint Positions for a Height of Travel of 0.4 m Following a Circular Path	111
Figure 6.20. Joint Velocities for a Height of Travel of 0.4 m Following a Circular Path	112
Figure 6.21. Joint Accelerations for a Height of Travel of 0.4 m Following a Circular Path	113
Figure 6.22. Allowed and Desired Circular Paths at 0.4 m	114
Figure 6.23. Joint Positions for a Height of Travel of 0.6 m Following a Circular Path	115
Figure 6.24. Joint Velocities for a Height of Travel of 0.6 m Following a Circular Path	116
Figure 6.25. Joint Accelerations for a Height of Travel of 0.6 m Following a Circular Path	117
Figure 6.26. Allowed and Desired Circular Paths at 0.6 m	118
Figure 6.27. Allowed and Desired Circular Paths at 0.2 m With Decreased Accuracy	120
Figure 6.28. Allowed and Desired Circular Paths at 0.4 m With Decreased Accuracy	121
Figure 6.29. Allowed and Desired Circular Paths at 0.6 m With Decreased Accuracy	122
Figure 6.30. Ditch Crossing for a CoG Height of 0.3 m	124
Figure A.1. Planar View of a Leg	142
Figure A.2. Torque Requirements to Move the Legs during one Cycle of the Creeping Gait	146
Figure A.3. Torque Requirements to Support the Body for one Cycle of the Creeping Gait	148

Nomenclature

Symbol Explanation

a	Represents the distance between the z_i and z_{i+1} axis
A^*	A^* Search Algorithm
b	Polynomial co-efficient
c	A vector representing the position of the corresponding reference frame
CM	Centre of Mass
CoG	Centre of Gravity
CoP	Centre of Pressure
CSIC	Industrial Automation Institute
d	Represents the distance between the z_i and z_{i+1} axis
DH	Denavit-Hartenberg
DKP	Direct Kinematic Problem
DoF	Degree of Freedom
ENSI	École Nationale Supérieure d'Ingénieurs
F	Force
g	Gravity, 9.8 m/s^2
G	Matrix of gravity terms
GE	General Electric
h	Height
H	Matrix of centrifugal and coriolis terms
I	Moment of inertia
IKP	Inverse Kinematic Problem
J	Jacobian Matrix
L	Length of a given link
m	Mass
M	Mass Matrix
n	Represents the number of a given object
p	Position
P	The stroke pitch of a gait. The distance between the stroke centres of adjacent legs
PID	Proportional Integral Derivative
q	Generalized co-ordinate
\dot{q}	Derivative of the generalized co-ordinate
Q	Rotation Matrix

R	The stroke length. The distance the leg travels relative to the CoG during the body movement phase
RMC	Royal Military College
S_E	Energy Stability Margin
S_l	Longitudinal Stability Margin
S_m	Stability Margin
SPLMF	Straight Line Periodic Monotonically Forward
SSA	Statically Stable Area
t	Time
T	Kinetic energy
t_l	Time to Complete One Leg Movement
U	Potential energy
W	Generalized external forces
ZMP	Zero Point Momentum

Greek Symbols

α	Crab angle measured from the forward axis of the robot
β	Duty cycle of a gait. The fraction of the gait cycle that a leg is on the ground
η	Gear efficiency
θ	Joint position
$\dot{\theta}$	Joint velocity
λ	Stride Length of a gait. The distance traveled by the CoG during one locomotion cycle
μ	Gear ratio
v	Velocity
\dot{v}	Acceleration
ξ	The relative angle measured in the clockwise direction between the reference frame of link 1 and link 2
τ	Torque
v	The relative angle measured in the clockwise direction between the reference frame of link 2 and link 3
ϕ	The angle between the x axis in the global reference frame and the x axis in the CoG reference frame
ψ	The angle of re-orientation measured from the forward y axis
ω	Angular velocity

Subscript

<i>a</i>	Denotes the actual value
CoG	Denotes the CoG reference frame
CM	Centre of mass
<i>d</i>	Denotes the desired value
<i>i</i>	Integer that is specific to the object being described
<i>f</i>	Refers to the final value
Global	Denotes the global reference frame
<i>m</i>	Refers to a motor
<i>o</i>	Refers to the initial value

Units

cm	Centimetres
kg	Kilograms
m	Metres
rad	Radians
s	Seconds
°	Degrees

Chapter 1

Introduction

1.1 Thesis Motivation

A group of robots being used to complete a task may be referred to as collaborative robots. Certain tasks are better achieved by a different number of robots. For a task in a small workspace at one location, usually one robot will suffice. The addition of other robots makes the task more complicated [5]. In other cases, adding more robots can decrease the time required to complete the task at hand. Two robots should be able to search an area more quickly than one robot. Additional robots may be able to accomplish certain tasks that simply cannot be done using one robot. This could arise if two different tasks at two different locations needed to be synchronized [5]. Multiple robots also increase redundancy, if one robot fails, the task is not necessarily a lost cause.

Collaborative robots can be placed into two main categories: homogeneous teams and heterogeneous teams [6]. In homogeneous teams, all the robots are identical and have the same capabilities. Heterogeneous robot teams have at least two robots that are not identical, this could be as simple as merely having the ability to demonstrate different behaviours or as obvious as having a completely different mechanical structure; legs versus wheels for example. Heterogeneous robots can allow for diversity of abilities, this may be beneficial for less structured more loosely defined tasks. They may also be more adaptable to different tasks. For example, if the task requires a room to be searched in the quickest time possible, wheeled robots would be well suited to the task. However, if a multi-level building needed to be searched, another type of robot would be required as most wheeled robots cannot climb stairs. If damage had been done to the building and certain obstacles existed, wheeled robots could also encounter difficulties accomplishing the task. In these cases, it would be beneficial to have a member of the robot team with a different ability, such as walking or climbing.

In such a task, the strength of both wheeled and legged robots can be used in order to complete a task more efficiently.

Currently in the RMC Mechanical Engineering Robotics Lab, there are several wheeled robots that are being used to conduct research in collaborative systems and formation control. In order to widen the capabilities of the robot team and to increase the degree of heterogeneity, it is desired to incorporate the special abilities of a legged robot.

Legged robots would enable the robot team to investigate different locations and to access areas that currently cannot be reached by the wheeled robots. However, before being able to incorporate a legged robot into the collaborative robot team, it must be able to follow a given path. In order to follow a path, a robot uses a trajectory planner to produce the joint variables to be sent to the actuators.

Legged robots have several very different considerations in terms of trajectory planning when compared to wheeled robots. It is not sufficient to simply select required motor positions and velocities for a set amount of time.

1.2 Aim of the Thesis

The aim of this thesis was to design an off-line trajectory planning method for a quadruped robot for use with two dimensional paths on even terrain, while maintaining static stability.

In order to develop an appropriate trajectory planner to achieve the aim of this thesis, investigations on appropriate gaits, static stability measures and leg and body trajectories as well as the development of the robot's kinematics were required. The focus of the investigation however, was on the trajectory planning program, which was created using MatLab.

1.3 Background

The word robot was introduced in Karel Capek's play *Rossum's Universal Robots* in 1920 [7]. Generally, a robot is a mechanism that operates with a certain degree of

autonomy. Robots can be described as mechanical workers. They can be autonomous, programmed to do certain tasks, or they can be controlled remotely in a master slave set up. Robots can perform repetitive, strenuous, boring or dangerous tasks in several different environments. The first programmable robot was designed in 1954 by George Devol [7]. According to [8], in 2006 there were over 800,000 industrial robots in operation and over 600,000 household robots in use worldwide. These numbers include artificial limbs, autonomous vacuum cleaners, satellite repair robots, and assembly robots to name a few. Robots can be divided into two main categories: manipulator robots or mobile robots.

1.3.1 Stationary Robot Manipulators

Some of the first working robots were robot arm manipulators. Many robot manipulators are in the form of robotic arms which are fixed at the shoulder. These robots are designed to perform repetitive tasks and are found mainly in industry for applications such as automotive assembly etc. The first industrial robot was the Unimate robot arm in 1961. This robot was used in a General Electric plant for hot-die casting [9]. Robotic manipulators have since become a common staple in industry and in industrial applications and are said to comprise over a two billion dollar industry [10]. The main disadvantage of robotic manipulators is a lack of mobility and a limited workspace.

1.3.2 Mobile Robots

Mobile robots can be used in many different applications. Such man made machines can venture into different environments that may be too dangerous for humans. Possible tasks could include search and rescue of contaminated areas or exploration of hazardous environments on Earth or elsewhere.

Robot locomotion can generally be divided into three basic types: rotation, wheels or tracks for example, articulated bodies, and legs [11]. Different types of locomotion may be better suited to different environments and/or tasks.

Wheels are the most popular locomotion mechanism for mobile robots as well as for other man made locomotion systems [10]. An example of a wheeled mobile robot is the Sojourner robot that was used in the Pathfinder mission for the exploration of Mars. One of the reasons for the popularity of wheeled robots is the fact that wheels are relatively simple to implement and control with respect to locomotion. Most man made locomotion vehicles have wheels. In order to be used however, roads or tracks have been developed for wheeled locomotion. Wheeled robots are very effective on even ground. Wheels require continuous contact with the ground and on soft surfaces, wheels loose energy efficiency. Articulated body robots would include snake like robots. As with wheeled robots, continuous contact points are required for locomotion. According to [12], less than half of the Earth is accessible to wheeled or tracked vehicles. The fact that the wheel does not seem to appear in nature and in biological systems is a possible indication that it is not an ideal form of locomotion in our environment.

Legged robots can offer a greater degree of maneuverability on varying terrain. Unlike wheeled or articulated body robots, legged robots only require discrete contact points making them much more versatile and better suited to locomotion on uneven terrain. Legged robots are more complicated than wheeled robots due to the higher number of degrees of freedom. A popular legged robot is the Sony AIBO robot that is a toy dog. This robot can walk and perform different movements that mimic dogs. Legged robots can be made to crawl, walk, run or even hop depending on the task or mission. Because of these advantages, the study of legged robots is expanding and research is being conducted on bipeds [13], quadrupeds [1], hexapods [14], octopods [15] and even robots with one leg [16].

The choice of the appropriate number of legs to use for a legged robot is an important one. The choice can affect stability, maneuverability and simplicity of implementation. In nature, most mammals have two or four legs whereas insects have six or perhaps even eight. Odd numbers of legs do not seem to occur naturally. The more legs a robot has the easier it becomes to maintain stability. In terms of stability, there are generally two different ways to describe legged robots: dynamically

stable or statically stable [17].

Dynamic stability requires a constant effort in order for it to be maintained. This is why it takes a couple of years for human infants to be able to walk properly and maintain verticality; they must learn how to maintain their dynamic stability.

In order to be statically stable a minimum of three different contact points are required and the centre of gravity must be in the support polygon that is formed by these points [18]. If, when moving, less than three legs are on the ground then the mechanism has become statically unstable. Therefore, in order to have statically stable locomotion, a minimum of four legs are required [18]. Having more than four legs lends itself to greater mobility and stability. However, adding legs to a mechanism is not necessarily the best option. More legs mean more complicated modeling, more mass and a requirement for more power. A four legged robot is capable of statically stable locomotion while remaining relatively simple in design.

Robot legs can have varying degrees of freedom and varying designs. The selection of these may depend on the desired use of the robot. The number of degrees of freedom that a leg possesses can be defined by the number of independent variables required to locate all parts of the leg [19]. Usually for an open chain, each joint position can be defined by a single variable and the number of degrees of freedom is therefore equal to the number of joints [19]. Legs that are designed with three degrees of freedom are used on many robots with different numbers of legs. Most robots also tend to have identical legs, although this is not always the case. Three degrees of freedom per leg allows for a robot to move on uneven terrain in three dimensions [17]. There are, however, robots with only two or one degree of freedom per leg, this can make for complication locomotion strategies such as hopping. Adding degrees of freedom to a leg, four for instance, adds complexity to the system, but may make it more agile. For a simple leg that allows for locomotion on uneven terrain, the three degrees of freedom per leg design can be used. This leg type is used by many robots and is a simplified version of an insect leg [20].

1.4 The Trajectory Planner

The main purpose of trajectory planning is to produce the required joint variables that would be sent to the actuators to allow the robot to follow a given path. The main components that are incorporated into the trajectory planner are forward and inverse kinematics, gait selection, stability analysis, and appropriate leg and body trajectories. These components are used by the trajectory planner in order to determine the joint positions, velocities and accelerations that can be used to allow for statically stable locomotion along a desired path. The path is entered by the user in the form of multiple waypoints that lie along the desired path. The user also enters the desired height of the robot's centre of gravity to be maintained during locomotion.

First the appropriate type of gait is selected, then a search is performed to find a specific stable gait of that type. The term gait is used to describe the cycle of leg and body movements that are pieced together to allow for locomotion. The joint variables are then calculated, using the inverse kinematic equations, for the required leg and body movements along pre-determined trajectories that join the gait together.

The main consideration when deciding on appropriate gaits was the ability to maintain static stability and simplicity of implementation while still retaining flexibility in the ability to produce valid joint variables for various 2D paths. With this in mind, two gaits were selected, one that allowed for straight line motion and another that allowed for rotation about the centre of gravity (CoG).

In order to successfully carry out locomotion, it is essential that the robot remain statically stable. By incorporating a static stability check into the trajectory planner it was ensured that the produced joint variables would allow for static stability. There are many different methods used to determine the static stability of a legged robot. The method described by [21] was implemented as the aim was to maintain static stability and not necessarily to optimize it. This method involves determining if the CoG lies within a support polygon by determining the areas of different triangles formed between the projection of a robot's CoG and the different footholds.

The stable sequence of leg and body positions determined using the gait must

be joined using set trajectories. These trajectories can be defined in either joint or cartesian space depending on the required movement. From these trajectories the required joint variables can be obtained. Whether or not the path actuated by the trajectory planner would be closely followed by the mobile robot depends on the robots actuators, its control system and other physical aspects. The actual amount of time taken to move the leg is determined by the size and speed of the actuator. For this reason, a normalized time is used in this thesis where the time it takes to complete a leg transfer, t_l , represents one unit of time.

1.5 Thesis Organization

The following chapter, Chapter 2, gives a review of the literature that exists concerning walking robots. A description of the selected robot model used in this thesis is also given in Chapter 2. A review of different approaches to trajectory planning for legged robot is the focus of this chapter and is broken down into different components. These components correspond to the different aspects of leg locomotion that must be addressed by the trajectory planner in order to produce appropriate joint variables. These include stability measures, the selection of appropriate gaits, and selection of appropriate leg and body trajectories to join positions determined by the gait.

Chapter 3 begins with a summary of the Denavit-Hartenburg method for solving the forward kinematic problem. The solution to the forward and inverse kinematic problems for the SILO 4 robot are then developed. The velocity and acceleration equations are found and a singularity analysis is performed. Finally the leg workspace is determined.

Chapter 4 commences with an investigation and explanation of different gaits and their uses. This chapter details the selection of appropriate gaits for the purpose of this thesis. Specific gait attributes are discussed and determined.

Chapter 5 discusses the determination of the leg and body trajectories. The use of the chosen stability criterion is explained and the different reference frames are also discussed. This chapter also includes how all the components are brought together in order to create the trajectory planner.

Chapter 6 presents the results of the trajectory planner. This chapter shows the time history of the joint variables produced by the trajectory planner for different paths. The results for travel at different CoG heights are also compared in this chapter. An example of the advantages offered by a legged robot over a wheeled robot is given in the form a ditch crossing simulation.

Finally, Chapter 7 summaries the work completed and the results of this thesis. Recommendations for improvement as well as for future work are also included in this chapter.

Chapter 2

Literature Review

In this chapter, the literature on different aspects of legged locomotion will be reviewed. These aspects include the legged mechanisms that have been created and trajectory planning methods which encompass the development and analysis of gaits, stability measures and leg and body trajectories.

2.1 Legged Robots

The first legged mechanism was created in the 1870s by Chebyshev. It was a four legged mechanism that could perform a trot gait [22]. Most of the significant work on legged mechanisms, however, did not begin until the 1960s [14]. During the 1960s, the General Space Corporation started to develop legged mechanisms for exploration in space. The machines that were investigated were of six and eight legs. These machines lacked the required degrees of freedom to be useful [14]. In 1962, the GE walking truck was developed. This mechanism was a quadruped that weighed 1400 kg. The main problem with the GE walking truck was the fact that the driver had to coordinate all joint movements. From this, the importance of developing an automatic cycling system was recognized. In the mid to late 60s, a robot known as Big Muskie was created. Big Muskie was one of the largest legged vehicles ever built weighing 13500 tonnes. It was designed for use in open air mines and was used until 1991 [22].

The Phony Pony was created in 1996 and it was the first legged vehicle to walk autonomously [14]. This robot weighed 50 kg and had two degrees of freedom per leg. McGhee carried on from the Phony Pony in 1997 creating the Ohio State University (OSU) Hexapod [22]. Shortly afterward, McGhee also created the Adaptive Suspension Vehicle (ASV) with Waldron [14].

Up until the 1980s, most of the mechanisms created were massive. Hirose created a much smaller and manageable robot. The Pre-ambulated Vehicle (PV-II) quadruped

weighed only 10 kg and used pantograph legs with three degrees of freedom each [22]. Hirose followed this with the creation of the TITAN robot series [23].

Raibert developed the first robots able to move with dynamic stability in the early 1980s. In 1983 he developed a one legged hopping machine with three degrees of freedom. Later, he created the first quadruped able to move using dynamic stability [16]. Many different kinds of robots continue to be developed. Generally more modern robots are less massive than their predecessors [22].

In order to select an appropriate robot for the aims of this thesis, a survey of different legged robots was conducted to determine the most appropriate architecture to be used. Important factors were: stability and maneuverability, as well as simplicity of implementation.

A total of thirty four different robots were surveyed [12, 15, 20, 24–53]. All robots had at least $2n$ feet, where n is an integer larger than 1, as the aim of this thesis involves the maintenance of static stability. Twelve robots were quadrupeds [12, 26, 29, 30, 36–43], nineteen were hexapods [24, 25, 27, 28, 31, 33–35, 44–52, 54], and three had eight legs [15, 32, 53]. Twenty one of the robots used three revolute joints per leg to give three degrees of freedom in each leg [15, 20, 25, 29–31, 33, 34, 36, 38, 40–47, 50, 51, 54]. An additional two robots had three degrees of freedom per leg, but they used a combination of two revolute joints plus one prismatic joint [24, 53]. Six of the robots had two degrees of freedom in each leg using mainly revolute joints [28, 32, 35, 39, 48, 52]. One robot used just one revolute joint in each leg [27], and two robots had four degrees of freedom per leg, one using all revolute joints [26], and the other using one spherical joint and one revolute joint [37].

In the course of the survey, a general architecture was prominent in both the four and in the six legged robot. A total of fourteen robots had the same general architecture [15, 20, 29–31, 33–36, 43, 45, 46, 51, 54]. The common architecture consists of either a square or rectangular body with three degree of freedom legs evenly spaced along the sides, as for an animal or insect. Figure 2.1 shows the simple architecture as applied to a quadruped robot.

Generally the legs were designed with two revolute joints (or an equivalent uni-

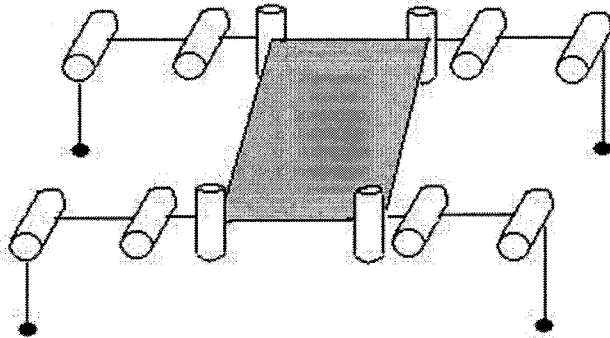


Figure 2.1: Quadruped Robot With Simple Legs

versal joint) at the hip and a third revolute joint at the knee, as shown in Figure 2.2.

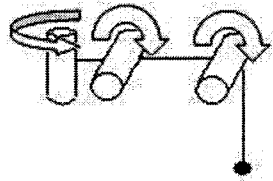


Figure 2.2: Three Degree of Freedom Leg

An equivalent form of the three degree of freedom leg also appeared to be used in a number of different robots such as the quadruped TITAN-VIII [29] and the hexapod ASV [51]. A pantograph leg is made up of four linkages, three passive revolute joints and three actuated revolute joints at the hip as shown in Figure 2.3. The grey circles in the figure represent passive revolute joints.

The pantograph linkage offers the advantage of amplifying hip motion at the foot. This also means, however, that loads at the foot are also magnified. The linkage also allows the actuators to be kept close to the body, reducing the chance of damaging them during walking [55].

The remaining robots surveyed showed some commonality, but a second general architecture does not stand out. The other robot architectures were usually more complicated than the general architecture discussed to this point adding extra degrees of freedom in the legs, ALDUBRO [37], or the body, BISAM [26]. Some models had

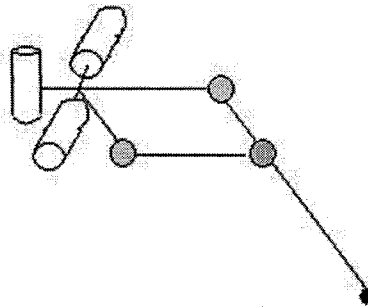


Figure 2.3: Pantograph Leg

only one or two degrees of freedom in each leg; RHex [27] and SCOUT [12] are examples of these. Though mechanically simpler in design than the robots with the general architecture, they do not have enough degrees of freedom for efficient walking on uneven terrain, making the locomotion strategies more complex.

Through a survey of several different legged mobile robots, a general robot architecture was determined. This general architecture is simple in design and allows for the required degrees of freedom for statically stable locomotion on uneven terrain. The general architecture has been seen in quadruped, hexapod and octopod robots. With simplicity in mind, the quadruped version of this general architecture, aptly represented by the SILO 4 robot, shown in Figure 2.4, was the model of choice for this thesis.

The SILO 4 robot was manufactured at the Industrial Automation Institute, CSIC, in Madrid as a research and educational platform. There are currently three SILO 4 robots; one in Madrid, one at the *École Nationale Supérieure d'Ingénieurs de Bourges-ENSI* in France and another at the University of Murcia in Spain [30]. SILO 4 is a spanish acronym that means “Sistema Locomotor de Cuatro Patas” [56] equivalently, quadruped locomotion system. The SILO 4 robot is made mainly of aluminum with a total body weight of 30 kg [1]. The centre of gravity(CoG) of the robot is assumed to be located at the centre of the robot’s body.

As discussed previously, each leg has three actuated joints. Each of the joints is actuated by a DC servomotor. The joints are PID controlled. SILO 4 has three options for foot configuration. These options differ by the number of passive joints,

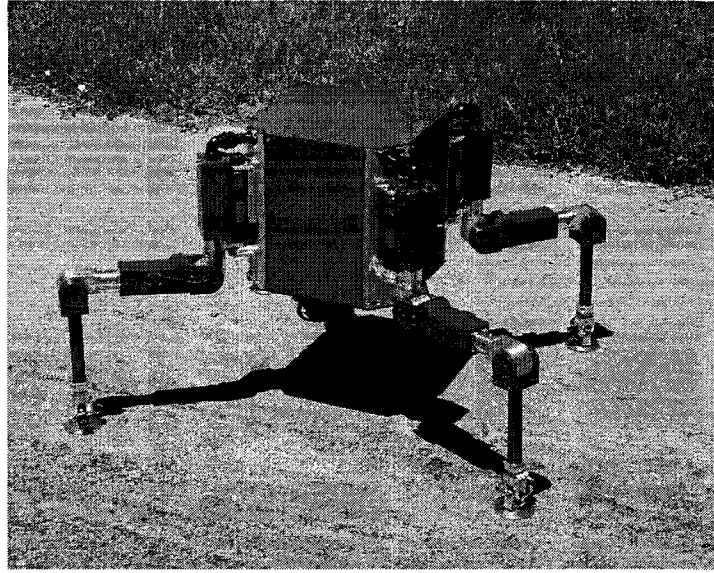


Figure 2.4: The SILO 4 Robot [3]

1, 3 or 0. The two feet with passive joints have a flat circular surface whereas the third foot is cone shaped and would therefore create a three degree of freedom passive joint when in contact with the ground. As this thesis considers the case of walking on a flat horizontal surface, a foot with one passive joint will be used. This means that the angle at the passive joint will always be equal to the sum of the second and third joint angles [30]. Specifics of the SILO 4 robot are shown in Table 2.1.

Table 2.1: Specifications of the SILO 4 Robot [1]

Length Link 1	0.06 m
Length Link 2	0.24 m
Length Link 3	0.24 m
Body Width	0.31 m
Body Height	0.30 m
Body Breadth	0.31 m

Although the specifics of the SILO 4 robot were used in the trajectory planner, the trajectory planner developed in this thesis can be applied to any quadruped robot with insect type legs.

2.2 Trajectory Planning

When a desired path is given to a robot the problem lies in determining how to actuate the motors to have the robot follow it. A trajectory planner takes the desired path and develops a plan to allow the robot to follow it. Trajectory planning can occur on-line or off-line [17]. On-line trajectory planning would be useful in dynamic environments where the desired path may change. However, as trajectory planning for a legged robot is complex and legged locomotion generally slow [22], on-line trajectory planning can be cumbersome to the robots computer, slowing down its process even more [17]. In off-line trajectory planning, the plan is already determined and needs only to be sent to the actuators.

For a wheeled robot the plan may take the form of motor velocities and accelerations. For a manipulator or legged robot this plan would be in the form of joint positions, velocities and accelerations. Looking at the example of a single manipulator, the required joint variables can be determined for a path defined in cartesian space by using the robots inverse kinematic equations, but what happens in the case where the base of the manipulator moves and when there are more than one manipulator attached to this base? This is the case of the legged robot and the determination of the required joint variables is much more complex. The body can be propelled along the path, but at some point in time the legs must also move forward or no further progress can be made. In trajectory planning for a legged robot certain problems must be addressed. These problems include:

1. How body and leg movements are joined together: the selection of appropriate gaits.
2. How to ensure static stability: stability maintenance .
3. How to join the leg and body movements: selection of leg and body trajectories.

When these problems are solved the trajectory planner can then, using the inverse kinematics, produce valid joint variables that would allow a robot to follow a desired path while maintaining static stability.

2.2.1 Gaits for Multi-Legged Robots

The study of gaits began as early as 1899 by Muybridge. Muybridge studied and photographed different animals in locomotion. Using the photographs, he determined and described the different gaits that were used by these animals. Although his work contained studies of humans and birds, his focus was on the quadruped. Muybridge described a total of eight different quadruped gaits that he observed in nature [4]. This work was carried on by Hildebrand who continued to study gaits in animals. Hildebrand, [57], began looking at gaits in a more analytical way. He defined the stride length during a locomotion cycle and introduced the gait diagram in order to be able to compare gaits. In [58], McGhee began the construction of a general theory of locomotion that could be applied to both animals and legged machines.

2.2.1.1 Statically Stable Periodic Continuous Gaits

McGhee and Frank investigated the Quadruped Creeping gait. In this work the authors established some of the key definitions involved in the study of legged locomotion. These include definitions for static stability, a legged locomotion machine, the support pattern, the static stability margin, and the creeping gait. This work investigated different quadruped creeping gaits with respect to stability. The authors showed that there are only three possible creeping gaits that maintain static stability, only one of which can be observed in nature [18]. During the same time frame, Bessonov and Umnov, [22], looked into statically stable gaits for hexapods.

Song and Waldron carried out substantial work on continuous gaits for hexapod robots. They were involved in the development the ASV robot. This hexapod is a large vehicle in which a human operator can sit. In their work they presented the important theory behind different periodic and non periodic gaits, focusing on a follow the leader gait. This gait places the feet on old, valid footholds, which means that only two new footholds must be determined rather than six [14].

The periodic gaits favored by McGhee and Bessonov, [18], were wave gaits. These are continuous gaits that allow for straight line motion [14]. Several works have

utilized a continuous periodic gait, such works include the work of Tee et al.. In that work, a wave gait is implemented on a quadruped robot in order to achieve straight line motion. The robot achieved speeds of only 0.0012 m/s [59]. The slow speed was related to problems with the design of the quadruped. The same type of gait was implemented on the TITAN-VIII quadruped with better results in [21]. However, the joint positions were not smooth. Inagaki and Kobayashi, [60], proposed a method for transitioning between different continuous periodic gaits such as the crawl and the gallop. The method used rhythm generators to switch smoothly between gaits. Linemann et al. implemented a continuous periodic gait on a scorpion robot with eight legs, and achieved a straight line walk on fair terrain with smooth accelerations. The velocities for the scorpion robot ranged between 0.05 m/s and 0.1 m/s. Although these and similar works are important to the development of the work on gaits, these gaits only allow for motion in one direction, along the forward axis of the robot [15].

Another periodic gait was developed that allows for straight line motion [61]. This gait is referred to as the crab wave gait. This gait was formulated by Song and Zhang, [61], in 1990. Using this gait, a robot could move in a straight line at different angles. The crab gait allows for motion at an angle α to the forward axis [62]. Jimenez and Gonzalez de Santos used a crab wave gait in conjunction with stroke control and velocity control to produce an adaptive gait on irregular terrain with the RHIMO quadruped robot. The resultant algorithm for the gait is not easily implemented and the required conditions to allow for locomotion are not evaluated until after a leg movement, meaning that on several occasions a leg transfer must be recovered. This is not an ideal situation as more movements occur than are necessary [63].

The crab wave gait was also successfully implemented on the TITAN-VIII robot [29]. Using this gait, TITAN-VIII was able to move along various paths in a two dimensional plane. The crab gait does allow for more diverse movement than the forward gaits, however several potential problems exist when using a wave crab gait. The crab gait does not allow the robot to re-orient its forward axis [62]. This means that the front of the robot is not necessarily pointed in the direction of travel. In addition, it is very difficult to transition between different crab gaits in a continuous setting,

restricting the omni-directionality of the proposed gait. Finally, Jimenez and Gonzalez de Santos, [64], showed that if stability is to be maintained, the crab angle has a maximum and a minimum value, specific to each individual robot. This means that not all points are necessarily accessible.

In order to orient a robot, turning gaits were developed. There are two common turning gaits, these are known as the spinning gait and the circling gait. The main difference between the two gaits is the turning centre. In the spinning gait, the robot rotates about the CoG contrary to the circulating gait where the robot rotates along a circumference while continuing to translate in the xy plane [65]. The circling gait was first proposed by Hirose [66]. Bien et al., [67], then proposed a scheme for a circling gait that allows for control of translation and orientation with special consideration for the longitudinal stability margin. Lie and Peisun, [68], successfully implemented a turning gait on the quadruped JTUWN-II robot. Zhang and Song went further into the study of turning gaits and generated the stable areas of the turning centres for both circling and spinning gaits. They also found that the stability in a wave circling gait was similar to that of a wave crab walking gait [65]. Circling gaits, like crab gaits are restricted to a certain range. If the turning radius is too small, a stable circling gait cannot be performed [64].

With the necessary gaits having been developed, omni-directional continuous locomotion could be achieved. In their paper, Hugel and Blazevic define six gaits to be used to create omni-directional locomotion. These gaits were variations of the forward gaits and turning gaits. Methods to transition between the different gaits were also discussed. These methods were specific to the gaits being transitioned. The gaits were tested separately on the Sony Pet Robot. Their spinning gait took 6 seconds to be completed and the forward gait was able to attain a walking speed of $0.07 \text{ m}/(\text{unit of time})$ [69]. The gait transition methods were not implemented on the robot.

The four variations of the crab gait, representative of the four directions along the x and y axes, and two variations of the circling gait, clockwise or counter clockwise, were implemented on the TITAN-VIII robot [70] and [71]. Gait transition methods were also developed and implemented. These transitions were composed of leg

movements from a current position to the start position for the next gait while maintaining stability. The work done with the TITAN-VIII robot was further studied, [72], allowing for omni-directional motion on a slope.

2.2.1.2 Statically Stable Periodic Discontinuous Gaits

Much of the work discussed so far explored continuous gaits. In a continuous gait, the body is in continuous motion with respect to a global reference frame [14]. This is not the only way to implement locomotion with a periodic gait. A discontinuous gait can also be used. In a discontinuous gait, body and leg motions occur separately [22]. Discontinuous gaits were first implemented on the walking robot, AMBLER. The gait used for AMBLER was named a circular gait, not to be confused with the above mentioned circling gait used for body re-orientation. The name was given because of the specific architecture of the machine that required the six legs to move in a circular fashion to achieve locomotion. AMBLER was designed to walk on rough terrain [73].

Pack and Kak, [74], introduced a discontinuous forward walking free gait that they named the SLPMF gait. For this gait the order of foot placement is determined by a method that uses diagonal lines in order to maintain a statically stable walk. The robot used in conjunction with this gait was a quadruped with two revolute and one prismatic joint in each leg. The robot was also physically attached to a computer during locomotion. The robot was able to walk successfully in a straight line using the SLPMF gait.

Much of the work carried out on discontinuous gaits has been done at the *Intstituto de Automatica Industrial* in Madrid, by Gonzalez de Santos, Garcia, Estremera and Armada [63]. They looked at the continuous wave, circling, and crab gaits and implemented equivalent discontinuous version of these gaits on the RHIMO quadruped robot [63]. They were able to show that discontinuous gaits could perform equally well if not better than continuous gaits. Discontinuous gaits are better suited to irregular terrain than continuous gaits. Because of their intermittent motion, discontinuous gaits offer better stability and lower power consumption than continuous gaits [22]. Taking a quadruped robot with three actuated joints for each leg as an example, if a

continuous gait is used, all twelve joints are actuated at all times. If a discontinuous gait is used instead, all the joints are actuated only in the body motion section of the gait, otherwise only three joints are actuated at once.

Their work, [64], also showed that, unlike previously assumed, the discontinuous gait was not necessarily slower than a continuous gait. In fact for a medium to high duty factor, discontinuous gaits were actually shown to have higher overall average speeds than continuous gaits. Discontinuous gaits also have the advantage of being simpler to plan and implement [14].

The work on discontinuous gaits continued on the quadruped platform SILO 4 [30]. New discontinuous gaits were investigated, and the creeping, crab and circling discontinuous gaits were further developed. Four main aspects were proposed for consideration when developing a discontinuous gait [22]:

1. If a leg is at the rear limit of its defined workspace, it should be moved to the forward limit of the workspace.
2. At the end of a body motion, at least one leg should be at the rear limit of its workspace.
3. A contra lateral non adjacent transfer leg should be moved to location that ensures that the CoG remains in a statically stable region.
4. The sequences of leg and body motion should be periodic.

Considering these aspects, discontinuous gaits can be developed. It can be shown that for a quadruped, a one phase discontinuous creeping gait, where only one body movement occurs per cycle, would operate on the brink of stability. It is possible to increase the number of body movements that occur. For instance after each time a leg is lifted and placed the body could be propelled forward, such a gait would be called a four phased discontinuous gait. The distance traveled by the CoG during one cycle of a one, two, three or four phased gait would be equal. Increasing body movements however, can increase the time needed to complete a cycle and, as shown by [22], an increase in body movements decreases in stability.

Estremera et al. proposed a two phased creeping gait for forward locomotion. A two phased discontinuous spinning gait was also purposed. This gait allows the orientation of the CoG with respect to the global reference frame to be changed. Unlike the circling gait, the spinning gait is not confined by a minimum and maximum angle of rotation. With such a spinning gait, the gait begins and ends with the same leg positions. In the proposed two phased spinning gait, two legs are moved followed by a re-orientation of the CoG by half the desired angle. Then the other two legs are moved and the CoG re-oriented again until it is pointed in the desired direction. Caution is required when determining the initial and final foot positions to ensure that static stability will be maintained during the locomotion cycle [22].

2.2.1.3 Dynamic Gaits

Dynamic gaits are gaits that allow for stable locomotion. In a dynamically stable gait, the robot maintains stability through controlled motion and the use of inertia [17]. Marc Raibert carried out extensive work in the area of dynamic gaits. The focus of his work was a single legged hopping robot. He used this robot to better understand the dynamics and active balance in legged locomotion. He used posture and velocity control to enable the robot to maintain dynamic stability. Raibert adapted the principles of the one legged hopper to quadruped and biped running, using the concept of the virtual leg. A virtual leg is a representation of a pair of co-ordinated legs. Using dynamic gaits, robots can move faster than with the static walking gait. With an eight degree of freedom quadruped robot, speeds close to 0.75 m/s were reached [16]. Raibert's experiments were run on flat even terrain and there was no pre-defined path for the robot to follow.

Chevallereau et al., [75], built on Raibert's work on the quadruped robot and developed a dynamic control law to allow a legged robot to follow a reference trajectory. The authors encountered problems because the size of the contact points were not considered. They showed that certain ground impacts would lead to a loss of stability.

Some of the problems related to these dynamic gaits, apart from the maintenance of stability, include large torque and energy requirements. In [76], an attempt to

optimize the torque and energy requirements for certain dynamic gaits was made. The maximum velocity achieved was for the amble gait and was 1.3 m/s. Again, these results were not tested on a physical robot. Although good results were achieved using dynamic gaits they are not much faster than statically stable gaits and are only suited to flat even terrain [22]. Stability maintenance and implementation of a dynamic gait are difficult when compared to statically stable periodic gaits. Dynamic gaits also required more energy in order to maintain dynamic stability [17].

2.2.1.4 Non Periodic Gaits: The Free Gait

The free gait is a non periodic gait designed for locomotion over rough or uneven terrain, or with forbidden areas. Terrain where a periodic gait would have difficulties functioning. The free gait has the advantage of being able to change direction at any time during locomotion. The foot placement and body motions in a free gait are not pre-set and are determined as a function of the trajectory and ground features in a more flexible way than in a periodic gait [22].

The free gait was first introduced by McGhee and Iswandhi [77]. For their algorithm, the terrain was divided into permitted and forbidden cells. During simulations the algorithm was tested on different types of terrain with different numbers of forbidden cells. Several shortcomings were discovered as the algorithm was not suitable for use with a quadruped robot. Another shortcoming of the algorithm is that it does not take terrain irregularities into account, much like a periodic gait.

In a free gait, the footholds must be determined. This is mainly done with one of two different methods [62]: (1) a rule based method or (2) a search based method. The rule based method was the first method employed to create free gaits [23]. Essentially, sequential leg and body movements are determined based on a set of rules. The determination of appropriate rules is essential to create stable locomotion. This process can also be a timely one, reducing the locomotion speed [62].

In an attempt to make the SILO 4 robot better suited to irregular terrain, a discontinuous crab free gait and discontinuous turning gaits were developed [62]. These gaits were implemented using rule-based algorithms to generate footholds. Again,

the free gaits presented require more computational time and are much more difficult to implement than periodic gaits. Consideration is also required in order to avoid deadlock situations when employing free gaits. All of the gaits proposed by [62], were successfully tested on the SILO 4 robot.

A rule based approach was also used [78], on a quadruped robot to produce a free gait. This gait also allowed for a change in body posture to allow the robot to avoid obstacles at different heights. With this approach, several deadlock situations occurred. A deadlock situation, when referring to legged locomotion, is a situation where a leg cannot be lifted without loosing stability or there exist no appropriate footholds, meaning the robot is unable to move. It should also be noted that this formulation of a free gait has not been used on irregular terrain.

The search based method involves the generation of several different robot actions. The actions are then evaluated to determine whether they would produce acceptable locomotion [62]. Depending on the exact method an infinite number of possible solutions could exist. The evaluation of possible options can be lengthly. Pal and Jayarajan, [79, 80], used a graph search based on the A* algorithm to produce a free gait. The A* algorithm finds the least cost path given an initial and goal node. In their papers, a simulation was run using their free gait on a simplistic model deemed “unrealistic” by the authors. A problem that occurred, even in the simplified model, was determining the depth of the search to minimize the possibility of deadlock, and maximize the speed of the algorithm. This is the main problem faced by search based methods to determine a free gait for legged locomotion.

A third method that has been successfully tested to implement a free gait is a reactive approach, which uses subsumption. This approach is a hierarchical approach where higher levels can subsume lower levels [6]. The hierarchy of different behaviours is decided by the operator. For example, the robot’s task is to walk forward in a straight line, while avoiding any obstacles. In this case, the avoidance of the obstacle would be a higher level in the hierarchy than the forward walk and this behaviour would take precedence. The reactive approach has been implemented on hexapod, [81], and octopod, [55], robots. Because subsumption is a purely reactive

approach and no planning occurs, it is very important that proper behaviours exist to accomplish a given task. It is quite possible that undesired emergent behaviours occur and the task at hand can not be completed. The more complicated the task, the more difficult it may be to accomplish it using subsumption [6]. This is part of the reason that such an approach has not proved successful on quadruped robots, as it is much more complicated to maintain their static stability [22].

Deadlock avoidance is one of the main problems with free gaits, even more so with quadruped robots [22]. The reason that quadrupeds are more prone to deadlock is that they have fewer legs and hence fewer locomotion options. Attempts to avoid deadlock situations have been made by trying to create an algorithm that identifies possibly deadlock options for locomotion. A different approach to deadlock avoidance was used by Ding and Scharf who proposed a quadruped with a fixed arm situated on the body. When a situation arose in the gait where the robot would be unable to lift a leg and still maintain static stability, the arm of the robot would be moved, not changing the physical location of the robot, but changing the robot's CoG, allowing for static stability. This approach did not take any possible dynamic effects of implementing such an arm into account. This method was tested through computer simulation [82].

2.2.2 Methods of Defining Stability

2.2.2.1 Dynamic Stability

In order to maintain dynamic stability, a robot uses dynamic modeling, inertia, and controlled robot motion [17]. If a robot is dynamically stable, stopping it in the middle of locomotion may cause a loss of stability. Locomotion using dynamic stability requires a complicated model of the robot dynamics and advanced control and locomotion processing [17]. It is possible to achieve dynamic stability with as little as one leg. Raibert has carried out extensive research by studying one legged hopping machines and dynamic stability. One of the main benefits of using dynamic stability is the ability to achieve higher speeds than when using static stability as well as a wider option of possible gaits [16].

Different criteria have been developed to define the dynamic stability of a legged robot. These include: the Zero Point Momentum (ZMP) [40], the Centre of Pressure (CoP) [83] and the control of an inverted pendulum [84].

2.2.2.2 Measures of Static Stability

Unlike dynamic stability, static stability can be maintained with no effort if no movement occurs [17]. Maintenance of statically stable locomotion requires at least three contact points on the ground at all times [85]. These contact points must also be appropriately placed to support the CoG if static stability is to be achieved. Many different methods and measures to determine static stability have been developed. These are many in number and only a small selection will be discussed here.

In order to discuss methods of determining stability, the idea of the support polygon must be explained. The support polygon is formed by joining the lines that join the supporting legs of a robot. A quadruped robot that has one leg in transfer phase for example, would have a triangular support polygon. The idea of the support polygon is the basis for many of the static stability measures.

One of the first measures of static stability was the idea of the Stability Margin, S_m , that was defined by McGhee [18]. According to McGhee, the S_m is the shortest distance between the projection of the robot's CoG and the boundaries of the support polygon. McGhee stated that if the S_m is negative then the robot is statically unstable. In other words, the projection of the CoG must be within the support polygon for the robot to be statically stable. This idea is illustrated for a triangular support polygon in Figure 2.5. Determination of a robot's stability can therefore be determined without directly calculating the S_m [21, 36]. This is beneficial because although the S_m is the optimum stability margin on horizontal, even terrain [22], it can be very complicated to calculate.

Another measure of static stability that is quite similar to the S_m is the Longitudinal Stability Margin, S_l [14]. The S_l is used by many when determining static stability because it is simpler to calculate than the S_m and offers a good approximation of it [86]. The S_l is defined as the minimum distance between the projection of

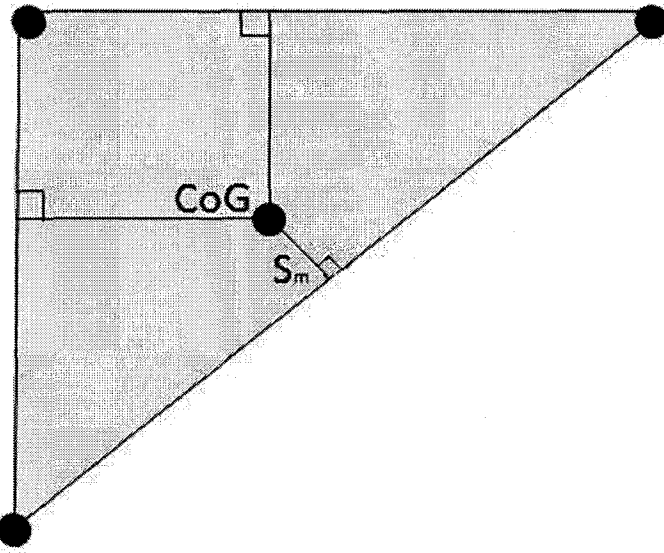


Figure 2.5: The Stability Margin

the CoG and the front and rear boundaries of the support polygon, with respect to the direction of motion [14]. This S_l illustrated in Figure 2.6.

Chen et al., [87], employed a method in a free quadruped gait to determine stability. The method uses lines from the two feet on the same side in support phase and the CoG to create what the authors call a Statically Stable Area (SSA), shown in Figure 2.7. The area allows for the selection of the next appropriate leg to change into the transfer phase as being the leg outside the SSA.

Though there are many different approaches for determining the static stability of a legged robot such as the use of S_m , S_l , or SSA, all of the above mentioned methods have the same foundation. The foundation is the support polygon. In order to maintain static stability, the CoG must remain within a support polygon.

The above mentioned methods work well on horizontal even terrain, but are not necessarily applicable to other situations: a robot on a steep slope for example. For such situations, another stability measure was developed [88], the Energy Stability Margin, S_E . This method takes the effects of gravity into account. The S_E is defined as the minimum potential energy required to cause the robot to fall. A normalized version of the S_E has also been employed by others such as in [89]. A positive S_E indicates static stability, but the CoG should also lie within the support polygon for

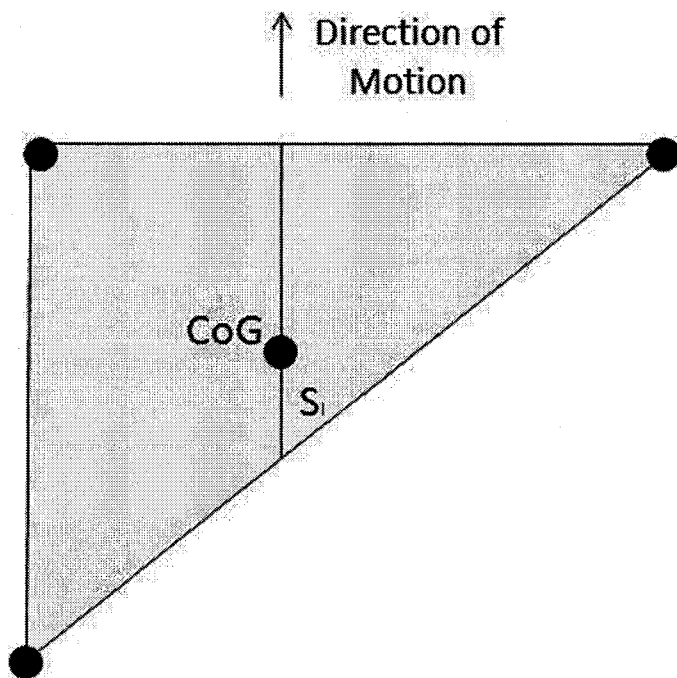


Figure 2.6: The Longitudinal Stability Margin

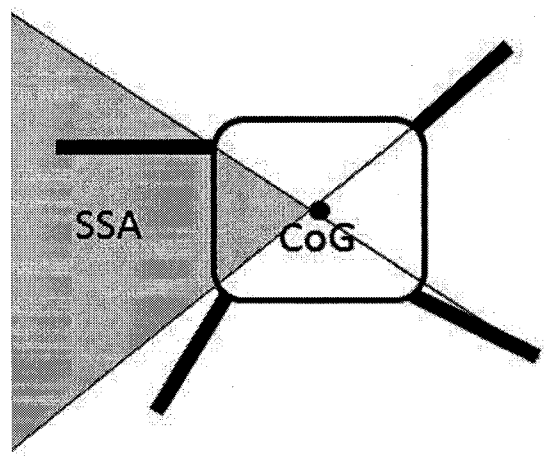


Figure 2.7: The SSA

static stability. This shows that the closer the CoG is to the slope the more stable it should be and the less likely that it will tip.

Several possible methods have been presented in order to determine the static stability of a robot. As the aim of this thesis does not include the optimization of stability, but just its maintenance, an exact value for stability is not required. This thesis also deals with horizontal even terrain, and therefore it is not necessary to determine the S_E . It is sufficient to know whether the projection of the CoG lies within the support polygon, as was done in [21] and [36].

2.2.3 Leg and Body Trajectories

The gait provides the required sequence of motions from point A to point B, but it does not provide the information about what those motions are. Leg and body trajectories provide the method to connect the initial and final configurations while satisfying any constraints that may apply [8].

When defining trajectories, there are two different options: joint space or cartesian space. Where joint space corresponds to the joint variables and cartesian space corresponds to the cartesian coordinates (x,y,z) . Whereas the path for the robot in this thesis is defined in terms of position and orientation (x,y,ϕ) , a trajectory is a function of time. There is an infinite number of different leg and body trajectories. Some are better suited than others for different tasks.

When discussing discontinuous legged locomotion, trajectories are required for leg movements and also for body locomotion. The main difference between the two is that in the case of a body movement, the end effector is the CoG of the robot and all twelve joints are used. It is important that the joints do not work against each other. For a leg movement, only the three joints in the leg move and the end effector is the foot. These differences must be considered when determining the appropriate trajectory to use and in what space it should be defined. In general, most of the trajectories for legged robots are defined in cartesian space because the constraints are more easily implemented. Such constraints include avoidance of obstacles such as irregularities in the terrain.

During the leg transfer phase, the leg must be lifted off the ground and moved forward. The start and end velocities of the leg trajectory are zero. The shortest distance is a straight line, but this would mean dragging the leg on the ground or creating jerky velocity and acceleration profiles. For this reason a curve is a popular choice. The shape of the curve can be determined based on different requirements, such as stepping over an obstacle. The simplest curve to implement would be a sine curve. A sinusoidal leg trajectory was implemented, [71], for a quadruped robot using a continuous gaits for omni - directional motion. Sakakibara et al. showed that for a robot of roughly 300 kg at speeds of roughly 0.7 m/s, a sinusoidal leg trajectory incurred problems because of discontinuities at the initial and final positions. The main issue was the large impact forces upon contact with the ground. The authors concluded that these forces could be problematic in locomotion. This is more of a problem in continuous gaits where the motion of the robot may be interrupted. It is also important to note that most legged robots operate the legs at slower speeds than that tested, closer to 0.3 m/s. At such speeds the authors found that a sinusoidal foot trajectory created no problems to locomotion [90]. Also important to note is the fact that current robots tend to be less massive than the quadruped walking machine used by Sakakibara et al.. The SILO 4 robot for example weighs roughly 46 kg [1]. With a lower mass, such as that of the SILO 4 robot, the impact forces created would be significantly decreased.

Alternatively, where impact forces become a problem, a composite cycloid leg trajectory has been presented [90]. This trajectory is quite similar to the sine curve except that the ends curve in, smoothing the transition to the contact point. The difference between the two leg trajectories is illustrated in Figure 2.8.

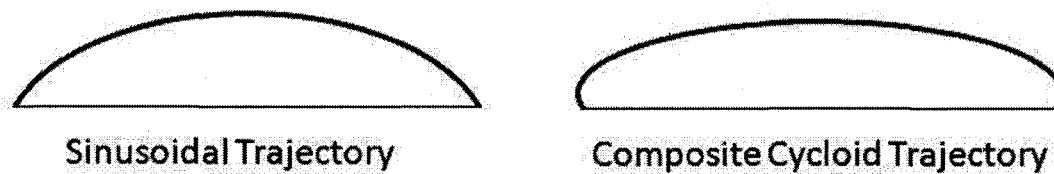


Figure 2.8: Examples of a Sinusoidal and a Composite Cycloid Trajectory

A cycloid function was implemented in work looking at quadruped and hexapod walking systems with two degrees of freedom per leg with a periodic continuous gait [91]. For a continuous gait, they found that a cycloid function improved hip and foot trajectory tracking. They also showed that there was little difference in performance between the two leg trajectories. Unlike the sinusoidal leg trajectory in [71], the cycloid function in [91] was not actually implemented on a physical robot.

Other types of curves have also been implemented. In bipedal walking, it is common for the trajectory to be defined by B-Splines [13, 92]. Bipedal walking is by definition dynamic locomotion. Smooth motion is therefore important to ensure that dynamic stability can be maintained. B-Splines are used to ensure that the trajectory is smooth and the body motion is continuous. Bezier curves have also been implemented in quadrupeds in order to satisfy certain constraints [93]. The constraints described by the authors would also be met by a sinusoidal curve. Even exponential functions have been used to develop leg trajectories. An exponential leg trajectory was used for the TITAN-VIII robot for use on uneven terrain [94]. The trajectory took into account the roughness of the ground profile, but in certain situations, such as steeping on top of a small hill, the motion was not smooth.

To increase simplicity for leg trajectories in continuous gaits, Jimenez and Gonzalez de Santos, [63] used a rectangular leg trajectory that is defined by four points joined by straight lines. A drawback of this trajectory, aside from discontinuous velocities and accelerations, is that collision with the terrain is not necessarily avoided. For a discontinuous gait this problem would not arise, but this trajectory would suffer the same minor limitations as a sinusoidal trajectory, and is just as simple to implement.

Most of the works detailing trajectory generation for legged robots deal with the transfer phase of the leg. That is because the body trajectory is generally dictated by the gait. The most common body trajectories are straight lines, for gaits such as wave gaits, and simple curves, for the circling gaits. When moving the body, it is important to first define the trajectory in cartesian space and then transform this information into joint variables for each point on the trajectory because the legs must

all move the CoG along the same cartesian path. A different situation occurs for gaits such as the spinning gait where no displacement of the CoG occurs, in this case defining the trajectory in joint space would be more appropriate as only the joint position are changed.

Chapter 3

Kinematics of an Insect Type Leg

The trajectory planner requires the ability to switch between cartesian and joint variables to determine the position of the feet and to calculate the required joint variables. In order to determine the relationship between the joint variables and the position of the mechanism, a kinematic analysis is performed. The kinematic analysis can be broken up into two separate problems [7]: (1) The direct kinematic problem (DKP) which is used to determine the mechanism's position given the joint variables. The DKP is used by the trajectory planner to check that given joint variables will provide statically stable positions. (2) The inverse kinematic problem (IKP) describes the case where the mechanisms position is known and can then be used to find the joint variables. Depending on the mechanism and its architecture, there is a possibility of several solutions for each problem. In order to solve these problems, the Denavit-Hartenberg (DH) representation will be used.

3.1 Forward Kinematic Equations

Mechanisms consist of several different links and joints. This can make the kinematic analysis, quite complicated. Although there are several different approaches used to solve the DKP of a mechanism, the DH representation is a widely used convention that helps to simplify the development of a mechanism's kinematics. Each link of the mechanism is assigned a number from 0 to n and a reference frame is assigned to each joint. In this way, the problem is equated to finding the relative position of each frame. Let i be a number from 0 to $n + 1$ representing the i^{th} reference frame. The rules that apply to assigning the reference frames are as follows [95]:

1. The z_i axis is along the axis of revolution of the i^{th} joint.
2. The x_i axis is defined as the common perpendicular between the z_i axis and the z_{i-1} axis in the direction toward the z_i axis.

3. It follows that the y_i axis can then be determined using the right hand rule.

Using the above mentioned rules, the reference frames for a leg of the quadruped can be determined and are shown in Figure 3.1.

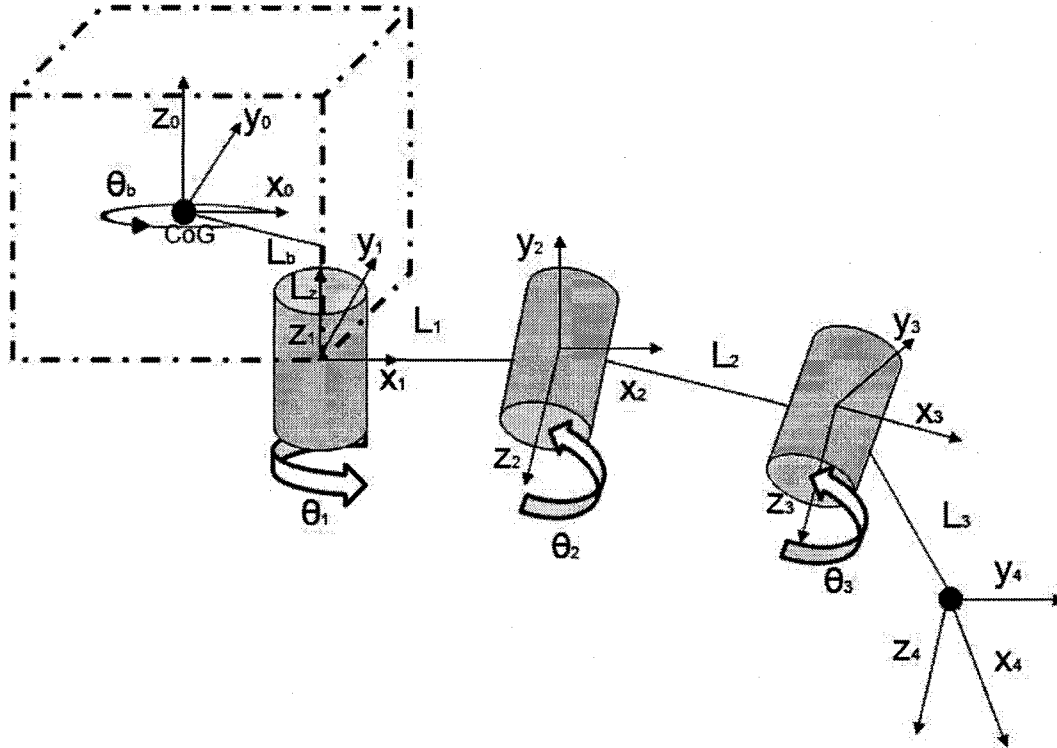


Figure 3.1: DH Reference Frames for the Robot Leg

Next the DH parameters must be determined. These parameters are four in number and help to describe the mechanism's architecture and configuration [95].

a_i : This parameter describes the distance between the z_i axis and the z_{i+1} axis. If the two axes intercept, then a_i is equal to zero.

d_i : This parameter describes the z_i co-ordinate of the intersection between the x_i axis and the z_{i+1} axis.

α_i : This parameter describes the angle between z_i axis and the z_{i+1} axis and is measured about the x_{i+1} axis.

θ_i : This parameter describes the angle between the x_i axis and the x_{i+1} axis and is measured about the z_i axis. In the case of the given leg, θ_i represents the joint variables.

The application of these rules to the quadruped leg shown in Figure 3.1 give the following parameters which are summarized in Table 3.1.

Table 3.1: DH Parameters

i	a_i	d_i	α_i	θ_i
0	L_b	$-L_z$	0	θ_b
1	L_1	0	$\pi/2$	θ_1
2	L_2	0	0	θ_2
3	L_3	0	0	θ_3

θ_b is known. For the SILO 4 robot θ_b is $3\pi/4$ for leg 1, for leg 2 θ_b is $\pi/4$, for leg 3 θ_b is $-3\pi/4$ and for leg 4 θ_b is $-\pi/4$. L_b is 0.22 m and L_z is equal to 0.15 m. The link lengths are those given in Table 2.1.

Associated with each reference frame is a vector, c_i and a rotation matrix $Q_{i+1 \rightarrow i}$. These variables give the $i + 1$ frame's orientation and position with respect to frame i . They can be described as follows [95]:

$$c_i = \begin{bmatrix} a_i \cos \theta_i \\ a_i \sin \theta_i \\ d_i \end{bmatrix} \quad (3.1)$$

$$Q_{i+1 \rightarrow i} = \begin{bmatrix} \cos \theta_i & -\cos \alpha_i \sin \theta_i & \sin \alpha_i \sin \theta_i \\ \sin \theta_i & \cos \alpha_i \cos \theta_i & -\sin \alpha_i \cos \theta_i \\ 0 & \sin \alpha_i & \cos \alpha_i \end{bmatrix} \quad (3.2)$$

In combining all c_i and $Q_{i+1 \rightarrow i}$ for each frame, the orientation and position of the end effector can be determined with respect to the base reference frame, located at the CoG.

$$p = c_0 + Q_{1 \rightarrow 0}c_1 + Q_{1 \rightarrow 0}Q_{2 \rightarrow 1}c_2 + Q_{1 \rightarrow 0}Q_{2 \rightarrow 1}Q_{3 \rightarrow 2}c_3 = \begin{bmatrix} x \\ y \\ z \end{bmatrix} \quad (3.3)$$

Using the DH parameters found in Table 3.1 and substituting into Equations 3.1, 3.2 and 3.3, the position of the foot with respect to the CoG of the leg can be determined to be:

$$p = \begin{bmatrix} (L_b \cos \theta_b + L_1 \cos(\theta_1 + \theta_b) + L_2 \cos(\theta_1 + \theta_b) \cos \theta_2 \\ + L_3 \cos(\theta_1 + \theta_b) \cos \theta_2 \cos \theta_3 - L_3 \cos(\theta_1 + \theta_b) \sin \theta_2 \sin \theta_3) \\ (L_b \sin \theta_b + L_1 \sin(\theta_1 + \theta_b) + L_2 \sin(\theta_1 + \theta_b) \cos \theta_2 \\ + L_3 \sin(\theta_1 + \theta_b) \cos \theta_2 \cos \theta_3 - L_3 \sin(\theta_1 + \theta_b) \sin \theta_2 \sin \theta_3) \\ L_2 \sin \theta_2 + L_3 \sin \theta_2 \cos \theta_3 + L_3 \cos \theta_2 \sin \theta_3 - L_z \end{bmatrix} \quad (3.4)$$

This can be simplified to give:

$$p = \begin{bmatrix} L_b \cos\theta_b + \cos(\theta_1 + \theta_b)(L_1 + L_2 \cos\theta_2 + L_3 \cos(\theta_2 + \theta_3)) \\ L_b \sin\theta_b + \sin(\theta_1 + \theta_b)(L_1 + L_2 \cos\theta_2 + L_3 \cos(\theta_2 + \theta_3)) \\ L_2 \sin\theta_2 + L_3 \sin(\theta_2 + \theta_3) - L_z \end{bmatrix} \quad (3.5)$$

The x , y and z coordinates of the end effector in the hip's frame of reference can now be determined given the joint variables θ_1 , θ_2 , and θ_3 . The orientation of the end effector is not required and will not be developed here.

3.2 Inverse Kinematic Equations

There are many possible approaches to solving the IKP of a serial mechanism. In this case the position is relatively simple, consisting of three equations and three unknowns and can be solved using an algebraic approach. From Equation 3.5, we have:

$$x = L_b \cos\theta_b + \cos(\theta_1 + \theta_b)(L_1 + L_2 \cos\theta_2 + L_3 \cos(\theta_2 + \theta_3)) \quad (3.6)$$

$$y = L_b \sin\theta_b + \sin(\theta_1 + \theta_b)(L_1 + L_2 \cos\theta_2 + L_3 \cos(\theta_2 + \theta_3)) \quad (3.7)$$

$$z = L_2 \sin\theta_2 + L_3 \sin(\theta_2 + \theta_3) - L_z \quad (3.8)$$

Taking the fact that x and y are quite similar, Equations 3.6 and 3.7 can be combined to solve for θ_1 .

$$\frac{x - L_b \cos\theta_b}{\cos(\theta_1 + \theta_b)} = \frac{y - L_b \sin\theta_b}{\sin(\theta_1 + \theta_b)} \quad (3.9)$$

$$\theta_1 = \text{atan2}(y - L_b \sin\theta_b, x - L_b \cos\theta_b) - \theta_b \quad (3.10)$$

Physically θ_1 must be between -90° and 90° for all legs. If Equation 3.6 is multiplied by $\cos(\theta_1 + \theta_b)$ and Equation 3.7 multiplied by $\sin(\theta_1 + \theta_b)$ they can be added together to give:

$$(x - L_b \cos\theta_b) \cos(\theta_1 + \theta_b) + (y - L_b \sin\theta_b) \sin(\theta_1 + \theta_b) = L_1 + L_2 \cos\theta_2 + L_3 \cos(\theta_2 + \theta_3) \quad (3.11)$$

This can be rearranged as:

$$\cos(\theta_2 + \theta_3) = \frac{(x - L_b \cos\theta_b) \cos(\theta_1 + \theta_b) + (y - L_b \sin\theta_b) \sin(\theta_1 + \theta_b) - L_1 - L_2 \cos\theta_2}{L_3} \quad (3.12)$$

Equation 3.8 can also be arranged to give:

$$\sin(\theta_2 + \theta_3) = \frac{z + L_z - L_2 \sin\theta_2}{L_3} \quad (3.13)$$

Equations 3.12 and 3.13 can be squared and added together to give an equation in terms of θ_1 , now a known value, and θ_2 . Let:

$$A = 2L_2(y - L_b \sin\theta_b) \sin(\theta_1 + \theta_b) + 2L_2(x - L_b \cos\theta_b) \cos(\theta_1 + \theta_b) - 2L_2L_1 \quad (3.14)$$

$$B = 2L_2(z + L_z) \quad (3.15)$$

$$\begin{aligned} C = & (\cos^2(\theta_b + \theta_1)(x - L_b \cos\theta_b)^2 \\ & + 2(x - L_b \cos\theta_b)(y - L_b \sin\theta_b) \sin(\theta_b + \theta_1) \cos(\theta_b + \theta_1) \\ & - 2L_1(x - L_b \cos\theta_b) \cos(\theta_b + \theta_1) - L_3^2 + \sin^2(\theta_b + \theta_1)(y - L_b \sin\theta_b)^2 \\ & - 2L_1(y - L_b \sin\theta_b) \sin(\theta_b + \theta_1) + L_1^2 + (z + L_z)^2 + L_2^2) \end{aligned} \quad (3.16)$$

By combining Equations 3.12-3.16, Equation 3.17 can be obtained:

$$A \cos\theta_2 + B \sin\theta_2 = C \quad (3.17)$$

In order to solve Equation 3.17, two identities, [96], must be used:

$$\cos\theta_2 = \frac{1 - \tan^2(\theta_2/2)}{1 + \tan^2(\theta_2/2)} \quad (3.18)$$

$$\sin\theta_2 = \frac{2\tan(\theta_2/2)}{1 + \tan^2(\theta_2/2)} \quad (3.19)$$

Equations 3.18 and 3.19 can be substituted into Equation 3.17 to get a quadratic expression which can be solved using the quadratic formula.

$$(C + A)\tan^2(\theta_2/2) - 2B\tan(\theta_2/2) + (C - A) = 0 \quad (3.20)$$

$$\tan(\theta_2/2) = \frac{2B \pm \sqrt{4B^2 - 4C^2 + 4A^2}}{2(C + A)} \quad (3.21)$$

$$\theta_2 = 2\tan^{-1}(\tan(\theta_2/2)) \quad (3.22)$$

This gives two different solutions for θ_2 . Note that if $B^2 + A^2 < C^2$, then the two angles have imaginary parts. Angles with imaginary parts are not valid solutions

and indicate that the desired waypoint cannot be reached. In order to solve for θ_3 Equations 3.12 and 3.13 can be combined to give:

$$\tan(\theta_2 + \theta_3) = \frac{z + L_z - L_2 \sin \theta_2}{(x - L_b \cos \theta_b) \cos(\theta_b + \theta_1) + (y - L_b \sin \theta_b) \sin(\theta_b + \theta_1) - L_1 - L_2 \cos \theta_2} \quad (3.23)$$

Finally Equation 3.23 can be solved for θ_3 .

$$\theta_3 = \text{atan2} \frac{(z + L_z - L_2 \sin \theta_2, (x - L_b \cos \theta_b) \cos(\theta_b + \theta_1) + (y - L_b \sin \theta_b) \sin(\theta_b + \theta_1) - L_1 - L_2 \cos \theta_2)}{\theta_2} \quad (3.24)$$

The IKP of the robot leg can be described by Equations 3.10, 3.22 and 3.24. There exist two solutions for θ_3 one for each value of θ_2 . These two sets of solutions correspond to the knee up or knee down configurations show in Figure 3.2.

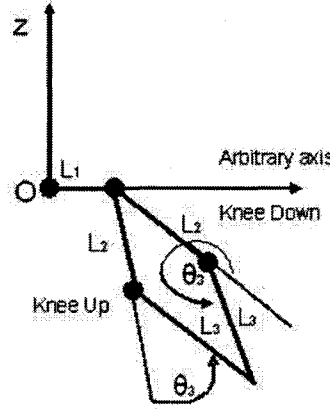


Figure 3.2: Knee up and Knee Down Leg Configurations

For a walking robot the knee down configuration is more desirable. This means that the appropriate selection of θ_3 is the one between π and 2π . The knee up value of θ_3 can be discarded along with the equivalent θ_2 leaving one value of θ_3 and θ_2 .

3.3 Velocity Equations

The velocity equations can be expressed by the following:

$$\dot{p} = J\dot{\theta} \quad (3.25)$$

Where J is the Jacobian matrix. The Jacobian can be found by differentiating the position with respect to θ_1 , θ_2 , and θ_3 .

$$J = \begin{bmatrix} J(1, 1) & J(1, 2) & J(1, 3) \\ J(2, 1) & J(2, 2) & J(2, 3) \\ J(3, 1) & J(3, 2) & J(3, 3) \end{bmatrix} \quad (3.26)$$

Where

$$\begin{aligned} J(1, 1) = \frac{\delta P(1, 1)}{\delta \theta_1} = & (-L_1 \sin(\theta_1 + \theta_b) - \frac{1}{2} L_2 \sin(\theta_1 + \theta_b - \theta_2) \\ & - \frac{1}{2} L_2 \sin(\theta_1 + \theta_b + \theta_2) - \frac{1}{2} L_3 \sin(\theta_1 + \theta_b - \theta_2 - \theta_3) \\ & - \frac{1}{2} L_3 \sin(\theta_1 + \theta_b + \theta_2 + \theta_3)) \end{aligned} \quad (3.27)$$

$$\begin{aligned} J(1, 2) = \frac{\delta P(1, 1)}{\delta \theta_2} = & (\frac{1}{2} L_2 \sin(\theta_1 + \theta_b - \theta_2) - \frac{1}{2} L_2 \sin(\theta_1 + \theta_b + \theta_2) \\ & + \frac{1}{2} L_3 \sin(\theta_1 + \theta_b - \theta_2 - \theta_3) - \frac{1}{2} L_3 \sin(\theta_1 + \theta_b + \theta_2 + \theta_3)) \end{aligned} \quad (3.28)$$

$$J(1, 3) = \frac{\delta P(1, 1)}{\delta \theta_3} = \frac{1}{2} L_3 \sin(\theta_1 + \theta_b - \theta_2 - \theta_3) - \frac{1}{2} L_3 \sin(\theta_1 + \theta_b + \theta_2 + \theta_3) \quad (3.29)$$

$$\begin{aligned} J(2, 1) = \frac{\delta P(2, 1)}{\delta \theta_1} = & (L_1 \cos(\theta_1 + \theta_b) + \frac{1}{2} L_2 \cos(\theta_1 + \theta_b - \theta_2) + \frac{1}{2} L_2 \cos(\theta_1 + \theta_b + \theta_2) \\ & + \frac{1}{2} L_3 \cos(\theta_1 + \theta_b - \theta_2 - \theta_3) + \frac{1}{2} L_3 \cos(\theta_1 + \theta_b + \theta_2 + \theta_3)) \end{aligned} \quad (3.30)$$

$$\begin{aligned} J(2, 2) = \frac{\delta P(2, 1)}{\delta \theta_2} = & (-\frac{1}{2} L_2 \cos(\theta_1 + \theta_b - \theta_2) + \frac{1}{2} L_2 \cos(\theta_1 + \theta_b + \theta_2) \\ & - \frac{1}{2} L_3 \cos(\theta_1 + \theta_b - \theta_2 - \theta_3) + \frac{1}{2} L_3 \cos(\theta_1 + \theta_b + \theta_2 + \theta_3)) \end{aligned} \quad (3.31)$$

$$J(2, 3) = \frac{\delta P(2, 1)}{\delta \theta_3} = -\frac{1}{2} L_3 \cos(\theta_1 + \theta_b - \theta_2 - \theta_3) + \frac{1}{2} L_3 \cos(\theta_1 + \theta_b + \theta_2 + \theta_3) \quad (3.32)$$

$$J(3, 1) = \frac{\delta P(3, 1)}{\delta \theta_1} = 0 \quad (3.33)$$

$$J(3, 2) = \frac{\delta P(3, 1)}{\delta \theta_2} = L_2 \cos \theta_2 + L_3 \cos \theta_3 \cos \theta_2 - L_3 \sin \theta_3 \sin \theta_2 \quad (3.34)$$

$$J(3, 3) = \frac{\delta P(3, 1)}{\delta \theta_3} = L_3 \cos \theta_3 \cos \theta_2 - L_3 \sin \theta_3 \sin \theta_2 \quad (3.35)$$

When the joint positions are known, the Jacobian matrix can be used to change between cartesian velocities and joint velocities. For the purposes of this thesis the

interest lies in the joint velocities. Generally the trajectories are defined in cartesian space. In order to determine the joint velocities, the inverse Jacobian will be used.

3.4 Acceleration Equations

The acceleration equations can be determined by taking the derivative of Equation 3.25. This gives:

$$\ddot{p} = J\ddot{\theta} + \dot{J}\dot{\theta} \quad (3.36)$$

Where \dot{J} is defined by the following equations:

$$\begin{aligned} \dot{J}(1,1) = & (-L_1 \cos(\theta_1 + \theta_b) \dot{\theta}_1 - \frac{1}{2} L_2 \cos(\theta_1 + \theta_b - \theta_2) (\dot{\theta}_1 - \dot{\theta}_2) \\ & - \frac{1}{2} L_2 \cos(\theta_1 + \theta_b + \theta_2) (\dot{\theta}_1 + \dot{\theta}_2) - \frac{1}{2} L_3 \cos(\theta_1 + \theta_b - \theta_2 - \theta_3) (\dot{\theta}_1 - \dot{\theta}_2 - \dot{\theta}_3) \\ & - \frac{1}{2} L_3 \cos(\theta_1 + \theta_b + \theta_2 + \theta_3) (\dot{\theta}_1 + \dot{\theta}_2 + \dot{\theta}_3)) \end{aligned} \quad (3.37)$$

$$\begin{aligned} \dot{J}(1,2) = & (\frac{1}{2} L_2 \cos(\theta_1 + \theta_b - \theta_2) (\dot{\theta}_1 - \dot{\theta}_2) - \frac{1}{2} L_2 \cos(\theta_1 + \theta_b + \theta_2) (\dot{\theta}_1 + \dot{\theta}_2) \\ & + \frac{1}{2} L_3 \cos(\theta_1 + \theta_b - \theta_2 - \theta_3) (\dot{\theta}_1 - \dot{\theta}_2 - \dot{\theta}_3) \\ & - \frac{1}{2} L_3 \cos(\theta_1 + \theta_b + \theta_2 + \theta_3) (\dot{\theta}_1 + \dot{\theta}_2 + \dot{\theta}_3)) \end{aligned} \quad (3.38)$$

$$\dot{J}(1,3) = \frac{1}{2} L_3 \cos(\theta_1 + \theta_b - \theta_2 - \theta_3) (\dot{\theta}_1 - \dot{\theta}_2 - \dot{\theta}_3) - \frac{1}{2} L_3 \cos(\theta_1 + \theta_b + \theta_2 + \theta_3) (\dot{\theta}_1 + \dot{\theta}_2 + \dot{\theta}_3) \quad (3.39)$$

$$\begin{aligned} \dot{J}(2,1) = & (-L_1 \sin(\theta_1 + \theta_b) \dot{\theta}_1 - \frac{1}{2} L_2 \sin(\theta_1 + \theta_b - \theta_2) (\dot{\theta}_1 - \dot{\theta}_2) \\ & - \frac{1}{2} L_2 \sin(\theta_1 + \theta_b + \theta_2) (\dot{\theta}_1 + \dot{\theta}_2) - \frac{1}{2} L_3 \sin(\theta_1 + \theta_b - \theta_2 - \theta_3) (\dot{\theta}_1 - \dot{\theta}_2 - \dot{\theta}_3) \\ & - \frac{1}{2} L_3 \sin(\theta_1 + \theta_b + \theta_2 + \theta_3) (\dot{\theta}_1 + \dot{\theta}_2 + \dot{\theta}_3)) \end{aligned} \quad (3.40)$$

$$\begin{aligned} \dot{J}(2,2) = & (\frac{1}{2} L_2 \sin(\theta_1 + \theta_b - \theta_2) (\dot{\theta}_1 - \dot{\theta}_2) - \frac{1}{2} L_2 \sin(\theta_1 + \theta_b + \theta_2) (\dot{\theta}_1 + \dot{\theta}_2) \\ & + \frac{1}{2} L_3 \sin(\theta_1 + \theta_b - \theta_2 - \theta_3) (\dot{\theta}_1 - \dot{\theta}_2 - \dot{\theta}_3) \\ & - \frac{1}{2} L_3 \sin(\theta_1 + \theta_b + \theta_2 + \theta_3) (\dot{\theta}_1 + \dot{\theta}_2 + \dot{\theta}_3)) \end{aligned} \quad (3.41)$$

$$\dot{J}(2,3) = \frac{1}{2} L_3 \sin(\theta_1 + \theta_b - \theta_2 - \theta_3) (\dot{\theta}_1 - \dot{\theta}_2 - \dot{\theta}_3) - \frac{1}{2} L_3 \sin(\theta_1 + \theta_b + \theta_2 + \theta_3) (\dot{\theta}_1 + \dot{\theta}_2 + \dot{\theta}_3) \quad (3.42)$$

$$\dot{J}(3, 1) = 0 \quad (3.43)$$

$$\dot{J}(3, 2) = -L_2 \sin \theta_2 \dot{\theta}_2 - L_3 \sin(\theta_2 + \theta_3)(\dot{\theta}_2 + \dot{\theta}_3) \quad (3.44)$$

$$J(3, 3) = -L_3 \sin(\theta_2 + \theta_3)(\dot{\theta}_2 + \dot{\theta}_3) \quad (3.45)$$

Knowing the joint positions and velocities, Equation 3.36 can be used to determine either the cartesian or the joint accelerations. As in the case of the velocity equations, Equations 3.27-3.35, the main interest is the joint accelerations that can be used with the dynamic equations, Appendix A, to determine torque requirements for the actuators. Using the inverse kinematic equations, the velocity equations and the acceleration equations, the trajectory planner can calculate the required joint variables.

3.5 Singularity Analysis

For serial manipulators, singularities occur when the determinant of the Jacobian is equal to zero. When this occurs, it is not possible to generate certain end effector velocities. The determinant of Equation 3.26 is shown in Equation 3.46.

$$\det(J) = -L_2 L_3 \sin \theta_3 (L_1 + L_2 \cos \theta_2 + L_3 \cos \theta_2 \cos \theta_3 - L_3 \sin \theta_2 \sin \theta_3) \quad (3.46)$$

Singularities therefore occur when θ_3 is equal to 0 or π . These configurations are represented in Figure 3.3.

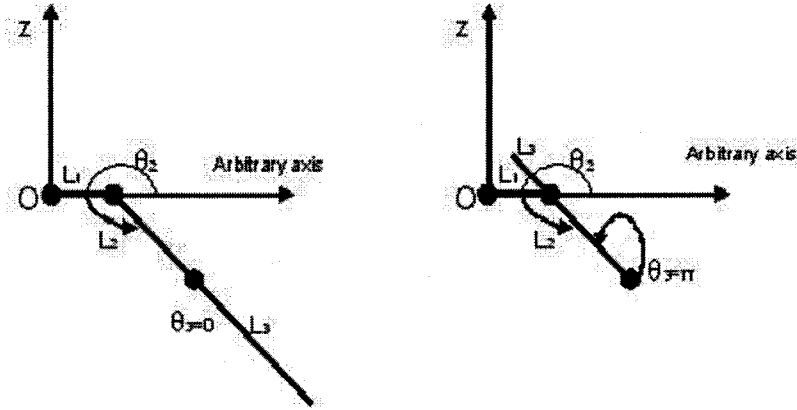


Figure 3.3: Singular Configurations

In these configurations, velocities cannot be produced by the foot in a direction parallel to links two and three. Singularities will also occur whenever $L_1 + L_2\cos\theta_2 + L_3\cos\theta_2\cos\theta_3 - L_3\sin\theta_2\sin\theta_3$ is equal to zero.

3.6 The Leg Workspace

The mechanism's workspace can be defined as the region in which the mechanism can operate. Generally, the workspace boundaries correspond to the mechanism's singular positions. For each leg, joint one rotates about the origin's z axis and joint two and three rotate about the origin's y axis. The workspace is shown in Figure 3.4 and is shaded in grey. Certain quadrants are not accessible to the end effector because the body acts as a physical constraint.

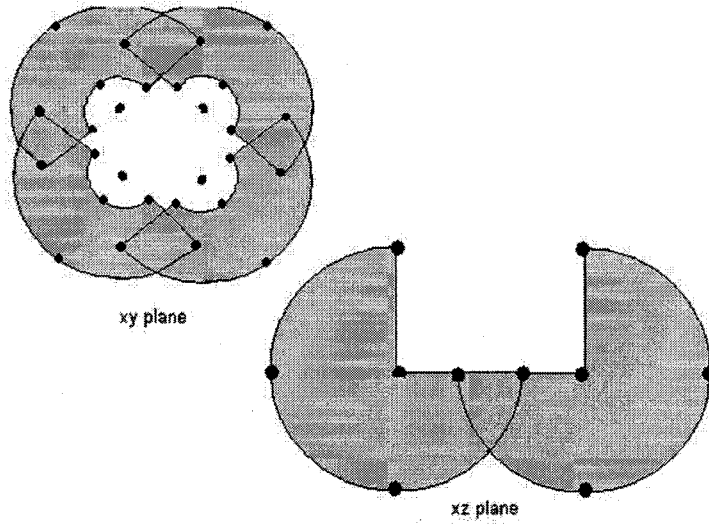


Figure 3.4: View of Leg Workspace

From Figure 3.4, it can be seen that these workspaces of the legs overlap. This means that there are certain configurations of the robot where the legs may interfere with one another. This must be taken into account when planning the gait to ensure that there is no interference.

If the desired Cartesian position of a leg is outside its reach, without considering the imposed physical constraints discussed above, the solution to the IKP will

involve imaginary numbers. If real solutions to the IKP exist, they must then be compared with the imposed physical constraints to determine if the position is within the workspace. The trajectory planner only produces valid joint variables with positions that are within the workspace.

Chapter 4

Selection of Appropriate Gaits

This chapter begins with an introduction to the concept of gaits. First some basic terminology is explained, then a description of many different types of gaits and their classifications is given. Lastly, the gaits that were selected to achieve the aim of this thesis are described in detail. The selected gaits act as a skeleton providing a plan of foot and body positions to be joined together, using appropriate trajectories, to be used by the trajectory planner to create the required joint variables to allow a robot to follow a desired path.

4.1 Background

4.1.1 Gait Terminology

In order to properly discuss gaits there are several important terms used to describe a gait that must first be explained.

- Gait: this word is used to describe a series of leg and body movements used by a legged system in order to move from point A to point B [10].
- Leg stroke, R: The distance the leg travels relative to the CoG during the body movement phase. This value also represents the distance traveled by the CoG when the body is being moved forward. The leg stroke must be within the limits of the leg workspace which is defined by R_x and R_y [22], Figure 4.7.
- Stroke Pitch, P: Used to describe the difference between the centre of the workspaces of adjacent legs. The stroke pitch is defined in terms of distances in x and y directions: P_x and P_y [22], Figure 4.7.
- Stride Length, λ : The distance traveled by the CoG during one locomotion cycle [14], Figure 4.7.

- Duty factor, β : The fraction of the locomotion cycle that a leg is on the ground [14].
- Gait diagram: Used to illustrate the gait. When a leg is in support phase, it is represented by a line. When all the legs are in support phase, a body movement phase is carried out. An example of a gait diagram for a quadruped gait with a β of $5/6$ is shown in Figure 4.1.

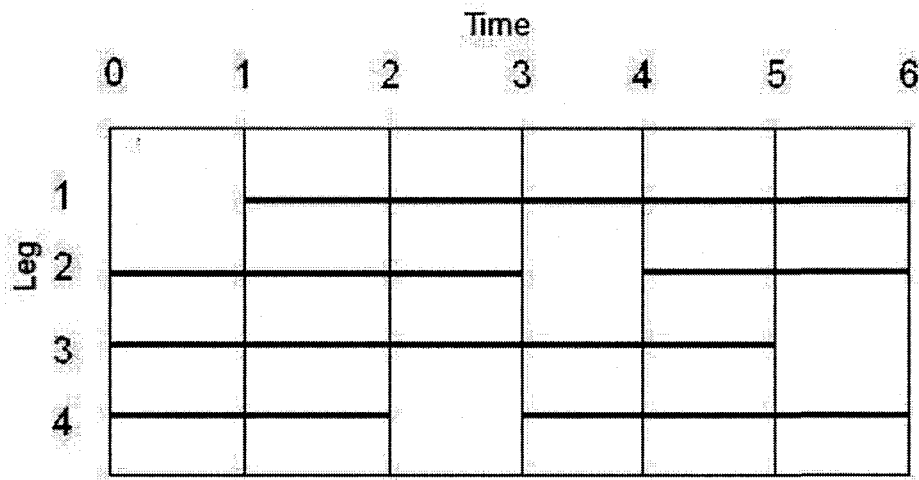


Figure 4.1: Gait Diagram

The numbers that run along the top of the diagram represent increments of time. Those that are along the side of the diagram represent the different legs. Different leg numbering strategies are used, but for this thesis, legs will be numbered from the front of the robot and from left to right. For example leg one would be the forward leg on the left, leg two the first leg on the right. The number is done with respect to the CoG's y axis. All the legs on the left hand side are odd.

4.1.2 Gaits in General

The study of gaits began as early as 1899 when Muybridge studied the locomotion of different animals using photographs [4]. Since then, a wide variety of different gaits have been discovered and studied. Different gaits are appropriate for different

applications and environments. The selection of an appropriate gait can depend on the task at hand, stability and velocity requirements, and the type of terrain that is to be traversed. In general gaits can be sub-divided into two different categories: non periodic gaits and periodic gaits.

In a non periodic gait, footholds and motion sequences are selected on-line based on the terrain. Non periodic gaits are the more flexible of the gaits and therefore suitable for locomotion on rough and difficult terrain where a repetitive cycle of movements cannot be determined. Non periodic gaits are also useful in situations where unknown obstacles need to be avoided or traversed [22].

Different non periodic gaits include free gaits and follow the leader gaits [14]. In free gaits, leg and body motion is determined by rule based or search based methods. They have proved very successful with hexapod robots. They are, however, more susceptible to deadlock situations than periodic gaits. This is even more so when discussing free gaits for quadruped robots due to the fewer numbers of options for leg movements [22]. Follow the leader gaits place the feet in a previous foothold during locomotion which assures that the foothold is suitable. In general non periodic gaits are also more difficult to implement than periodic gaits, but they are the only option on rough and uneven terrain [14].

According to Song, in a periodic gait, “similar states of the same leg during successive strokes occur at the same interval for all legs, that interval being the cycle of time” [14]. Essentially, if there is not an established pattern of leg and body movements that is repeated at a regular interval, then the gait is not periodic.

Muybridge identified eight different periodic gaits used by quadrupeds during locomotion. These gaits include: the walk, the amble, the trot, the pace, the canter, the transverse gallop, the rotary gallop and the ricochet. During the walk, only one leg is lifted at a time. The walk is the slowest form of locomotion. For a continuous walking gait, β is equal to $3/4$. The amble is faster than the walk. No more than two legs are in contact with the ground at one time during the amble. During the trot, shown in Figure 4.2, the body is supported by diagonal legs and the body is unsupported at certain points in the gait. For a continuous trot gait, β is equal to

1/2. The pace is similar to the trot, with the same duty factor, but the legs that are

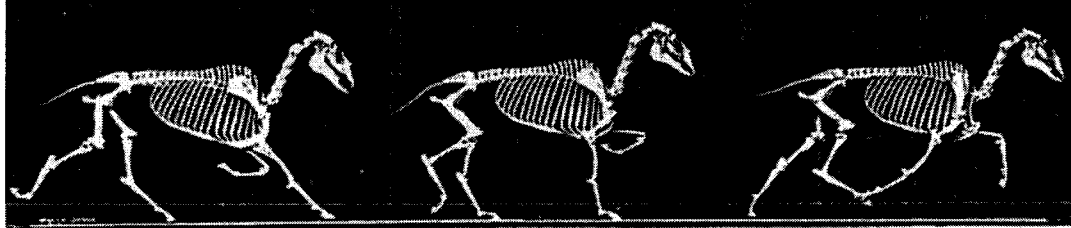


Figure 4.2: The Quadruped Trot Gait [4]

in support stance are lateral as opposed to diagonal. The canter has the same footfall movement as the walk, but it does not have the same regularity of intervals. For a continuous rotating galloping gait, β is equal to 5/16. The gallop, shown in Figure 4.3, is the fastest of the quadruped gaits. The rotary or transverse prefix describes

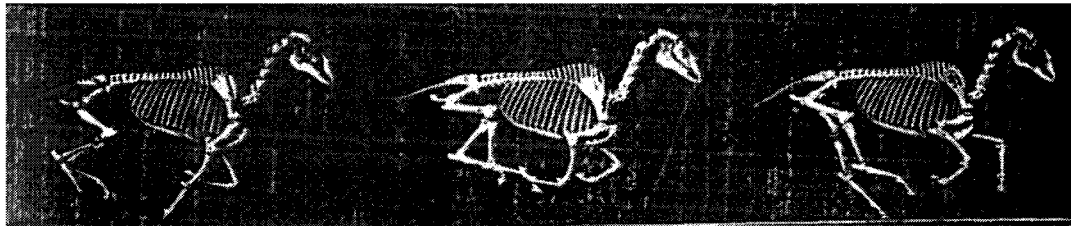


Figure 4.3: The Quadruped Gallop [4]

the foot fall sequence in that gait. The ricochet is a skipping or bounding action like that seen in a kangaroo [4].

Periodic gaits work very well for smooth terrain and also can work in fair terrain. Before continuing further into periodic gaits, it is important to be aware of two further subcategories of gaits. Locomotion gaits can be classified further into continuous or discontinuous gaits, these subcategories can be applied to both periodic and non periodic gaits [22].

In continuous gaits, the body travels at a constant speed with respect to the terrain [14], the body is always in motion. Conversely, discontinuous gaits refer to gaits where body and leg motion occur separately. Continuous gaits can be faster than discontinuous gaits, but this is not always the case [64]. Continuous gaits also generally have higher power consumption than discontinuous gaits and are more difficult to

implement [14]. Because a discontinuous gait moves the legs and body separately, these types of gaits offer more stability.

The main categories of continuous periodic gaits are wave gaits, backwards phase gaits, and equal phase gaits. Of these gaits, it is to be noted that wave gaits provide an optimum stability margin. The wave gait has been observed in insects and also in animals and is defined as a periodic, regular, symmetric and constant phase incremented gait [14].

Wave gaits are characterized by their stepping sequence. The rear leg on a side is placed first, followed by the placement of the leg in front like a wave. When this is reversed the gait becomes a backward wave gait. The crawl gait is another continuous gait which is essentially a wave gait specific to a quadruped robot. Figure 4.4 shows an example of a gait diagram for a hexapod wave gait.

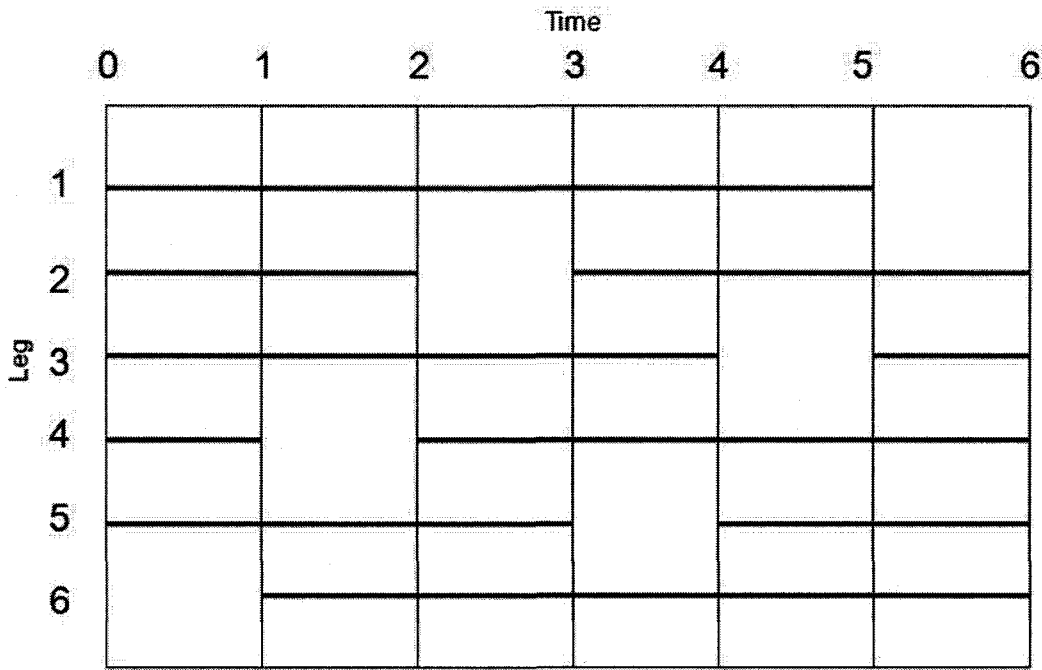


Figure 4.4: Hexapod Wave Gait

Equal phase gaits are used in situations where even power consumption is a vital concern. Equal phase gaits have the same stepping sequence as wave gaits, but they equally distribute the leg motion during the locomotion cycle in order to decrease

power consumption fluctuations [14]. Figure 4.4 is also an example of an equal phase gait.

Different gaits can be implemented in discontinuous and continuous forms. Such gaits include tripod gaits, creeping gaits and crab gaits. Tripod gaits are mainly used by hexapod robots and can be compared to the quadruped trot gait. In a tripod gait, the legs move in two groups of three, where one of the legs is on the other side of the body. An example of a hexapod tripod gait is shown in Figure 4.5.

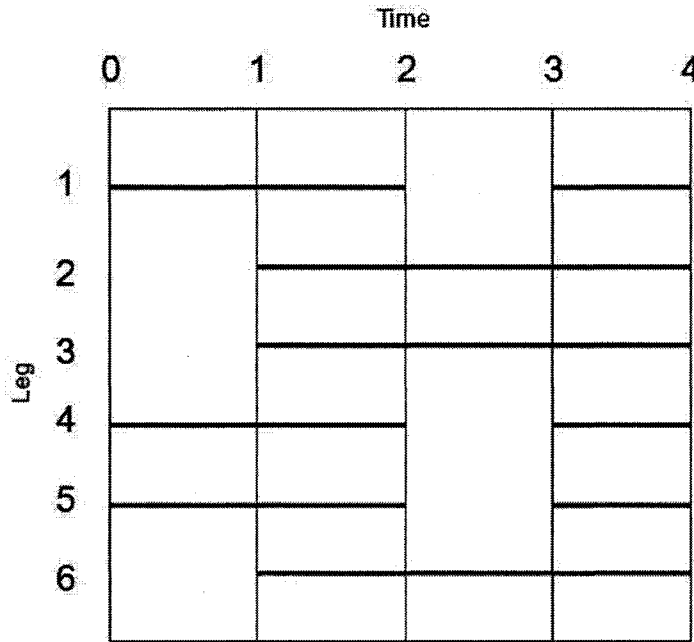


Figure 4.5: Hexapod Tripod Gait

A creeping gait, which can also be referred to as a walk, refers to a gait where at most one leg is lifted at a time. To achieve static stability a quadruped robot must use a form of creeping gait. According to McGhee, there are a total of six different creeping gaits for quadruped locomotion. Each of these gaits has a different order of leg placement: 1-2-3-4, 1-2-4-3, 1-3-2-4, 1-3-4-2, 1-4-2-3 and 1-4-3-2. Of the six gaits discussed by McGhee, only three are stable, 1-4-2-3, 1-2-4-3, 1-3-4-2, and only one of these, 1-4-2-3, has been observed in nature [18].

The above described gaits allow for motion that is more or less confined along the axis of the body. Crab gaits are gaits where the direction of locomotion is at a

crab angle, α , to the forward axis of the body [64]. In these gaits the body is not re-oriented and the body is moved along a straight line at the crab angle. This means that the robot can move to a point that is not along one of the main axes. Large crab angles, however, are not feasible due to stability constraints. The limits of the crab angle are defined by Equations 4.1 and 4.2. These equations were developed in [64] using the definition of the longitudinal stability margin.

$$\alpha_{max} = \cot^{-1} \left(\frac{P_x R_y + P_y R_x}{P_x R_x} \right) \quad (4.1)$$

$$\alpha_{min} = \cot^{-1} \left(\frac{-2P_y R_x + R_y R_x - 2P_x R_y}{2P_x R_x} \right) \quad (4.2)$$

Depending on the robot and its configuration, the crab angle may be quite small. When considering the SILO 4 robot, the crab angle usually falls between $\pm 30^\circ$. Therefore, in order to follow widely varying trajectories or to re-orient the body a different type of gait is required.

In order to solve this problem, a turning gait is introduced. Different gaits can be used with different turning gaits in order to reach all necessary points in a trajectory. There exist two main types of turning gaits, circling gaits and spinning gaits. The main difference between the two is the centre of rotation [65]. Circling gaits move the body on a circular path about a fixed point which corresponds to the centre of a circle that lies on the trajectory. This means that using a circling gait, a robot can change its orientation while continuing to follow the trajectory. Circling gaits become more unstable as the radius of the circle decreases [64]. Unlike circling gaits, spinning gaits rotate about a robot's CoG. With a spinning gait, no progress is made along the trajectory.

4.2 A Description of the Selected Gaits

Two main types of gaits were chosen to be used by trajectory planner in order to create a plan to allow a robot to follow different two dimensional paths. One gait provides trajectory planning for straight line paths along the robot's forward y axis. The other gait allows trajectory planning for re-orientation of the forward axis. The

gaits were selected with simplicity of implementation and stability in mind. It is clear that in order to create a statically stable trajectory plan, a creeping gait was required. The optimal creeping gait described by McGhee was selected. It was also decided to use a discontinuous gait as this increased static stability. The sequence for the selected gait, which is a version of McGhee's optimal quadruped gait, is 4-2-B-3-1-B, where B represents a body movement.

The spinning gait was selected over the circling gait because of the restrictions on the circling gait that depend on the turning radius. A spinning gait also means that the planned trajectory can be simpler than if a circling gait was used in conjunction with the creeping gait. This is because the planned trajectory would be a combination of straight lines joining the given waypoints.

4.2.1 A Two Phase Discontinuous Creeping Gait

In order to maintain stability and simplicity, periodic, discontinuous, quadruped creeping gaits will be used for this thesis. Four different creeping gaits will be developed each referring to a different direction along the main axes. The different creeping gaits will be defined by the direction in which they travel, along the $+x$, $-x$, $+y$ or $-y$ axis. The creeping gaits will all have the same basic structure and are broken down into two phases. The chosen gait, 4-2-B-3-1-B, has two support phases, when the body is propelled forward. Because each time the body is moved forward it moves a distance R , λ is equal to $2R$. It was decided that in this gait the body should be moved more slowly than the legs. This is because lower velocities would be desired in order to prevent a leg lifting from the ground when all the joints would be actuated. The time it takes to complete each leg transfer phase, t_l , represents one unit of time and a body movement represents two units of time. The reason for using a normalized time is because the speed at which a robot performs will be determined by its physical characteristics, such as its actuators. The selected creeping gait has a β of $7/8$. A gait diagram for the selected creeping gait is shown in Figure 4.6.

In order to determine the distance that the CoG moves forward during a body movement phase, R , the workspace of the legs must first be determined. This has

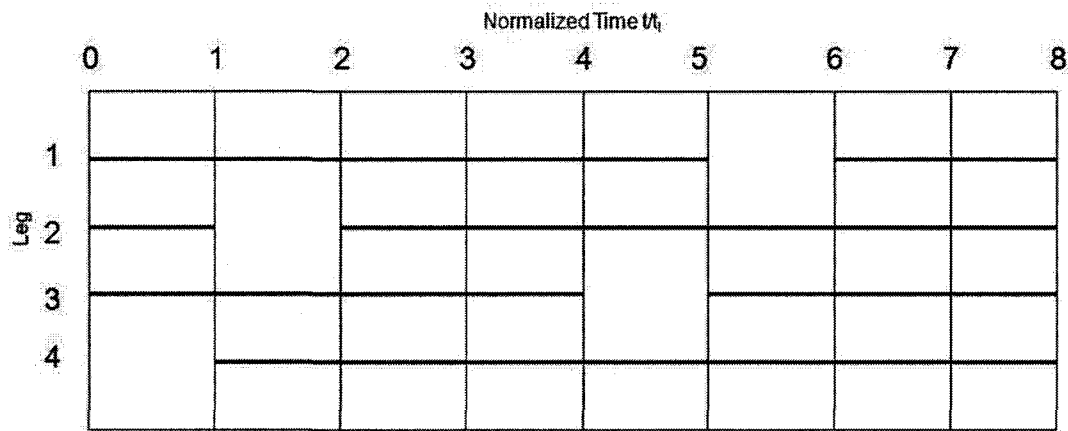


Figure 4.6: Discontinuous Creeping Gait Gait, $\beta = 7/8$

been done previously in the section on Kinematics. However, the previously defined workspace did not take into account the fact that in order to have the body lifted off the ground and the legs in contact with the ground, a minimum height of 0.15 m is required for the CoG. The physical maximum for the height of the CoG occurs at 0.63 m, when links two and three are aligned and vertical. The minimum and maximum values were determined using the value in Table 2.1.

In order to simplify the determination of the footholds for this gait, a simplified workspace in the form of a square is defined. The square is within the circular section that defines the workspace. Using a simplified workspace also ensures that the legs do not interfere with each other during the gait.

The simplified workspace can be found once a desired height of travel is selected for the plan. Geometry can be used to determine possible joint variables for θ_2 and θ_3 that would place the CoG at the desired height. These joint variables can then be inputted, with a value of θ_1 equal to zero, into the DPK to give a position of the foot at the required height. The values determined by the DPK now become the maximum x and y limits of the simplified workspace. The minimum x and y values are the position of the hips. The simplified workspace is defined by a square from the hip of the leg to the outstretched foot. This is illustrated below in Figure 4.7.

In order to plan for movement along a given direction, the chosen positions of the legs with respect to the body must change only along that direction. Three differ-

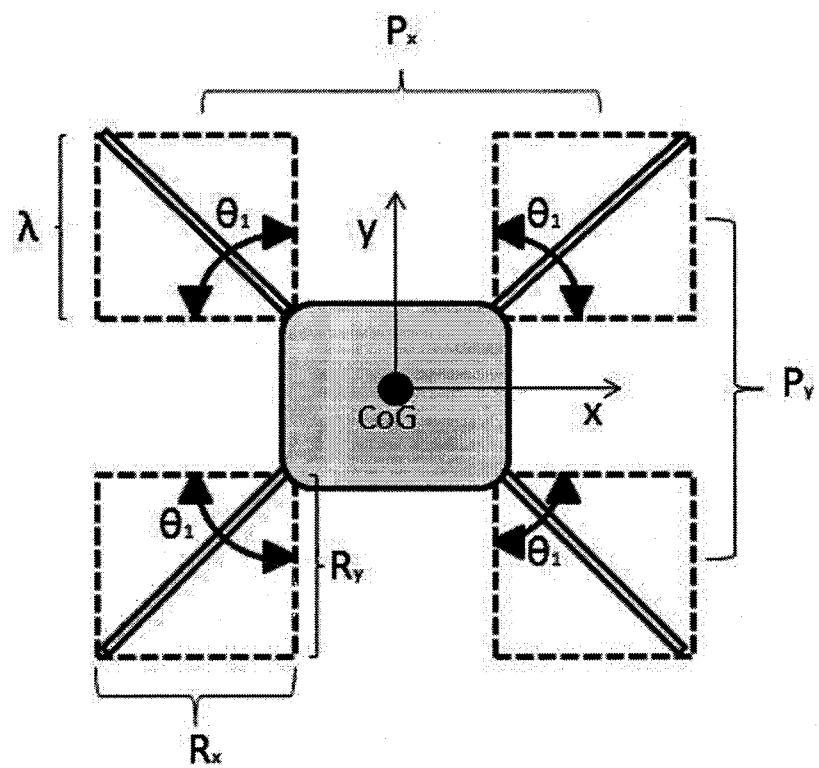


Figure 4.7: Redefined Workspace

ent footholds are determined using the limits of the workspace [22]. For movement along the positive y direction, the first foothold corresponds to $(y_{max}, x_{max}/2)$, the second foothold corresponds to $(y_{max}/2, x_{max}/2)$ and the third foothold equates to $(y_{min}, x_{max}/2)$. λ is equal to the distance between y_{max} and y_{min} . For the possible directions of travel these positions are illustrated in Figure 4.8.

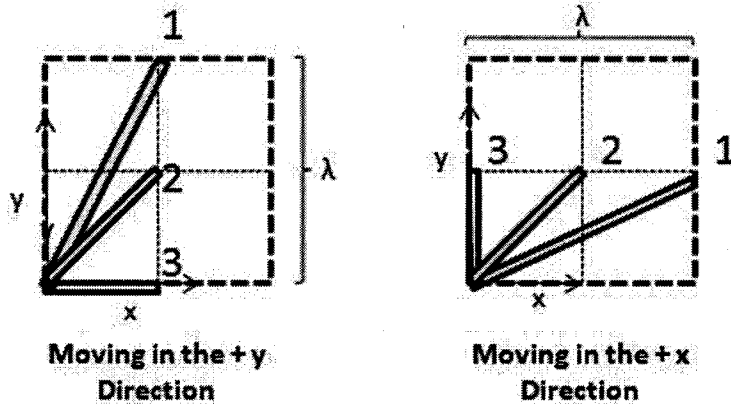


Figure 4.8: Foothold Positions

The trajectory planner will create a plan that will place the legs from positions one to positions three. The stride length is therefore equal to the difference between the minimum and maximum values of the workspace. A plan of different leg and body positions to allow one locomotion cycle to be carried out for the positive y creeping gait can now be described as follows:

1. Leg four is moved to the limit of its workspace, position 3.
2. Leg two is moved to the limit of its workspace, position 1.
3. The body is moved a distance R along the positive y direction.
4. Leg three is moved to the limit of its workspace, position 3.
5. Leg one is moved to the limit of its workspace, position 1.
6. The body is moved a distance R along the positive y direction.

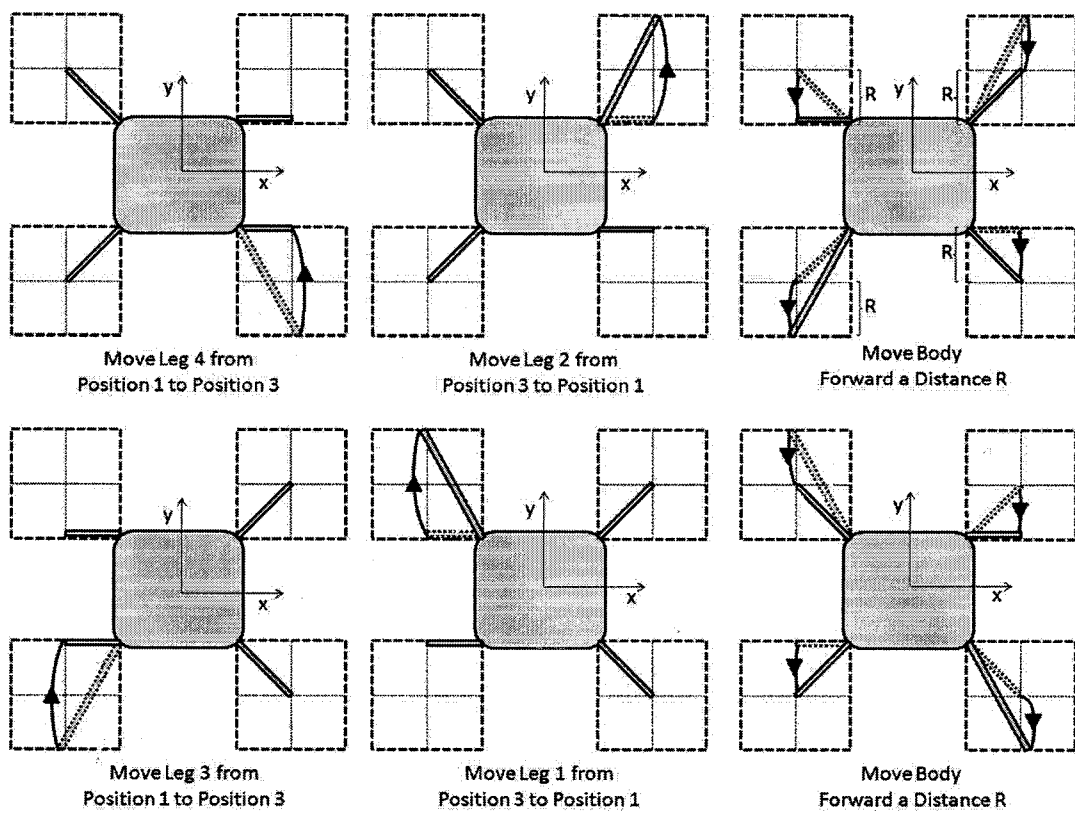


Figure 4.9: Gait Sequence for the Positive y Direction

This cycle is repeated until the desired position is reached, illustrated in Figure 4.9.

In order to allow for movement in the negative y direction the same gait is applied but as if the robot had been rotated 180° meaning that leg one now becomes leg four etc. The sequence is as follows:

1. Leg one is moved to the limit of its workspace, position 3.
2. Leg three is moved to the limit of its workspace, position 1.
3. The body is moved a distance R along the negative y direction.
4. Leg two is moved to the limit of its workspace, position 3.
5. Leg four is moved to the limit of its workspace, position 1.
6. The body is moved a distance R along the negative y direction.

In order to move in the positive x direction the same gait is also applied, but as if the robot had been rotated -90° meaning that leg two now becomes leg one etc. The sequence is as follows:

1. Leg three is moved to the limit of its workspace, position 3.
2. Leg four is moved to the limit of its workspace, position 1.
3. The body is moved a distance R along the positive x direction.
4. Leg one is moved to the limit of its workspace, position 3.
5. Leg two is moved to the limit of its workspace, position 1.
6. The body is moved a distance R along the positive x direction.

In order to allow for movement in the negative x direction the same gait is also applied, but as if the robot had been rotated 90° meaning that leg three now becomes leg one etc. The sequence is as follows:

1. Leg two is moved to the limit of its workspace, position 3.

2. Leg one is moved to the limit of its workspace, position 1.
3. The body is moved a distance R along the negative x direction.
4. Leg four is moved to the limit of its workspace, position 3.
5. Leg three is moved to the limit of its workspace, position 1.
6. The body is moved a distance R along the negative x direction.

In order to get an idea of the joint variables required to produce one locomotion cycle, a mid-range height for the CoG was selected, 0.39 m. This means that the hip would be situated at 0.24 m as the distance from the CoG to the hip is -0.15 m. This height is therefore equal to the length of link 3 meaning that one possible joint configuration would be $\theta_1 = 0$, $\theta_2 = 0$, and $\theta_3 = -\pi/2$. Inputting these joint positions into the DKP values of 0.3726 m for x_{max} and y_{max} can be obtained. y_{min} is a fixed value of 0.155 m. λ is the difference between y_{max} and y_{min} and becomes 0.2176 m. The trajectory planner was used to create a plan in order to complete one gait cycle, a total of 8 units of time. The joint positions for one cycle are shown in Figure 4.10.

From Figure 4.10, the planned support phase and transfer phases of the legs can be seen. The planned body movement is characterized by movement of the joints in more than one leg at once. Body movement is planned to occur between the normalized times 2-4 and 6-8. During these times very little change occurs in θ_2 or θ_3 which makes sense as the height does not change. The Figure also shows the planned pattern of leg movement: leg four followed by leg two. After a change in the body position, leg three and leg one should be transferred. All the joint positions are within the joint limits. The joint velocities are shown in Figure 4.11 and the joint accelerations are shown in Figure 4.12

The same information obtained from Figure 4.10 can be obtained from Figures 4.11 and 4.12. Figure 4.11 also shows a much higher velocity would occur during the transfer phase of a leg. The difference in the velocities is to be expected as the legs complete their trajectory in half the time than the body.

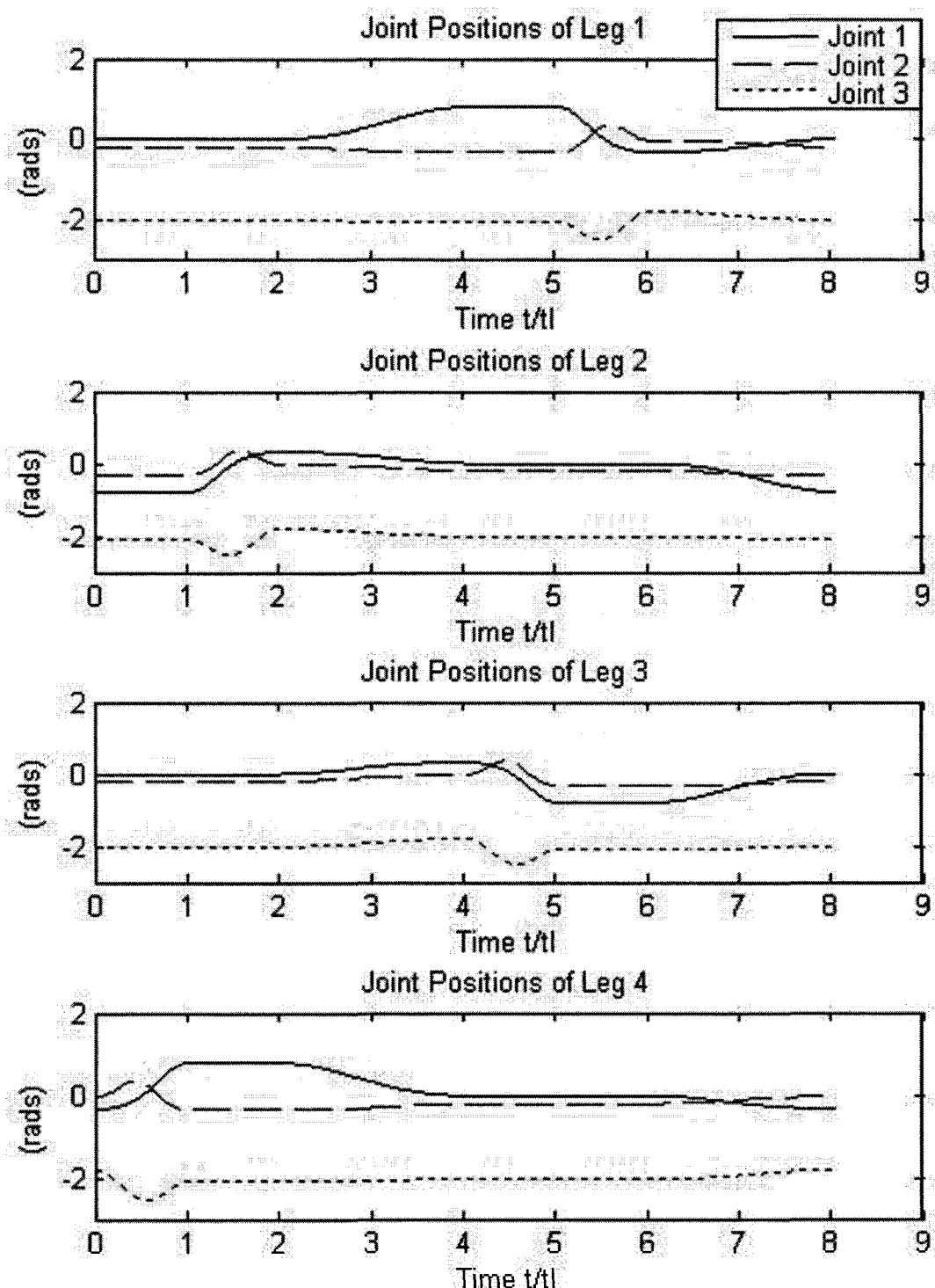


Figure 4.10: Joint Positions for one Creeping Gait Cycle

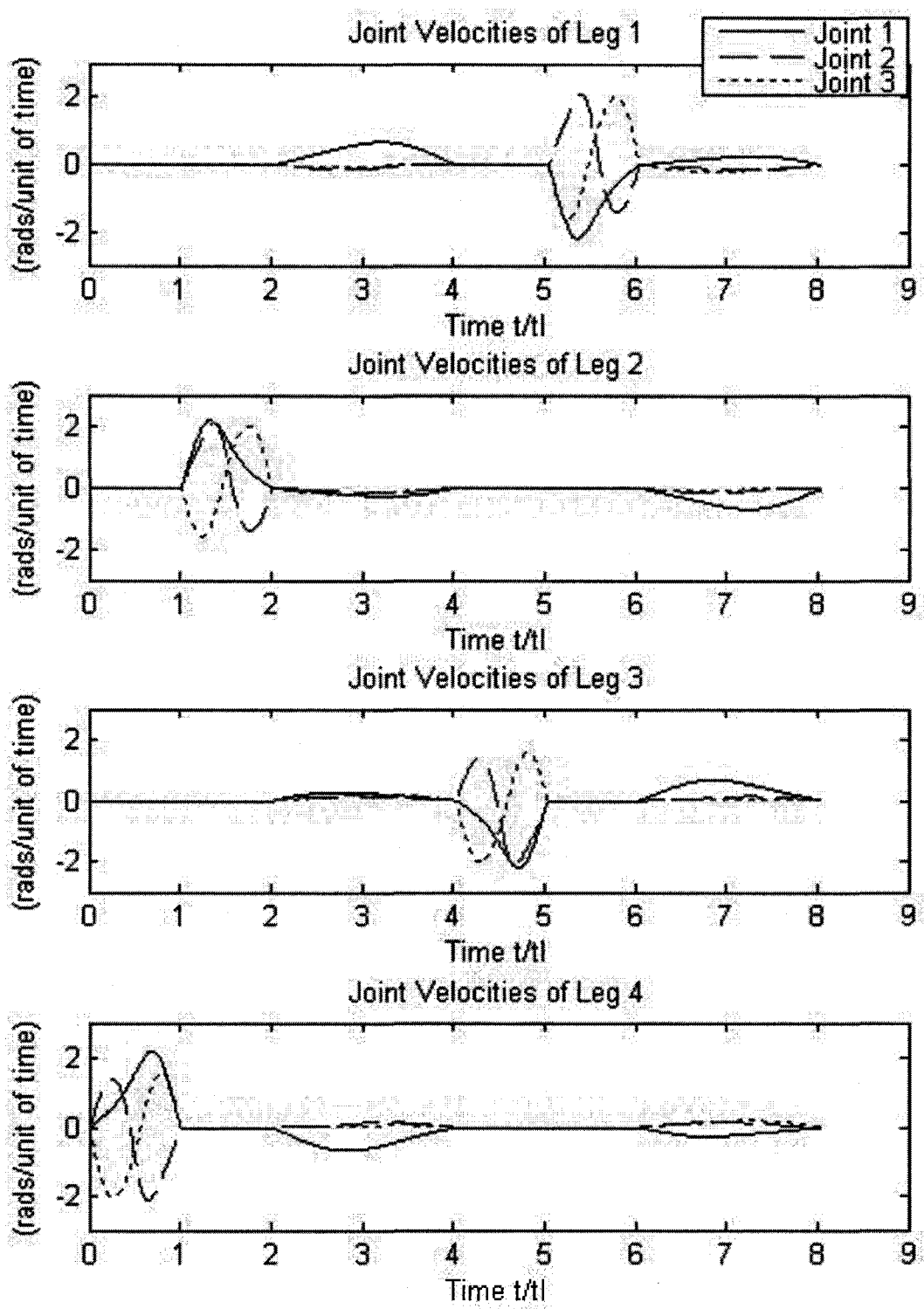


Figure 4.11: Joint Velocities for one Creeping Gait Cycle

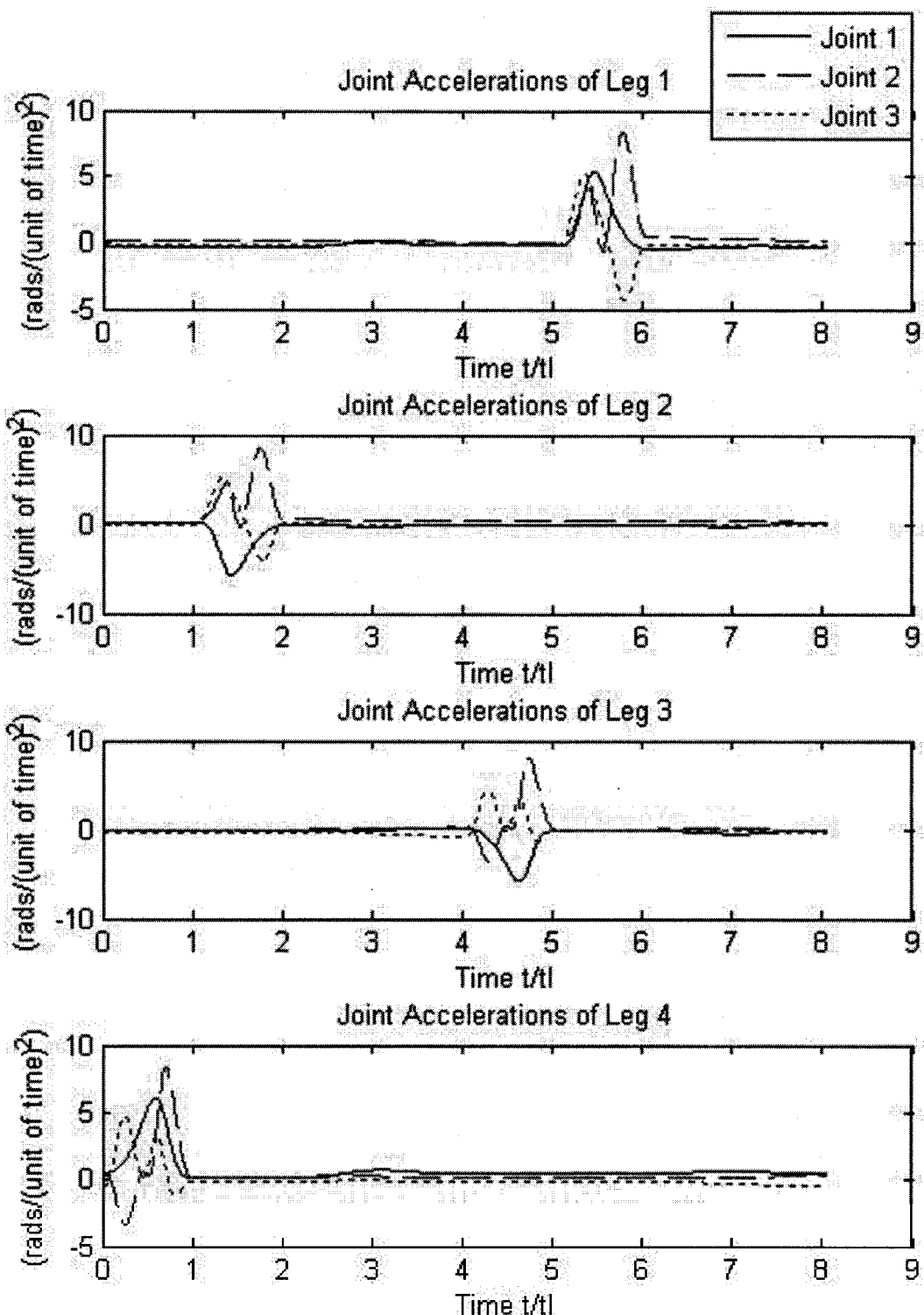


Figure 4.12: Joint Accelerations for one Creeping Gait Cycle

4.2.2 A Discontinuous Spinning Gait

In order to plan for re-orientation, a spinning gait was chosen. In the spinning gait, all the legs change their positions, followed by a change of orientation of the body. At first, it was attempted to plan a spinning gait that would begin in the same configuration as in the creeping gait, for ease of transition between the two gaits as they would both begin with the same leg and body positions. The starting configuration for the spinning gait had to be changed however, because using the same start configuration as the creeping gait it became difficult to provide joint variables that would allow for static stability. A planned transition is required to join the plan from the creeping gait to that of the spinning gait. The start position for this gait has all legs in position two, where θ_1 is equal to zero. The planned transition requires a change of position of legs 4 and 2. Therefore, the transition takes two units of time to complete. One cycle of the spinning gait, can provide a plan to turn a robot up to an angle ψ of $\pi/2$ rads. ψ is defined in the counterclockwise direction from the forward y axis of the CoG. If the required angle is greater than $\pi/2$, than the trajectory planner will plan for several cycles of the spinning gait to be joined together. The limitations on ψ are due to physical restrictions of the robot and the start positions of the gait.

Unlike the creeping gait, there are no set footholds for the leg. The required positions for placement of the feet depend on the angle that the CoG is planned to be moved. When that angle is determined, the hip vector is subtracted from the actual position of the legs with respect in the CoG reference frame and this is multiplied by the following rotation matrix:

$$Q_\psi = \begin{bmatrix} \cos\psi & -\sin\psi & 0 \\ \sin\psi & \cos\psi & 0 \\ 0 & 0 & 1 \end{bmatrix} \quad (4.3)$$

This gives the new leg positions. These new positions must then be changed back into the CoG reference frame by adding the relevant vector previously subtracted. The vectors for each hip are shown in Equations 4.4 to 4.7 and were determined using the values from Table 2.1:

$$Hip_1 = \begin{bmatrix} -0.155 \\ 0.155 \\ -0.15 \end{bmatrix} \quad (4.4)$$

$$Hip_2 = \begin{bmatrix} 0.155 \\ 0.155 \\ -0.15 \end{bmatrix} \quad (4.5)$$

$$Hip_3 = \begin{bmatrix} -0.155 \\ -0.155 \\ -0.15 \end{bmatrix} \quad (4.6)$$

$$Hip_4 = \begin{bmatrix} 0.155 \\ -0.155 \\ -0.15 \end{bmatrix} \quad (4.7)$$

The spinning gait dictates that each leg's position is moved to the new position one at a time. The order that the legs are to change positions is determined by a comparison of the possible leg movement sequences. When a stable leg movement sequence is found, it is adopted for the gait cycle. Once the legs have been placed the body is rotated so that the legs are in the same position that they were in at the beginning of the gait. One cycle of the spinning gait takes 6 units of time. The duty cycle for this gait is 5/6. The gait diagram is shown in Figure 4.13.

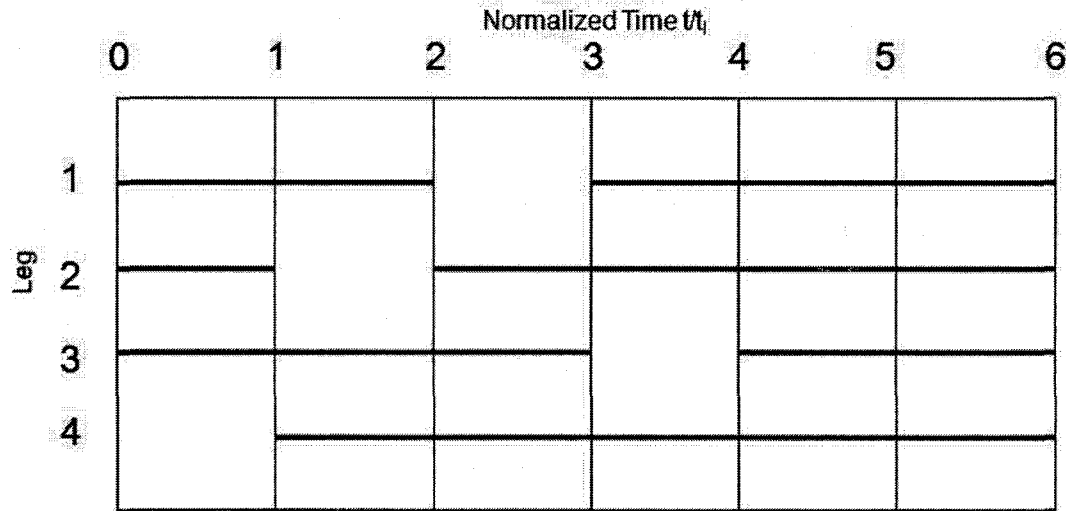


Figure 4.13: Discontinuous Spinning Gait Gait, $\beta = 5/6$

Once the spinning cycle is complete, another planned transition must occur to place the legs into the start position for the creeping gait. Again the transition takes two units of time and involves a change of position of legs 2 and 4.

Using the same selected height that was used in the trajectory planner with the creeping gait, 0.39 m, the trajectory planner was used to provide the joint variables

required for one gait cycle with the two planned gait transitions on either side of the gait. The angle ψ was set at $\pi/3$. The joint positions for one cycle are shown in Figure 4.14. As with the creeping gait, θ_1 undergoes the biggest change in position, which is expected. The leg transfer and body movement phases can clearly be seen in the figure where movement occurs in all four legs at the same time.

All the joints, also remain within the joint limits. The joint velocities and accelerations are shown in Figures 4.15 and 4.16. In the figures, the leg transfer phases are even more clearly identifiable. In the spinning gait, the legs would travel at higher velocities as they would be traveling a larger distance. Depending on ψ , this might not always be the case. The velocity of the joints when the legs would be lifted is much greater than the velocity of the joints when the body would be moved as a smaller distance is travelled over a larger period of time.

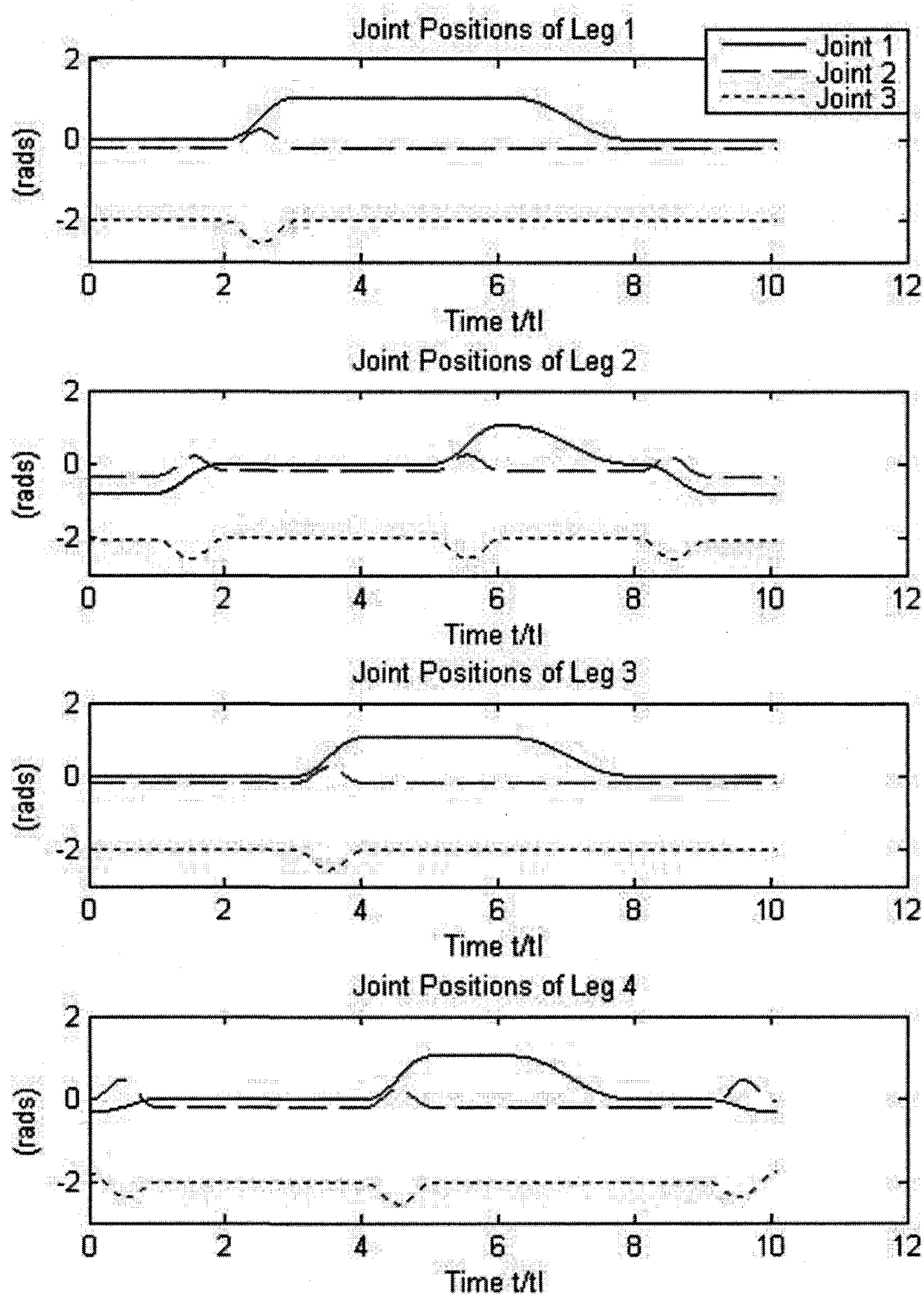


Figure 4.14: Joint Positions for one Spinning Gait Cycle, $\psi = \pi/3$

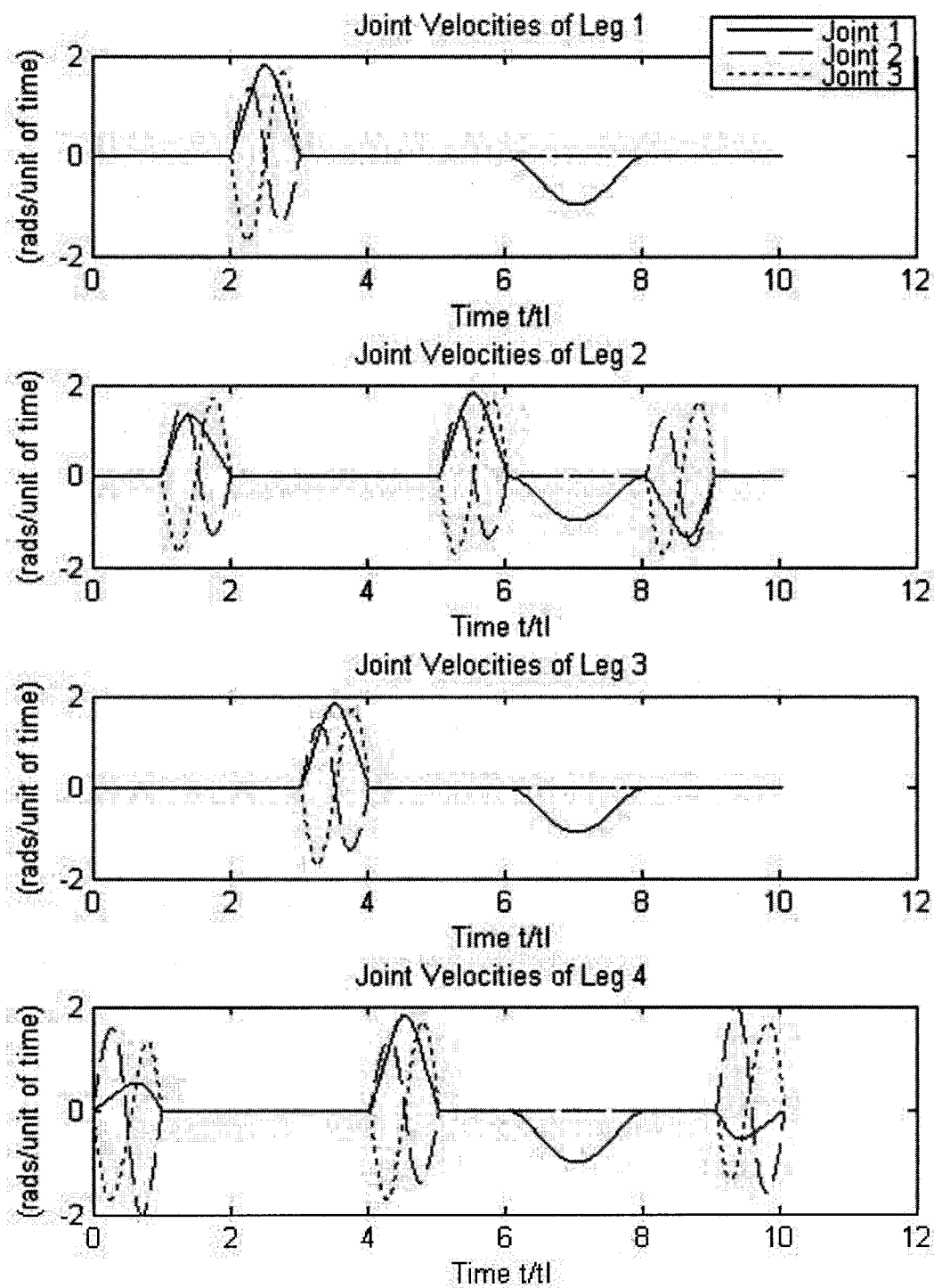


Figure 4.15: Joint Velocities for one Spinning Gait Cycle, $\psi = \pi/3$

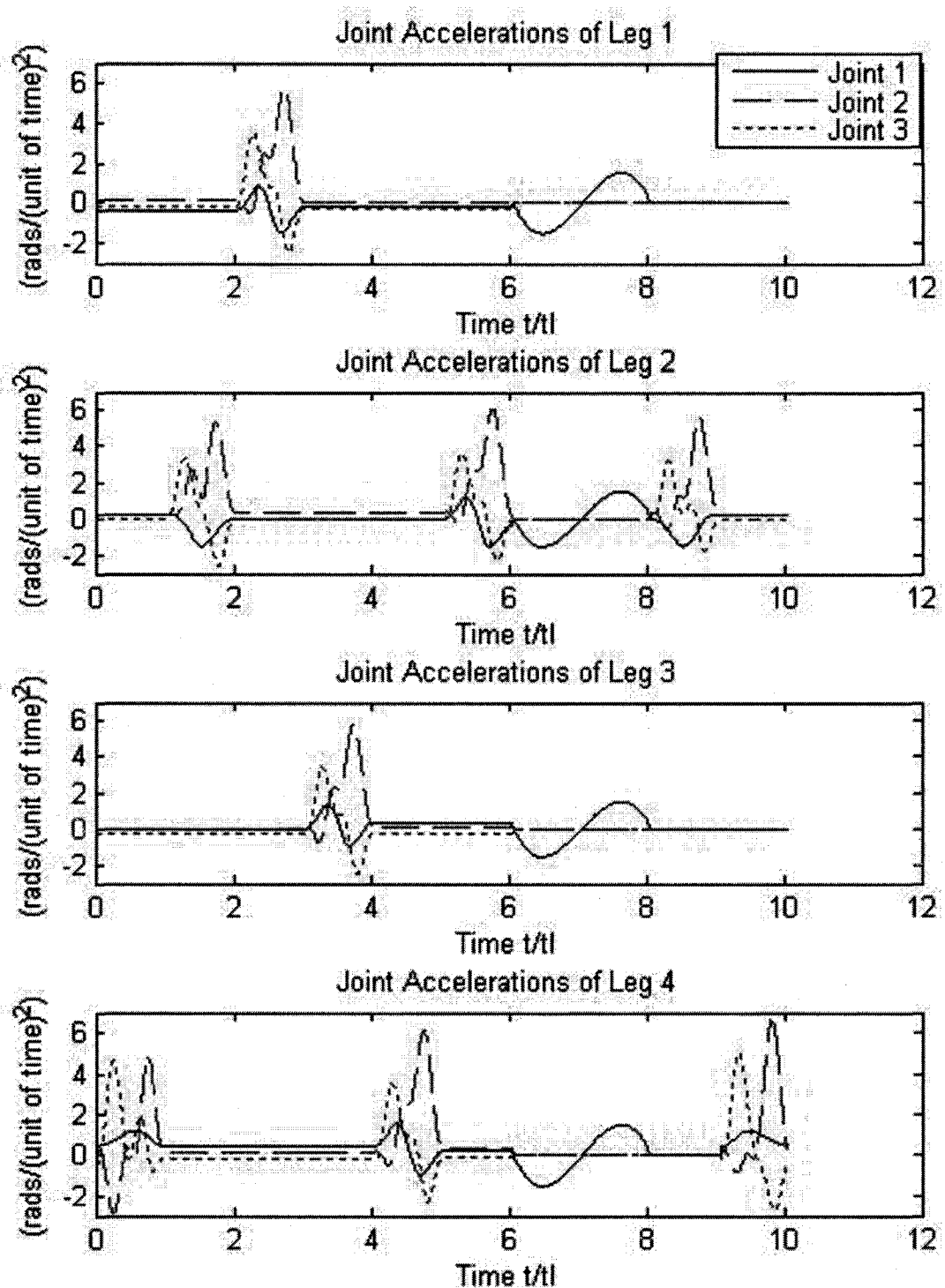


Figure 4.16: Joint Accelerations for one Spinning Gait Cycle, $\psi = \pi/3$

Chapter 5

Trajectory Planning for a Quadruped Robot

The aim of this thesis involved the design of a trajectory planning method for a quadruped robot. Much of the theory used by the trajectory planner to create a plan of joint variables to allow a quadruped to follow a given path was discussed in Chapters 3 and 4. In this chapter the application of the remaining theory used is explained. This remaining theory includes the implementation of a static stability margin, the definition of the leg and body trajectories used, and the different reference frames that are used by the trajectory planner. Finally, the process followed by the trajectory planning program that was created in order to achieve the aim of this thesis is detailed in this chapter.

5.1 Maintaining Static Stability

Stability is an important concern when considering legged locomotion. If a robot cannot remain stable, it is not very likely that it will be able to complete its mission and there is also a higher probability that it will be damaged. As previously mentioned in Chapter 2, there are two basic types of stability in reference to legged locomotion: dynamic stability and static stability. The work in this thesis is focused on maintaining static stability.

As discussed in Chapter 2, static stability refers to situations where the robot is stable at all times [17]. This means that even if the motion is halted during locomotion, stability would be maintained. To achieve statically stable locomotion, a minimum of three contact points with the ground are required. This means that a statically stable gait requires at least four legs. In order to maintain statically stable locomotion, at least three of the robot's four legs must be in the support stance at all times. To ensure that the trajectory planner provides joint variables that allow for statically stable locomotion, the feet and body positions provided by the gaits must

be statically stable options.

The positions of the leg's contact points with the ground can be joined together by lines to create what is called the support polygon. Static stability is maintained as long as the projection of the CoG is within the support polygon [18]. If the projection of the CoG is not within the triangle formed by the three contact points, the robot is not stable.

Before a leg's position is changed, it must be ensured that the CoG is within the triangle formed by the other three legs. Although this idea seems simple enough to visualize, some thought is required for its implementation. Chen et al., [21], proposed a simple method to determine if the CoG falls within the support triangle. Small triangles can be formed between the footholds of adjacent legs and the CoG. This gives a total of four triangles. If the area of the three smaller triangles is equal to the area of the support polygon, the projection of the CoG is within the support triangle. This idea is illustrated in Figure 5.1. Case A represents a stable configuration where the CoG is within the support triangle. Case B represents an unstable configuration.

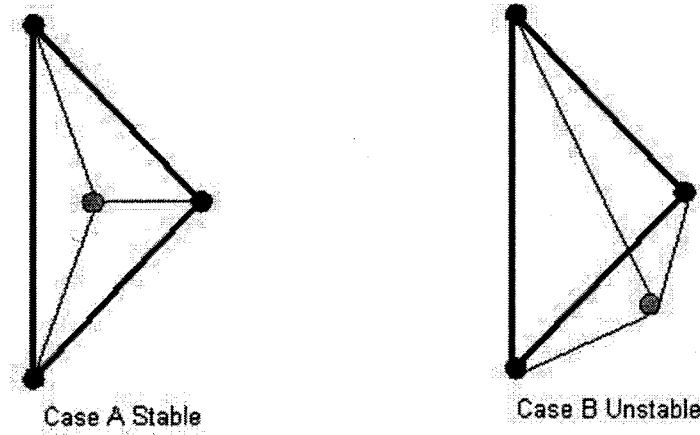


Figure 5.1: The Support Triangle

From Figure 5.1, it can be seen that in the stable configuration, case A, the area of the support polygon is equal to the sum of the areas of the three triangles formed between adjacent legs and the CoG. For case B this is not true. Using the idea of the three smaller triangles, the stability of a robot can be determined as long as the

positions of the support legs are known. The area of the triangles can be found using Equation 5.1 [96], where the vertical lines represent a determinant.

$$Area = \frac{1}{2} \begin{vmatrix} x_1 & y_1 & 1 \\ x_2 & y_2 & 1 \\ x_3 & y_3 & 1 \end{vmatrix} \quad (5.1)$$

The variables represent the x and y coordinates of the three points of the triangle. With this method, it can be ensured that the joint variables provided by the trajectory planner will allow for statically stable motion. If the trajectory planner determines that a certain movement would result in a loss of static stability that movement is not incorporated into the planned trajectory. In this way a robot can maintain static stability throughout locomotion. For the creeping gait, the footholds are always the same with reference to the CoG. This means that the trajectory planner must check for stability only once for each of the four leg transfer phases. For the spinning gait however, the footholds may differ with respect to the CoG depending on the planned angle of re-orientation. In this case, the trajectory planner must check each proposed leg transfer phase each time the spinning gait is used to plan leg and body positions. The stability for the entire proposed gait cycle is always carried out before any joint variables are calculated. This is done in order to avoid deadlock situations where the gait cannot be carried out as it is defined because a loss of stability would occur.

5.2 Leg Trajectories

In order to move between the planned leg and body positions provided by the gaits a trajectory must be followed. When the leg position is to be changed there is no planned movement of the position or orientation of the CoG. The initial and final foot positions for a leg transfer phase are defined in Cartesian space. In order to join the foot positions, a trajectory, also defined in Cartesian space, is used.

Many different types of leg trajectories have been used in the literature. Such trajectories include straight line rectangular trajectories and curved trajectories defined by sine waves or Bezier functions [93]. In this thesis the trajectory for a leg transfer is a sine wave defined in cartesian space.

When a leg is moved, it must be lifted up and moved forward from a starting velocity of zero. The movement must also finish with a velocity of zero. As even terrain is being used, the initial and final z positions are the same. This type of trajectory gives a much smoother velocity profile than a rectangular trajectory. The trajectory can therefore be modeled as a sinusoidal function and can be described by the following equations [71]:

$$x(t) = \left(\frac{x_o - x_f}{2} \right) \cos \left(\frac{\pi t}{t_f} \right) + \left(\frac{x_o + x_f}{2} \right) \quad (5.2)$$

$$y(t) = \left(\frac{y_o - y_f}{2} \right) \cos \left(\frac{\pi t}{t_f} \right) + \left(\frac{y_o + y_f}{2} \right) \quad (5.3)$$

$$z(t) = \left(\frac{h_{max}}{2} \right) \left(1 - \cos \left(\frac{2\pi t}{t_f} \right) \right) + z_o \quad (5.4)$$

$$\dot{x}(t) = - \left(\frac{x_o - x_f}{2} \right) \left(\frac{\pi}{t_f} \right) \sin \left(\frac{\pi t}{t_f} \right) \quad (5.5)$$

$$\dot{y}(t) = - \left(\frac{y_o - y_f}{2} \right) \left(\frac{\pi}{t_f} \right) \sin \left(\frac{\pi t}{t_f} \right) \quad (5.6)$$

$$\dot{z}(t) = h_{max} \left(\frac{\pi}{t_f} \right) \sin \left(\frac{2\pi t}{t_f} \right) \quad (5.7)$$

$$\ddot{x}(t) = - \left(\frac{x_o - x_f}{2} \right) \left(\frac{\pi}{t_f} \right)^2 \cos \left(\frac{\pi t}{t_f} \right) \quad (5.8)$$

$$\ddot{y}(t) = - \left(\frac{y_o - y_f}{2} \right) \left(\frac{\pi}{t_f} \right)^2 \cos \left(\frac{\pi t}{t_f} \right) \quad (5.9)$$

$$\ddot{z}(t) = 2h_{max} \left(\frac{\pi}{t_f} \right)^2 \cos \left(\frac{2\pi t}{t_f} \right) \quad (5.10)$$

Where the subscript o represents the initial value and f the final value. h_{max} is the maximum height to be achieved by the leg during its trajectory and must be determined beforehand. t_f is the time required to complete one leg movement. On flat terrain there is no need for the trajectory to be at a certain height as there would be on uneven terrain where for example stairs are being climbed. The foot must just leave the ground. It is preferable to have a lower value for h_{max} as large values may compromise a robot's stability. Originally, h_{max} was determined for each trajectory depending on the initial and final positions of the foot, and equal to half the height

of the total distance to be traveled by the leg. This was done in order to have a curve with a height that was smaller than the total distance traveled. This trajectory is described in Equation 5.11.

$$h_{max} = \frac{\sqrt{(x_o - x_f)^2 + (y_o - y_f)^2}}{2} \quad (5.11)$$

This value for the maximum height allowed joint variables to be produced at CoG heights that were mid-range to the maximum. Problems occurred when the height of the CoG was low and the stride length, or the distance traveled in the xy plane, was large. In these cases, the maximum height was not in the defined workspace as values for θ_3 were in the positive range.

A new method of determining a maximum height was chosen based on the height of the CoG. Using this method, h_{max} was determined and within the leg workspace. h_{max} was determined using the following equation:

$$h_{max} = \frac{z_{hip} - z_i}{2} \quad (5.12)$$

Where z_{hip} is equal to -0.15 m is the z location of the hip in the CoG reference frame. z_i is equal to the position of the ground in the CoG reference frame. This means that h_{max} is defined as half the distance between the ground and the hip.

Using Equations 5.2 to 5.10 and Equation 5.12 a leg trajectory can be created. For a leg transfer time of t_l and a leg moving from foot position three to foot position one, defined in Chapter 4, and with the CoG height at 0.39 m , plots of the trajectory can be obtained. These are shown in Figures 5.2, 5.3 and 5.4. As can be seen in the figures, there is no change in position in the x direction and the velocities are smooth starting and ending at zero.

5.3 Body Trajectories

The trajectory planner can create a plan where the body is moved either forward or rotated about the CoG. When the body is moved, the joints in all four legs must be actuated as opposed to only the joints in one leg that occurs when transferring a leg. The forward creeping gait is designed to allow for the trajectory of the body to be

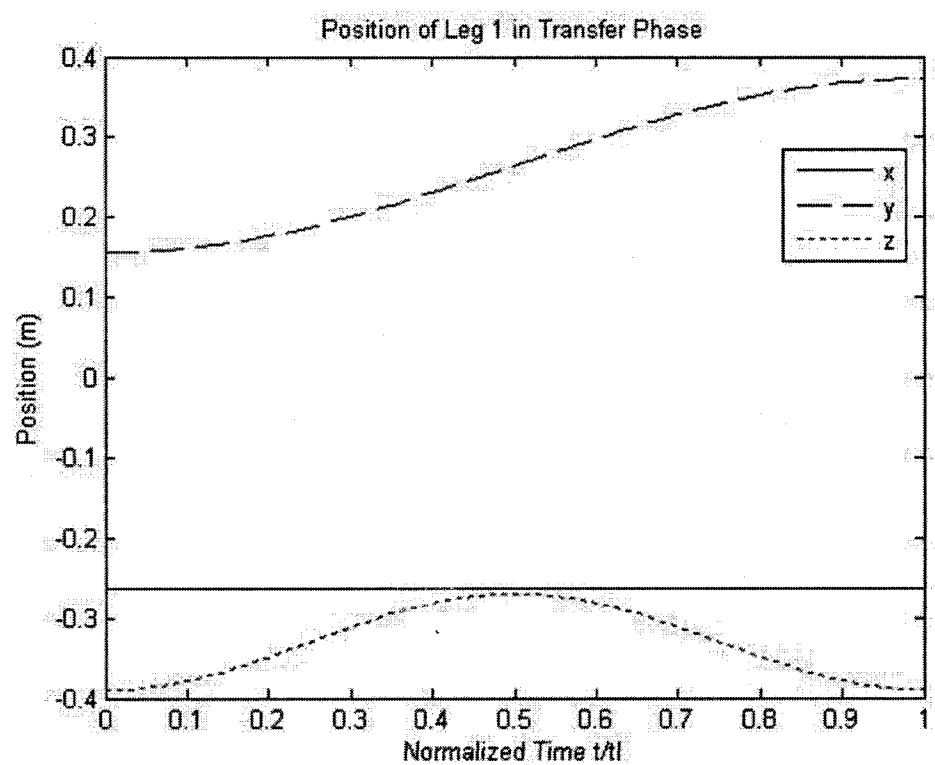


Figure 5.2: Position of Leg 1 in Transfer Phase

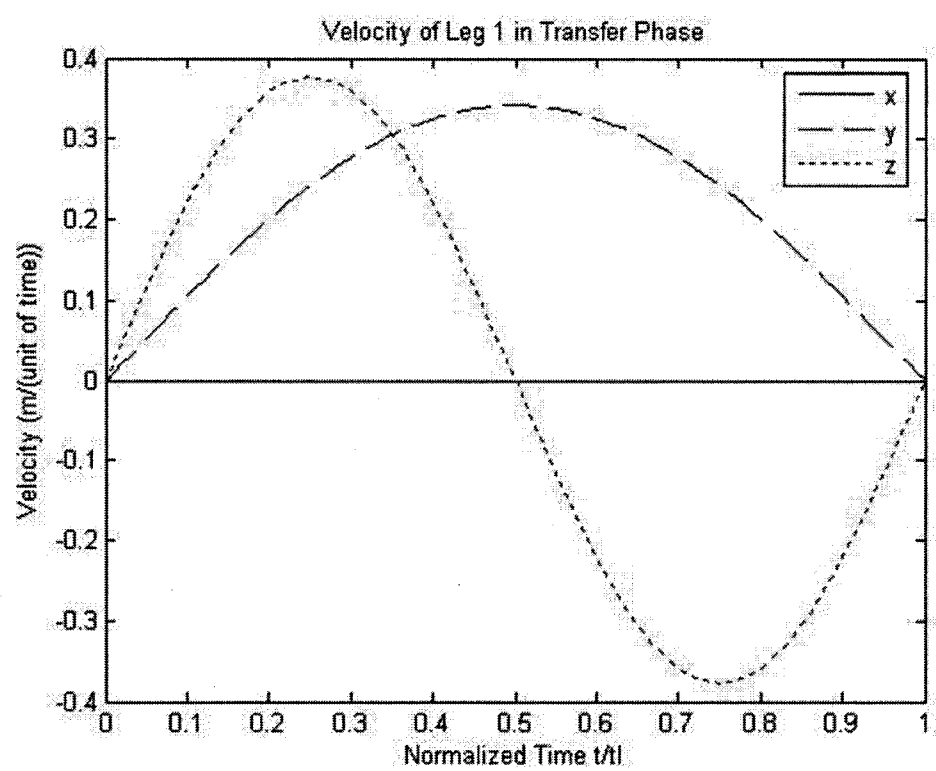


Figure 5.3: Velocity of Leg 1 in Transfer Phase

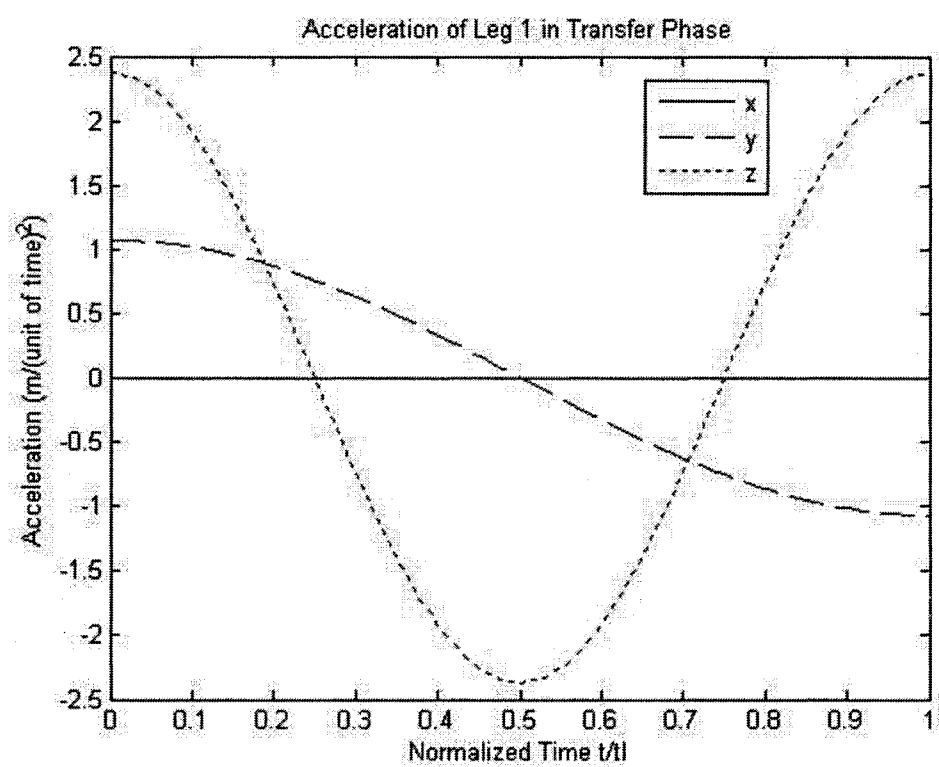


Figure 5.4: Acceleration of Leg 1 in Transfer Phase

defined as a straight line, where the CoG would move forward by $\lambda/2$. Because all the legs work together to move the CoG along a path, the trajectory for the body will be defined again in cartesian space. As with the trajectory for leg movement, the start and end velocities are both zero. The trajectory for the body movement phase of the creeping gait is defined by Equations 5.2, 5.3, 5.5, 5.6, 5.8 and 5.9. The position, velocities and accelerations in the z direction of the CoG reference frame are expressed by Equations 5.13, 5.14 and 5.15.

$$z(t) = \left(\frac{z_o - z_f}{2} \right) \cos \left(\frac{\pi t}{t_f} \right) + \left(\frac{z_o + z_f}{2} \right) \quad (5.13)$$

$$\dot{z}(t) = - \left(\frac{z_o - z_f}{2} \right) \left(\frac{\pi}{t_f} \right) \sin \left(\frac{\pi t}{t_f} \right) \quad (5.14)$$

$$\ddot{z}(t) = - \left(\frac{z_o - z_f}{2} \right) \left(\frac{\pi}{t_f} \right)^2 \cos \left(\frac{\pi t}{t_f} \right) \quad (5.15)$$

Here t_f is equal to the amount of time required to complete one body movement. As an example of the trajectories, let the transfer time for the body be two units of time, the initial position of the CoG in the body reference frame is [0,0,0] and the final position is [0, $\lambda/2$,0]. For a CoG height of travel of 0.39 m, $\lambda/2$ is equal to 0.1088 m. Using this information and equations that define the trajectory, the following trajectories are obtained and shown in Figures 5.5, 5.6 and 5.7. There is only a change in the y position, which increases with respect to time, meaning that the trajectory in the xy plane is a straight line. The velocity and accelerations are smooth.

The body also changes position during the spinning gait when it is rotated about the CoG. In this case, there is no change in the cartesian co-ordinates of the CoG, just its orientation. For this reason the trajectory will be defined for each joint in joint space. As with previous trajectories, the end and start velocities are zero. The beginning and end accelerations are also set to zero. The initial and final joint positions are known. This information can be used with a quintic polynomial to create a trajectory. A quintic polynomial eliminates the jerk that can arise in other types of trajectories, such as a cubic polynomial trajectory, allowing for smoother accelerations. The quintic polynomial for the position as a function of time can be

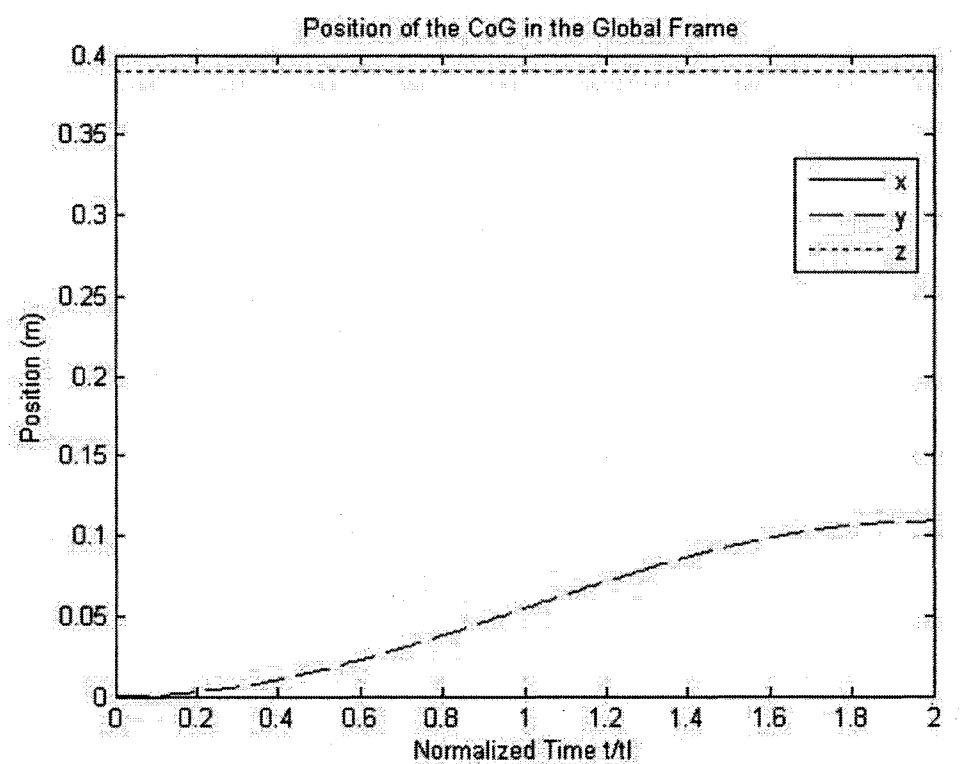


Figure 5.5: Cartesian Positions During the Body Movement Phase of the Creeping Gait

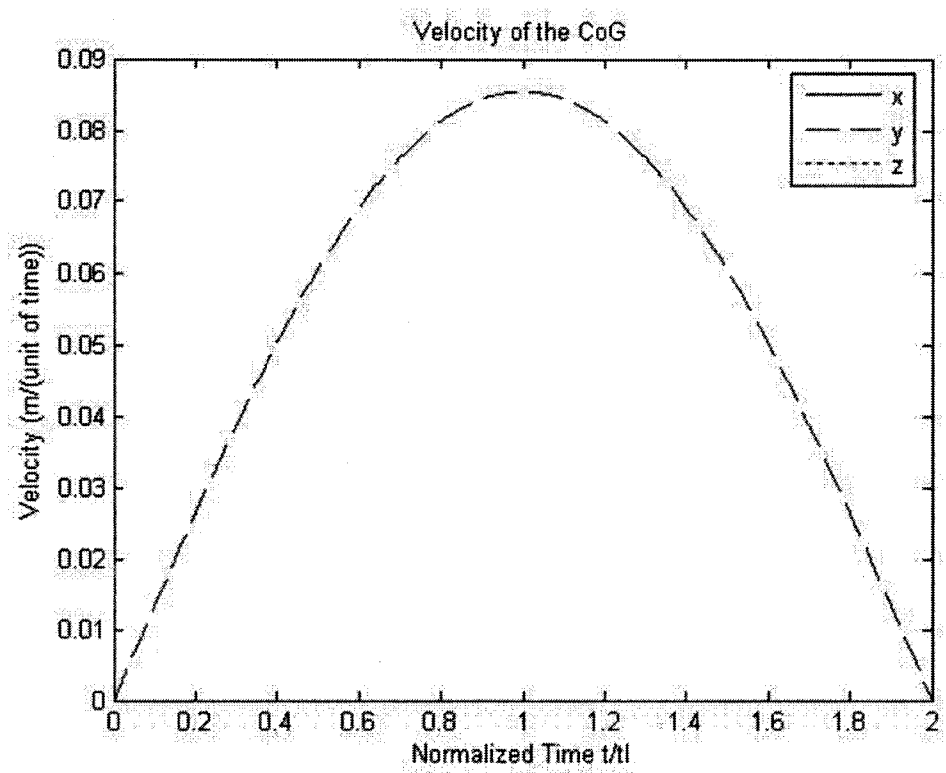


Figure 5.6: Cartesian Velocities During the Body Movement Phase of the Creeping Gait

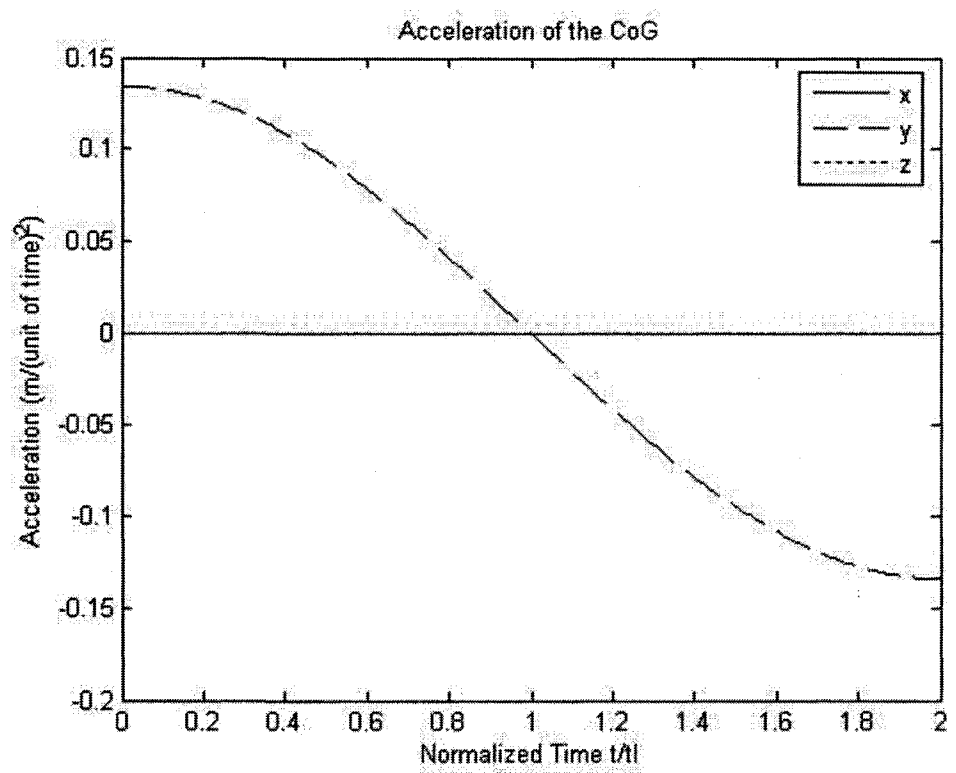


Figure 5.7: Cartesian Accelerations During the Body Movement Phase of the Creeping Gait

described by Equation 5.16 [8]:

$$p(t) = b_o + b_1 t + b_2 t^2 + b_3 t^3 + b_4 t^4 + b_5 t^5 \quad (5.16)$$

In order to define the trajectory, the coefficients $b_o, b_1, b_2, b_3, b_4, b_5$, must be determined. There are six unknowns so six equations are required to solve for these. The derivative of Equation 5.16, gives an expression for the velocity. An expression for the acceleration can also be determined by taking the derivative of the velocity expression. Each of these leads to two expressions for the initial and final values. These six equations are expressed by Equations 5.17 to 5.22 [8]:

$$p_o = b_o + b_1 t_o + b_2 t_o^2 + b_3 t_o^3 + b_4 t_o^4 + b_5 t_o^5 \quad (5.17)$$

$$p_f = b_o + b_1 t_f + b_2 t_f^2 + b_3 t_f^3 + b_4 t_f^4 + b_5 t_f^5 \quad (5.18)$$

$$\nu_o = b_1 + 2b_2 t_o + 3b_3 t_o^2 + 4b_4 t_o^3 + 5b_5 t_o^4 \quad (5.19)$$

$$\nu_f = b_1 + 2b_2 t_f + 3b_3 t_f^2 + 4b_4 t_f^3 + 5b_5 t_f^4 \quad (5.20)$$

$$\dot{\nu}_o = 2b_2 + 6b_3 t_o + 12b_4 t_o^2 + 20b_5 t_o^3 \quad (5.21)$$

$$\dot{\nu}_f = 2b_2 + 6b_3 t_f + 12b_4 t_f^2 + 20b_5 t_f^3 \quad (5.22)$$

The equations can be further simplified by setting t_o equal to zero. t_f is equal the amount of time required to complete one body movement phase. With this the following values can be obtained for the coefficients:

$$b_o = p_o \quad (5.23)$$

$$b_1 = 0 \quad (5.24)$$

$$b_2 = 0 \quad (5.25)$$

$$b_3 = - \left(\frac{10}{t_f^3} \right) p_o + \left(\frac{10}{t_f^3} \right) p_f \quad (5.26)$$

$$b_4 = \left(\frac{15}{t_f^4} \right) p_o - \left(\frac{15}{t_f^4} \right) p_f \quad (5.27)$$

$$b_5 = - \left(\frac{6}{t_f^5} \right) p_o + \left(\frac{6}{t_f^5} \right) p_f \quad (5.28)$$

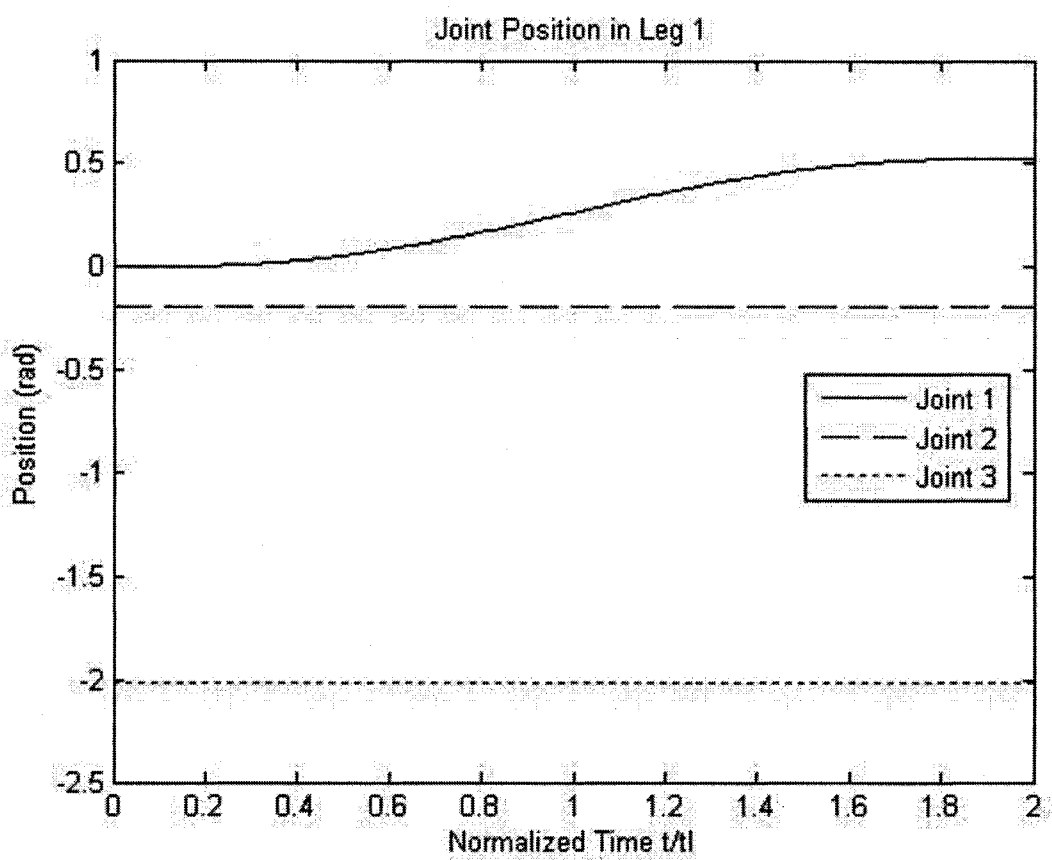


Figure 5.8: Joint Positions During the Body Movement Phase of the Spinning Gait

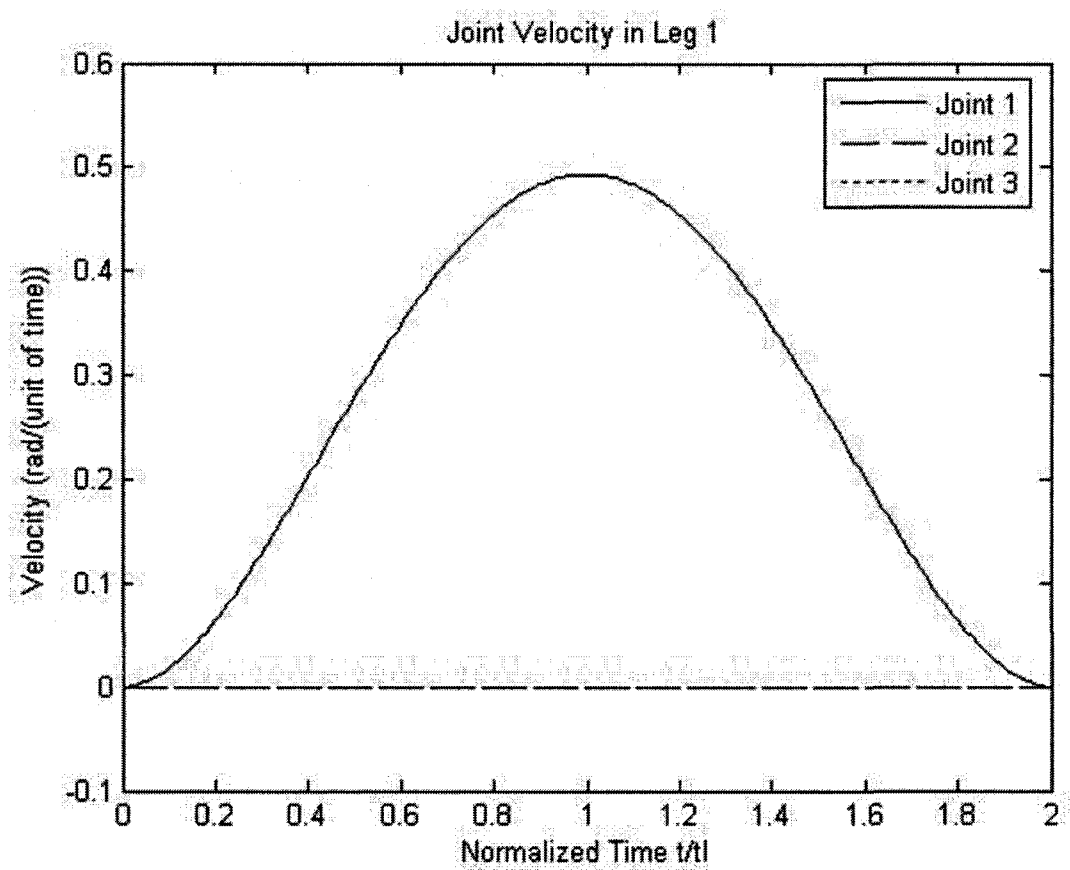


Figure 5.9: Joint Velocities During the Body Movement Phase of the Spinning Gait

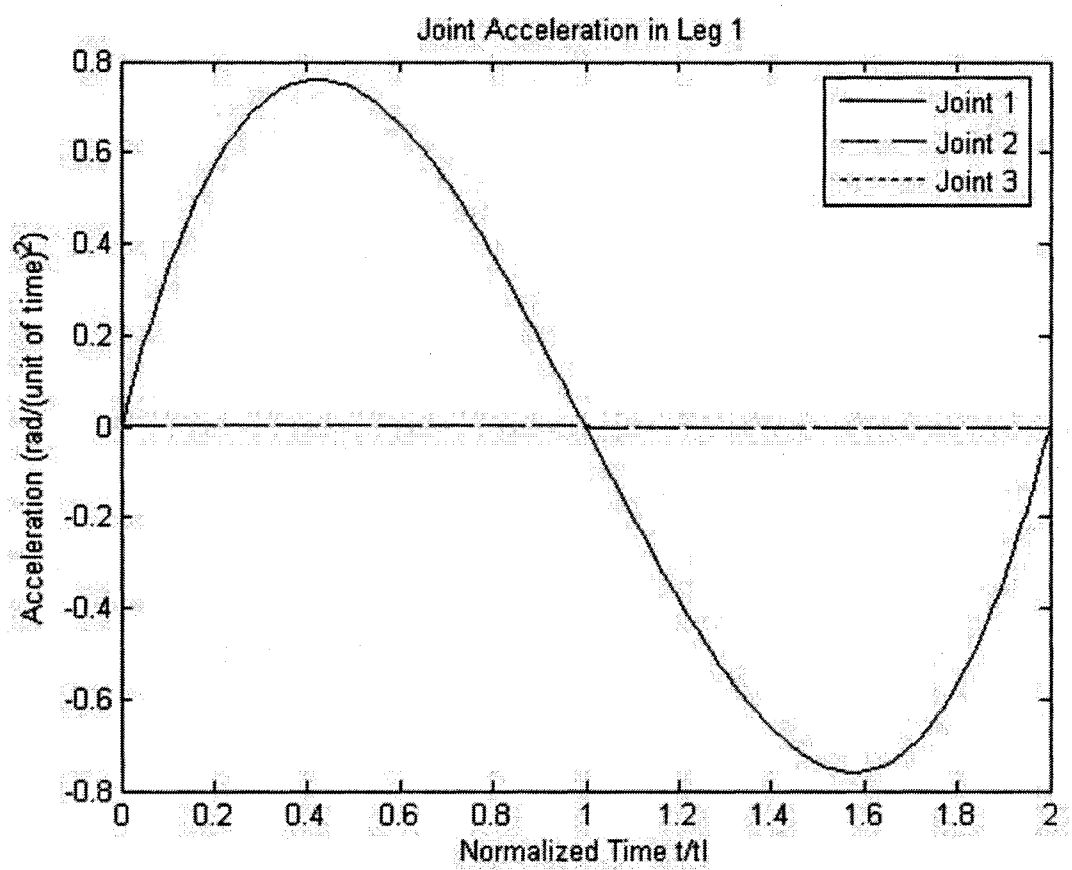


Figure 5.10: Joint Accelerations During the Body Movement Phase of the Spinning Gait

An example of the joint trajectories for a change in orientation of $\pi/6$, with a CoG height of 0.39 m is shown in Figures 5.8, 5.9 and 5.10. The legs begin and end in the same configuration with respect to the CoG, while maintaining the same height. This means that θ_1 should be the only joint to change, as seen in the Figures 5.8, 5.9, 5.10.

5.4 Changing Between the Global and CoG Reference Frames

As seen in previous sections, the IKP and DKP for each leg can be solved in the CoG reference frame. They could also be solved in the foot reference frame. Although the initial and final positions of the CoG can be calculated in the foot frame, there is added complexity using this frame as the orientation of the foot with respect to the CoG must be considered. Using the CoG reference frame, the concern was only in the foot position. For this reason the IKP and DKP for the CoG reference frame are used in determining the position and joint variables required to allow the CoG to move to a desired position in the global frame.

The desired path to be followed by the CoG of a robot is defined in a global reference frame. The joint variables required to transfer a leg can be determined in a CoG reference frame as the gaits specify leg positions in the CoG reference frame. When planning the number of gait cycles that should be carried out to achieve a desired waypoint, the waypoint must be transferred into the CoG reference frame. Once the IKP is solved and a body movement carried out, the new position should be changed into the global reference frame to allow for tracking of the CoG.

In the global reference frame, a planned trajectory begins at position $(0,0,z)$ and at orientation $\phi = 0$. ϕ is the angle between the x axis in the global frame and the CoG's x axis, shown in Figure 5.11. The waypoint, defined in the global frame, must be transferred into the CoG reference frame, this done using Equations 5.29 and 5.30.

$$Q_{CoG \rightarrow Global} = \begin{bmatrix} \cos\phi & -\sin\phi & 0 \\ \sin\phi & \cos\phi & 0 \\ 0 & 0 & 1 \end{bmatrix} \quad (5.29)$$

$$p_{f_{CoG}} = Q_{CoG \rightarrow Global}^{-1} (p_{f_{Global}} - p_{o_{Global}}) \quad (5.30)$$

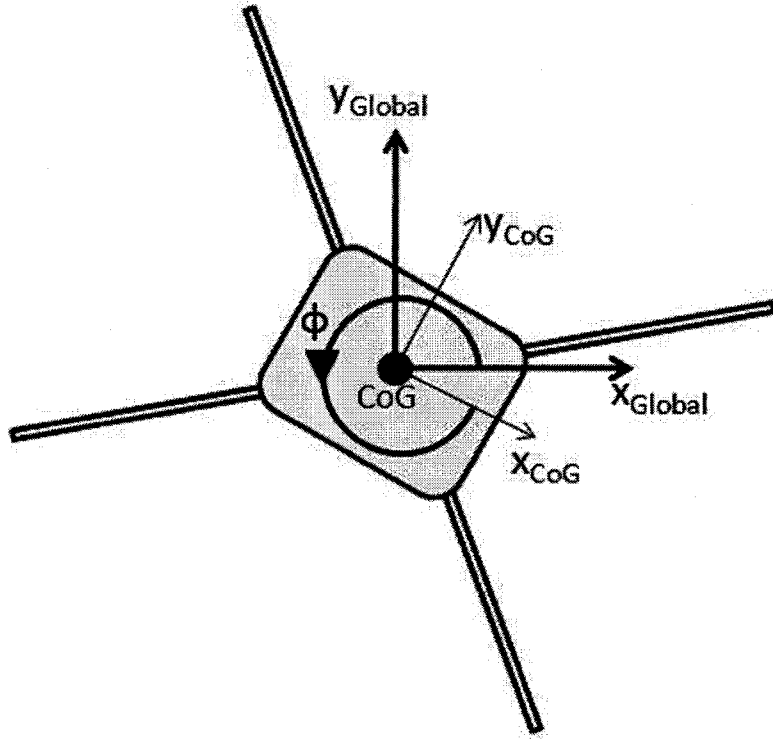


Figure 5.11: The Angle ϕ

Where $p_{f_{Global}}$ and $p_{o_{Global}}$ represent the final and initial positions of the CoG in the global reference frame. Given the initial joint variables, the positions of all the legs can be determined in the CoG reference frame. The final position of the foot with respect to the new position of the CoG can be determined by finding the vector between the initial position of the foot and the desired final position of the CoG in the CoG frame. This is shown in Figure 5.12 and Equation 5.31

$$p_{f_{foot_{CoG}}} = p_{o_{foot_{CoG}}} - p_{f_{CoG}} \quad (5.31)$$

The required joint variables can then be calculated for all legs. Once the new body position has been determined, its position in the global frame is calculated using Equation 5.32, allowing the CoG to be tracked.

$$p_{CoG_{Global}} = Q_{CoG \rightarrow Global}(p_{f_{CoG}}) + p_{o_{CoG_{Global}}} \quad (5.32)$$

It is possible that the orientation of the CoG with respect to the global frame changes. It is therefore important to recalculate ϕ after the body has been moved.

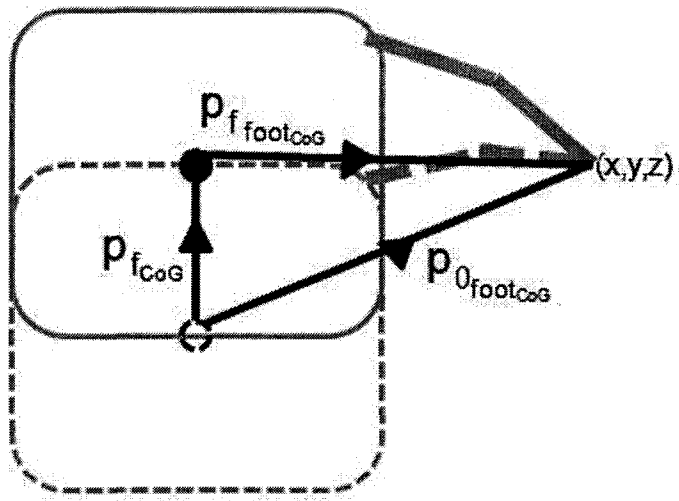


Figure 5.12: Determining the Position of the Foot with Respect to the New position of the CoG

The hips of the robot are rigidly attached to one another and when ϕ is equal to zero the line joining an odd numbered and an even numbered hip is parallel with the global x axis, it is always parallel to the CoG x axis. The initial and final positions of the hips can be determined using the DKP, these can then be changed into the global reference frame using the method described above. A line can then be drawn between an odd and even hip in order to determine the angle ϕ .

5.5 The Trajectory Planner

Once a desired path is selected by the user. A plan to follow the desired path, in terms of joint positions, joint velocities and joint accelerations is required. Producing these variables is the job of the trajectory planner.

The trajectory planner requires the input of the desired path in the global reference frame, in the form of waypoints defined in the xy plane. The desired traveling height of the CoG above the ground must also be defined. When creating a plan, first the re-defined workspace, presented in Section 4.2.1, is determined. Using the simplified workspace, the positions of the three footholds to be used in the creeping gait for each leg are defined. Then starting with the first waypoint, the waypoint is transformed into the CoG reference frame, as discussed in Section 5.4. The distance from the CoG

to the waypoint is determined in the x and y directions. If the CoG is not at the waypoint, there are two possibilities:

1. If the distance in the x direction is equal to zero and the distance in the y direction is larger than zero, the trajectory planner calls upon the creeping gait to provide the order of appropriate foot and body positions to reach the waypoint. All of the robot configurations defined by the gait for one gait cycle are checked for stability using the method described in Section 5.1.

The trajectories to move the legs between required footholds are produced using Equations 5.2 to 5.10. Trajectories are defined in the order that they are required for the gait. First a trajectory to move leg 4 from position one to position three is defined, then the required joint variables to allow the leg to follow the defined trajectory are calculated by solving the IKP, presented in Chapter 3, and stored. The same is done for moving leg 2 from position three to position one. Then the trajectory for a body movement is produced using the equations in Section 5.3. The IKP is again used for the body trajectory to produce the required joint variables and the position of the CoG is updated in the global frame. The trajectories and required joint variables are then produced for the movement of leg 3 from position one to position three, then for the movement of leg 1 from position three to position one and then finally for the second body movement. The position of the CoG is again updated in the global frame. Using this process, the trajectory planner produces the required joint variables to complete one cycle of the creeping gait. A flow chart for the creeping gait is shown in Figure 5.13.

To determine the appropriate number of cycles of the creeping gait to complete, the straight line distance from the CoG to the waypoint is divided by the stride length and rounded to a whole number. Once a plan to reach the given waypoint is achieved, the next waypoint is evaluated.

2. If the distance in the x direction is not equal to zero or the distance in the y

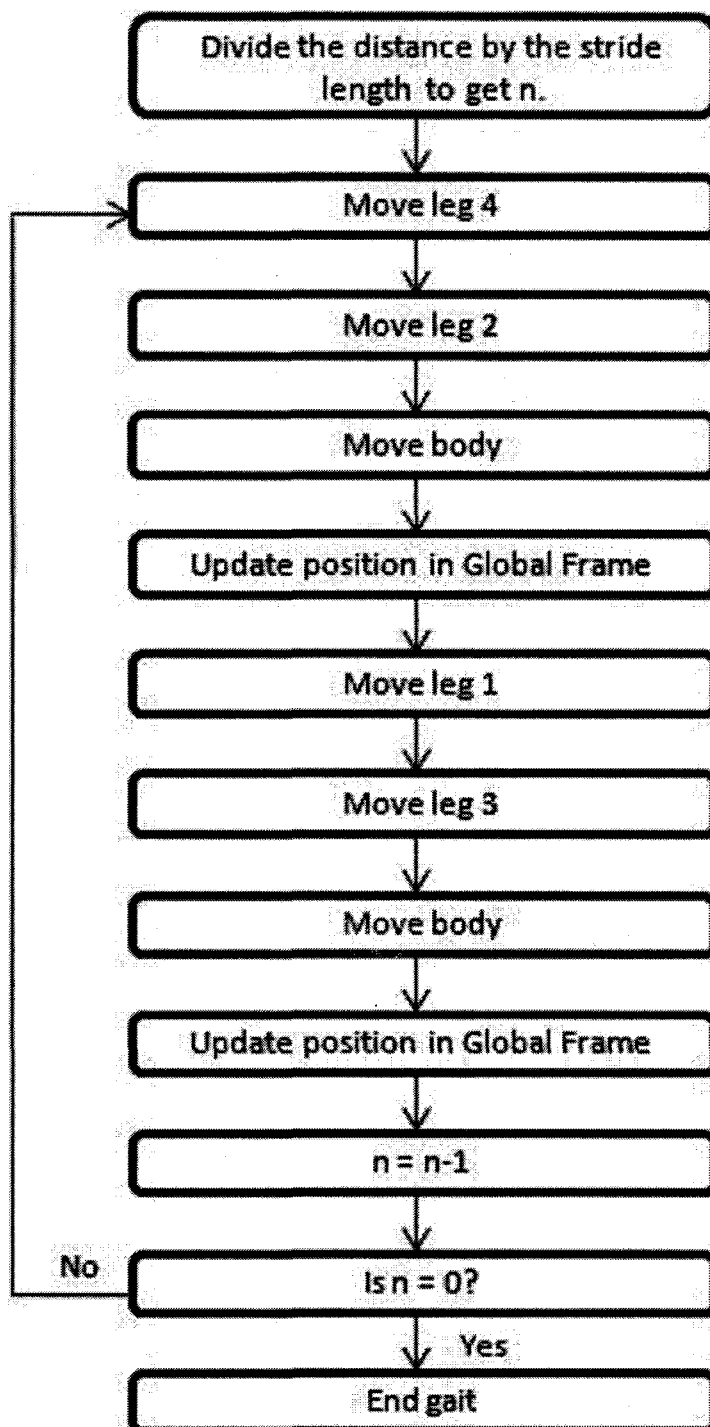


Figure 5.13: The Creeping Gait

direction is less than zero, the plan produced by the trajectory planner must allow for re-orientation, the spinning gait must be used. First a planned transition to the appropriate positions must occur to begin the spinning gait, as described in Section 4.2.2. Trajectories and joint variables to move legs 4 and 2 to position two are produced. The angle ψ , between the forward axis of the CoG and the waypoint is determined. If the value of ψ is larger than $\pi/2$, then ψ becomes $\psi/2$ until the value of the angle is less than $\pi/2$. The number of divisions that occur determine the number of cycles of the spinning gait that should be carried out.

For one cycle of the spinning gait, the new footholds are calculated using ψ and the method described in Section 4.2.2. The order of appropriate leg movements is determined by checking up to a possible total of 24 leg movement options for stability until a stable pattern of four leg movements to the new footholds is determined. The trajectories to join the foot positions are determined using Equations 5.2 to 5.10 and again the IKP is solved to produce the joint variables. The joint trajectories to re-orient the forward axis of the robot is determined using Equation 5.16 and its derivatives. In this case, the IKP is not used as the trajectory is already defined in joint space. Then the orientation of the robot is updated in the global frame. Using this process, the trajectory planner produces the required joint variables to complete one cycle of the spinning gait.

The spinning gait is carried out until all the required joint variables to allow the robot to have the desired orientation are produced. Once the planned trajectory allows the forward axis of a robot to be orientated in the right position, another planned transition must occur to the appropriate start position for the creeping gait and the required joint variables to follow the appropriate leg trajectories are produced. A flow chart for the spinning gait is shown in Figure 5.14. Then, the creeping gait is again used, in the same way as in the first possibility described above to achieve the waypoint.

This process is carried out until a plan allowing all of the waypoints to be achieved

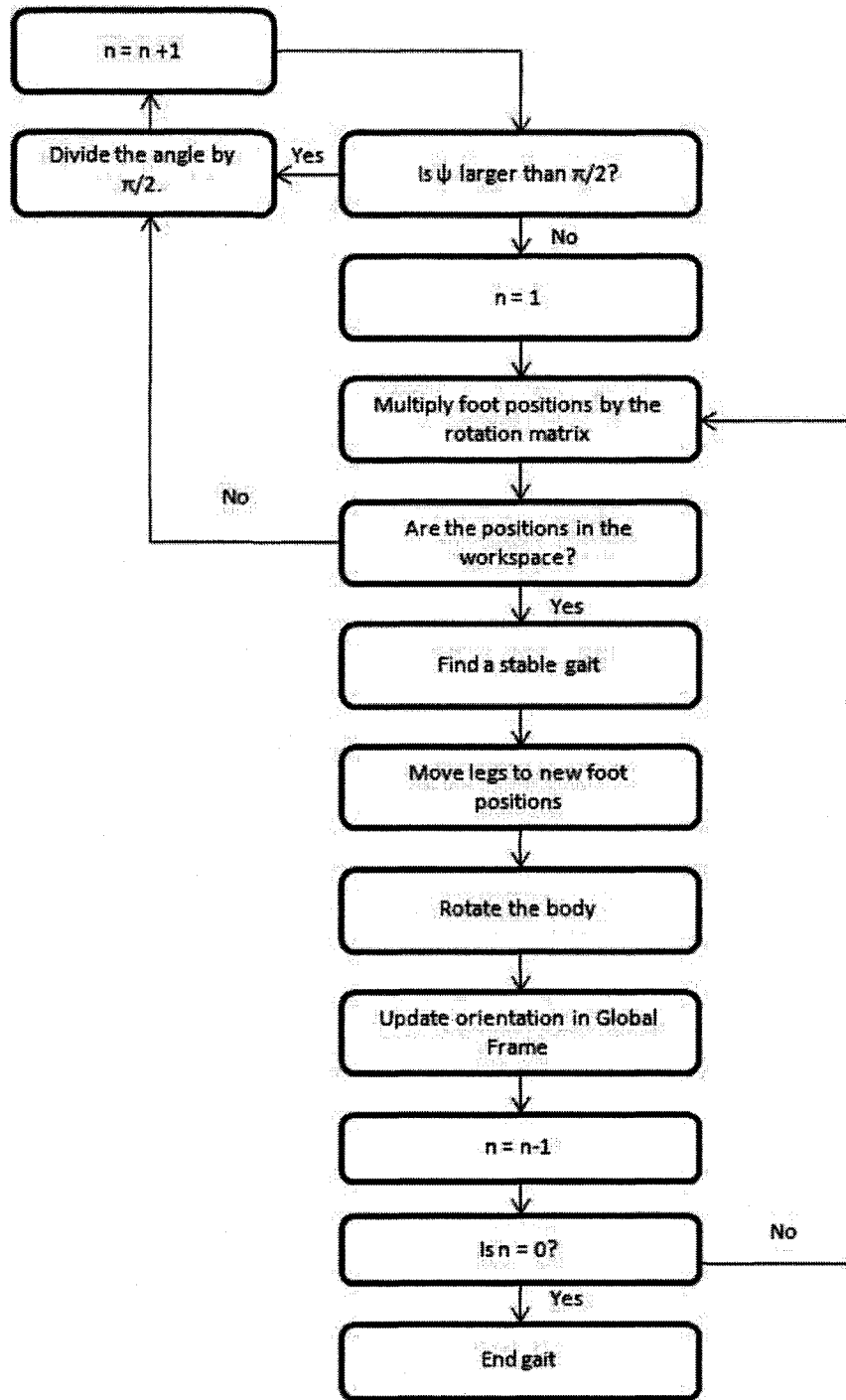


Figure 5.14: The Spinning Gait

is obtained. Joint variables are produced and stored for every period of one hundredth of the time required for one leg movement. Figure 5.15 illustrates the steps involved in the trajectory planner.

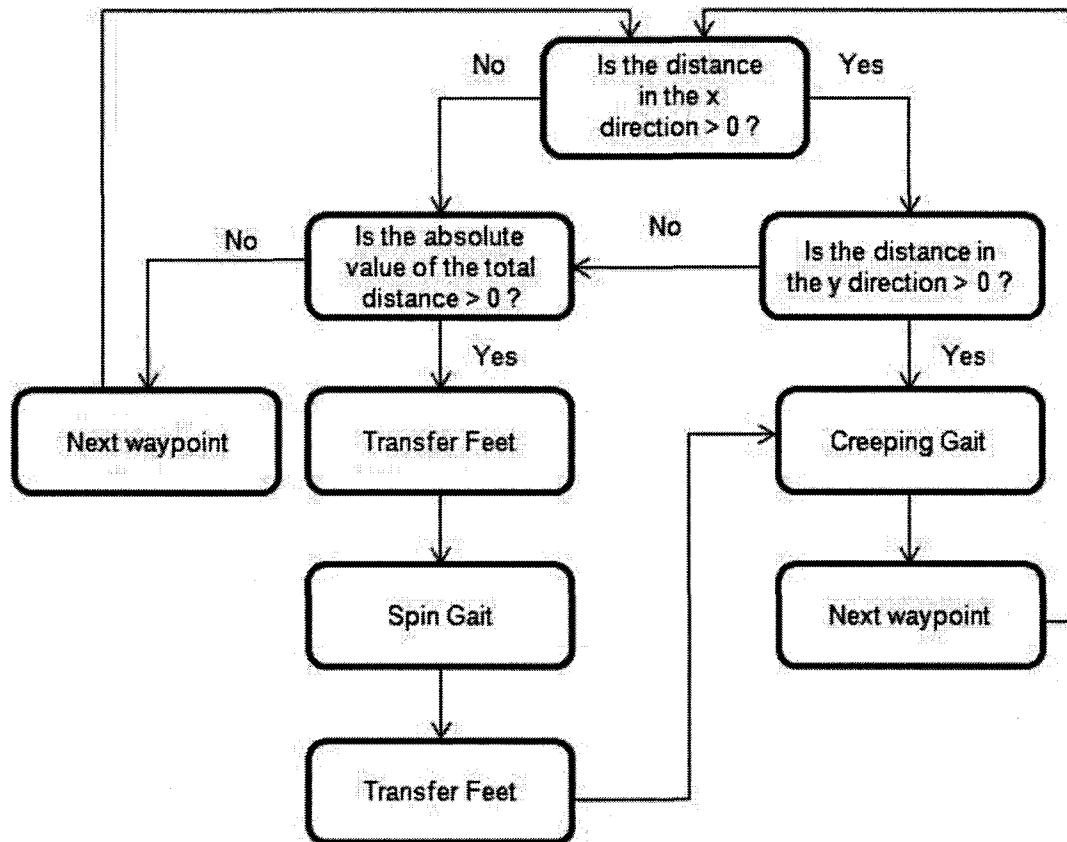


Figure 5.15: The Trajectory Planner

Chapter 6

Case Studies and Results

In this Chapter the results of the trajectory planner for several different case studies will be provided. The case studies involved different heights of travel for the CoG, 0.2 m, 0.4 m and 0.6 m, and different types of desired paths. This was done in order to give an indication of the performance near the extremes of the allowable height range as well as the performance with a height near to the mid range. The respective stride length at the three different heights were found using the method as in Chapter 4 and are as follows: 0.3787 m, 0.3328 m and 0.1613 m. Two different types of paths were used to test the performance of the trajectory planner: a path consisting only of straight lines and a circular path.

The error of the path that the plan provided by the trajectory planner would allow a robot to follow in reference to the desired path is determined by finding how far the CoG would be away from the desired waypoint once the waypoint would be achieved. The normalized error referred to in this chapter is the sum of these distances divided by the total number of waypoints. The normalized error is described by Equation 6.1:

$$E_n = \frac{1}{n} \sum \sqrt{(x_a - x_d)^2 + (y_a - y_d)^2} \quad (6.1)$$

Where the subscripts a and d represent the allowed and desired positions and n represents the number of waypoints. Also in this chapter is an investigation of how a decrease of accuracy can increase the overall average velocity. The investigation is carried out at all three of the above mentioned CoG heights for the circular path. Finally, the benefit of legged locomotion over wheeled locomotion is demonstrated in this chapter where an example of a ditch crossing is given.

6.1 Results of the Trajectory Planner for the Follow of a Straight Line Path

The straight line path is made up of a set of straight line segments between the following points in the xy plane: $(0,1)$, $(1,1)$, $(0,2)$, $(0,3)$. The path is illustrated in Figure 6.1. The distance of the desired path was a total of 4.41 m. The results for the straight line path are shown in Table 6.1 at the end of the section. A section of

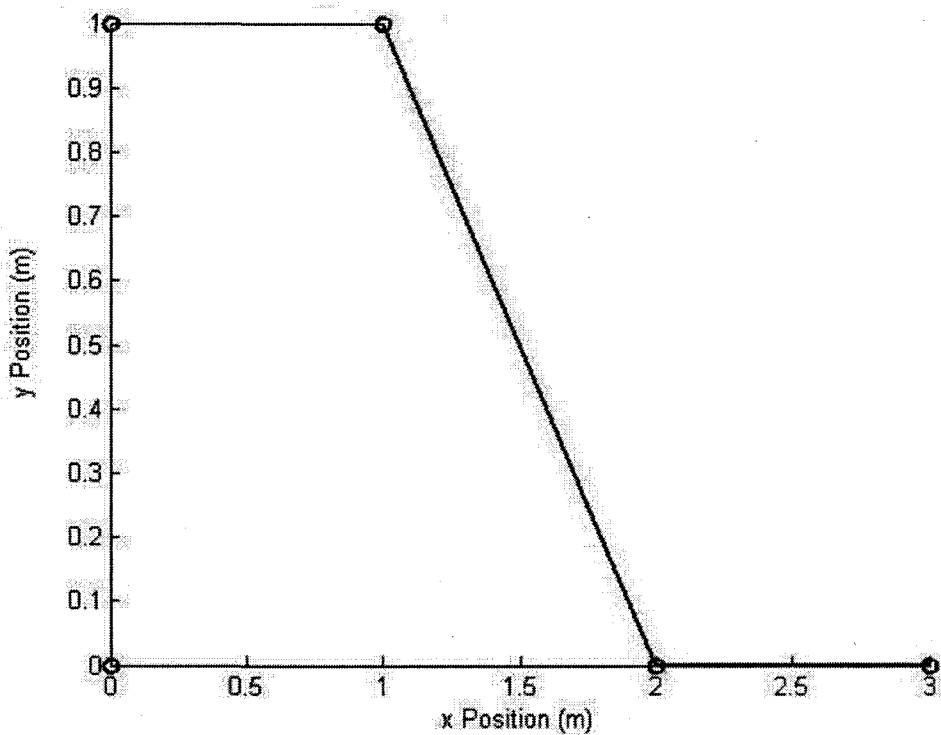


Figure 6.1: Straight Line Path

the joint variables produced by the trajectory planner to allow a robot to follow the desired path for a height of travel of 0.2 m are shown in Figures 6.2, 6.3 and 6.4. This section ranging from time period 16 to 40 shows the completion of one cycle of the creeping gait, the transitions of legs 4 and 2, two cycles of the spinning gait and the transitions of legs 2 and 4. This refers to the traveling in a straight line just before the first turn on the path shown in Figure 6.1 and the completion of the turn. It can be seen in Figure 6.5 that the magnitude of the angle required to re-orient the body

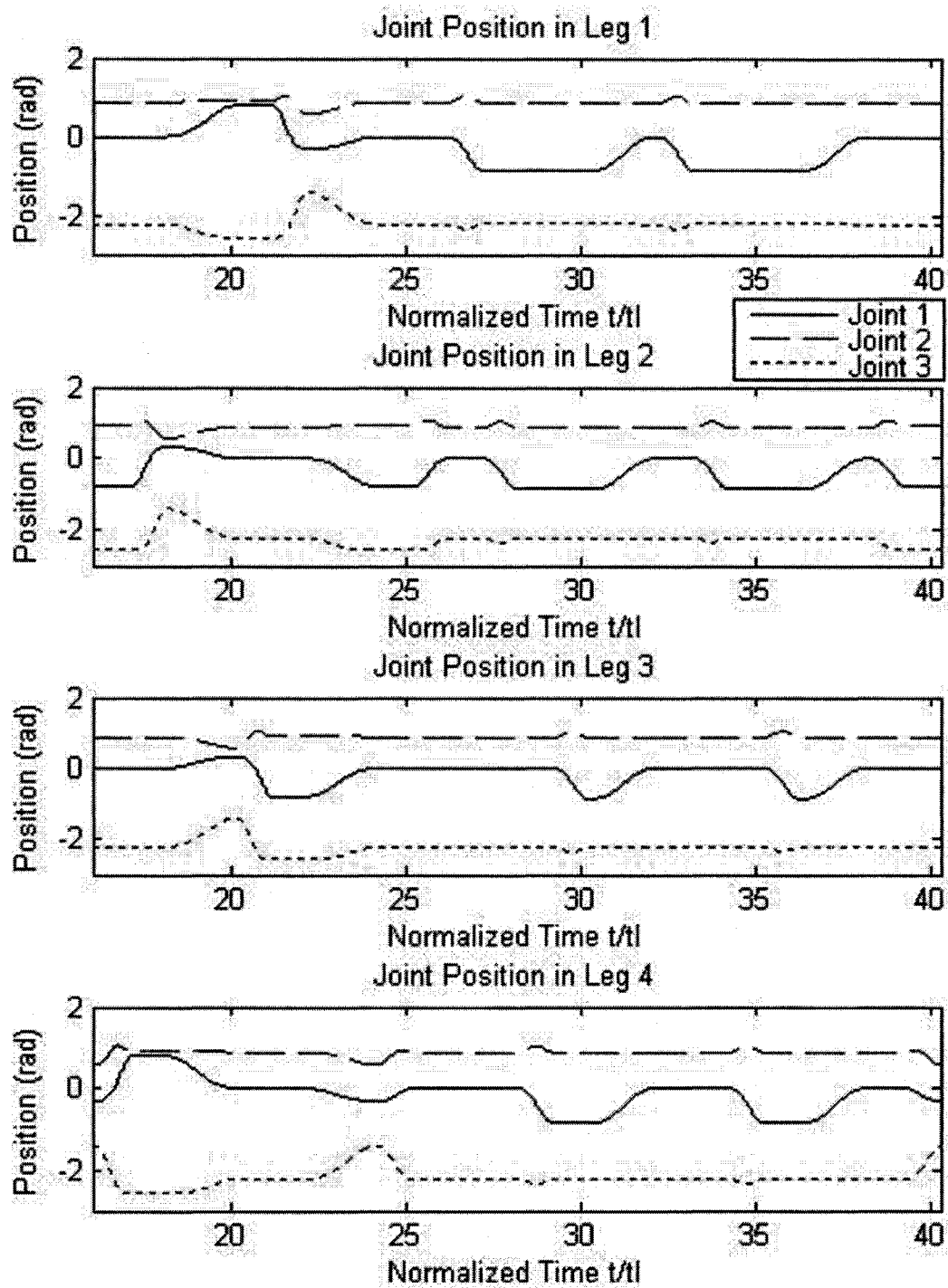


Figure 6.2: Joint Positions for a Height of Travel of 0.2 m Following a Straight Line Path

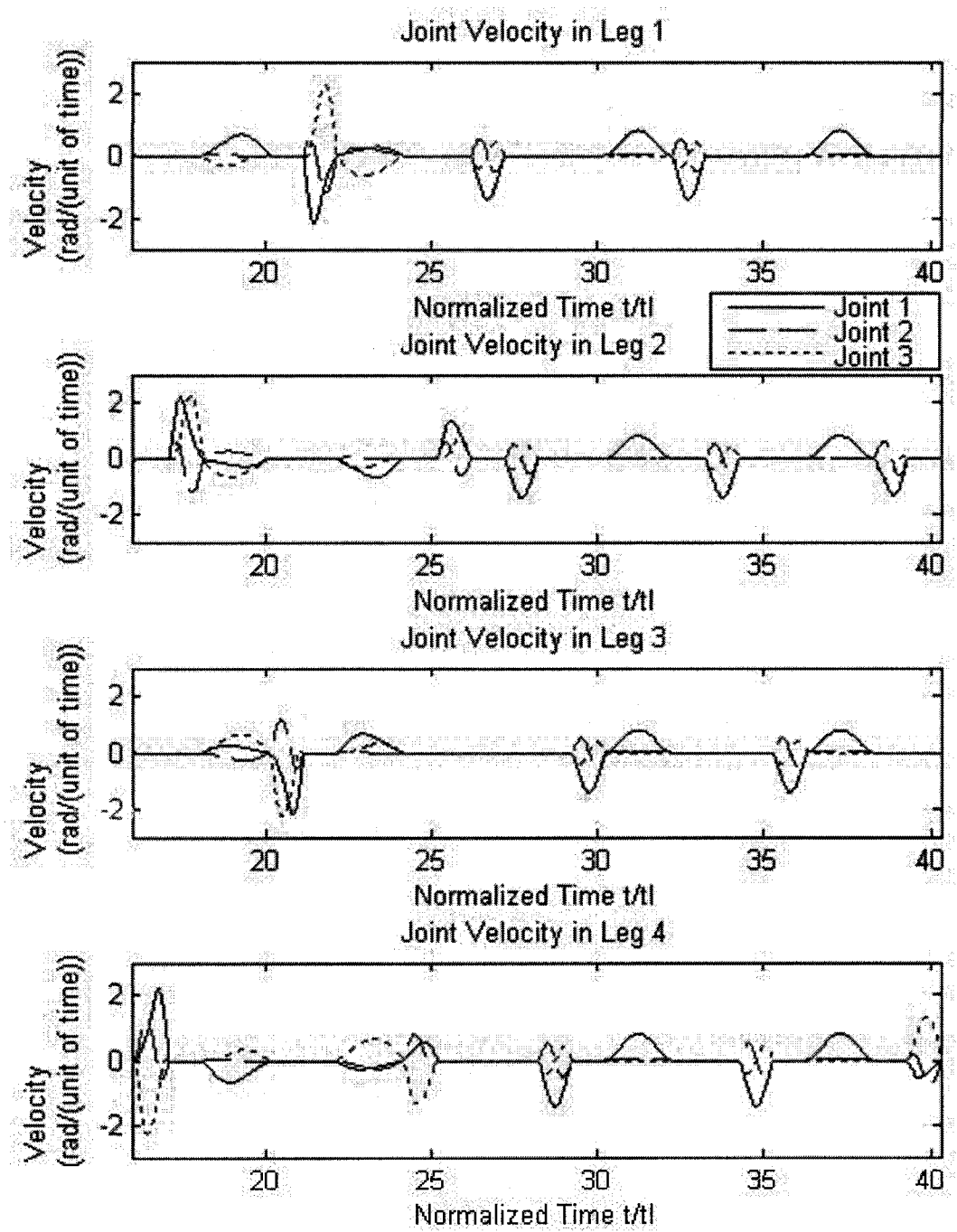


Figure 6.3: Joint Velocities for a Height of Travel of 0.2 m Following a Straight Line Path

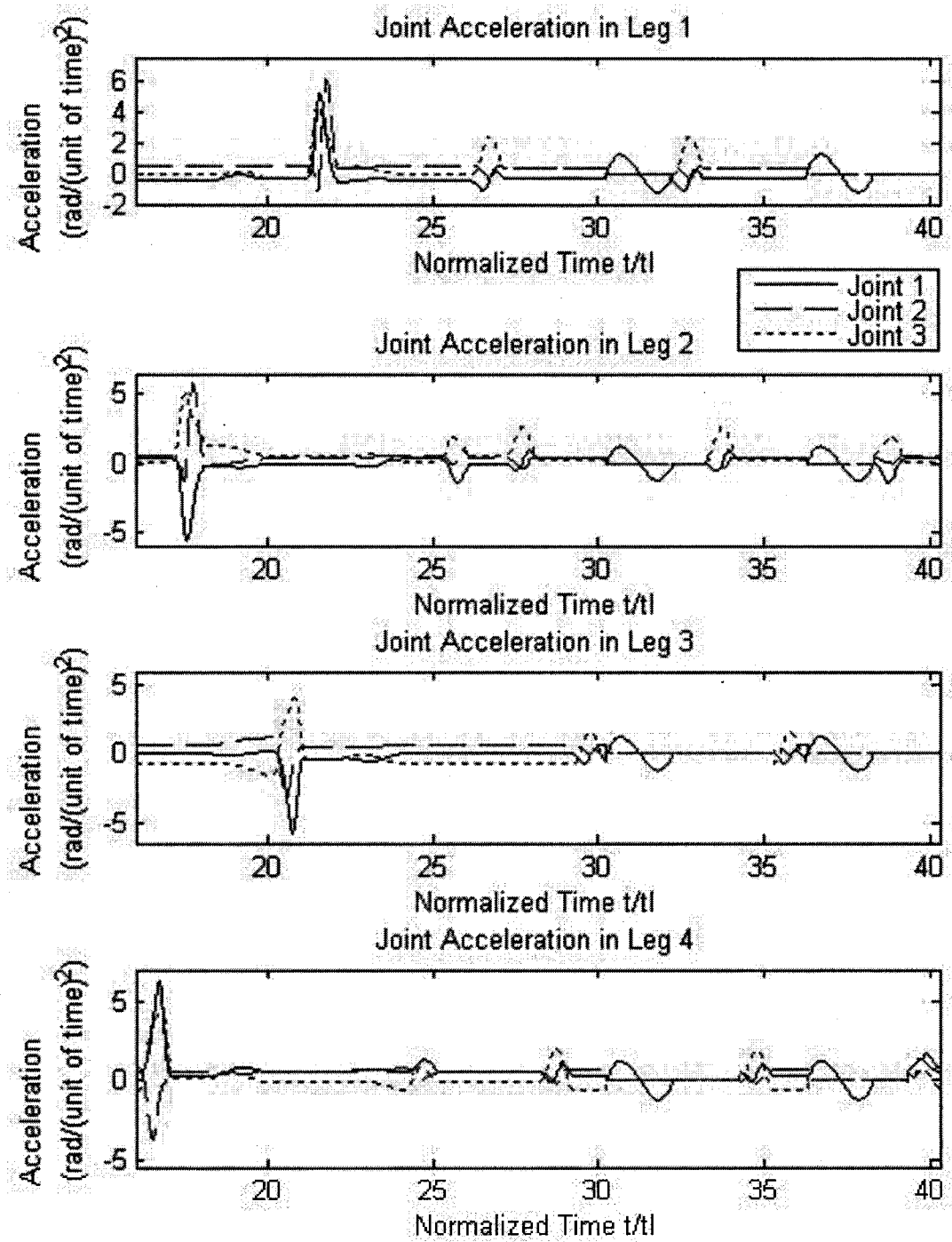


Figure 6.4: Joint Accelerations for a Height of Travel of 0.2 m Following a Straight Line Path

to face the second waypoint is larger than $\pi/2$. This is the reason why two cycles of the spinning gait are carried out.

From Figure 6.2 the creeping gait can be seen to be carried out from times 16-24. Leg 4 moves first, followed by leg 2 etc. At time 24, leg 4 is moved to position two followed by the move of leg 2 to position two. The leg movements for the spinning gait then occur between times 26 and 30 and it can be seen that they occur in the 1-2-4-3 order. The body is spun which can be seen during times 30 to 32 where movement occurs in all legs, but only for joint 1. The spinning gait can then be seen to be repeated once followed finally by transitions of legs 2 and 4. These movements are even more clearly pronounced when looking at Figures 6.3 and 6.4 and are representative of the movements that occur of the entire trajectory repeated at different intervals.

Also more clearly shown in Figures 6.3 and 6.4 is the fact that the largest velocities and accelerations occur during the leg movement phase of the creeping gait. This would not have been the case if it was possible to re-orient by the desired amount using only one cycle of the spinning gait.

The allowable path, marked with xs, that could be achieved using the planned trajectory is shown in Figure 6.5. The xs also mark the positions of the CoG provided by the gait which are a distance of $\lambda/2$ apart. For a height of travel of 0.2 m above the ground, the allowed trajectory took a total of 132 units of time to reach the end of the path. The normalized error of the allowed path was 0.11 m. The average speed for the planned trajectory was 0.034 m/(unit of time).

The same section of the joint variables produced by the trajectory planner when traveling at 0.2 m is shown for those produced for a height of travel of 0.4 m in Figures 6.6, 6.7 and 6.8. The same portion of the desired path is also represented in these figures. In Figure 6.6 the same body movements that can be seen in Figure 6.2 can be identified, but with different values, within a close range, due to a change in height and stride length. In Figure 6.7 it can be seen that although the velocities for joint 1 during a leg transfer phase of the spinning gait is similar to what can be seen in Figure 6.3, the joint velocities seen in the leg transfer phase of the spinning gait for joints 2 and 3 are much closer to having the same magnitudes seen in the leg transfer

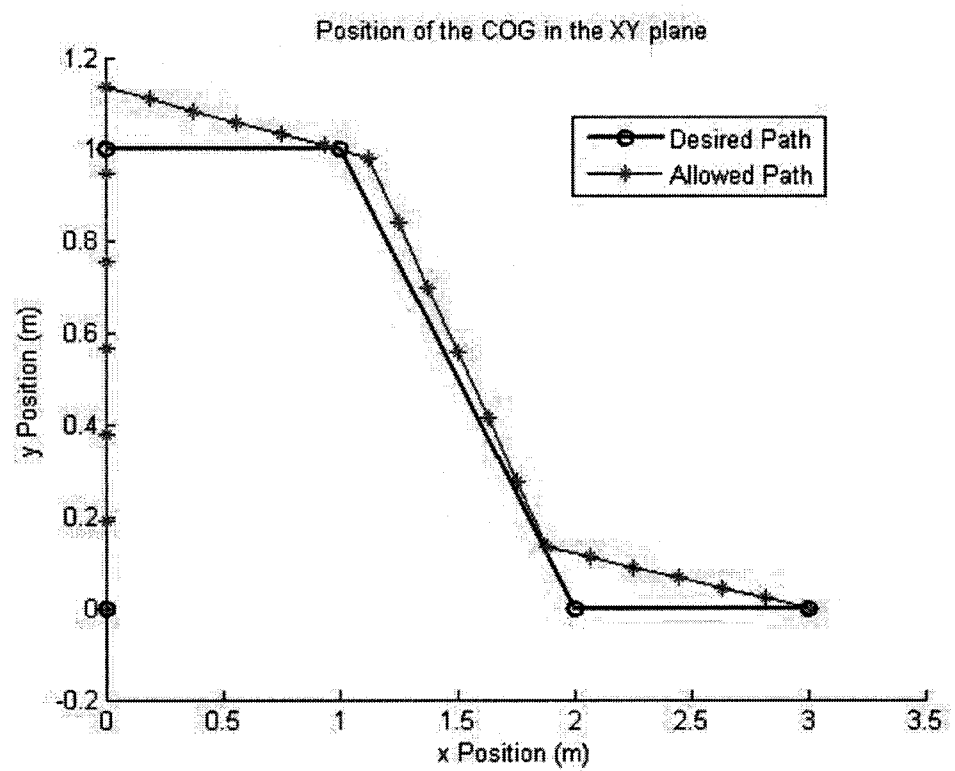


Figure 6.5: Allowed and Desired Straight Line Paths at 0.2 m

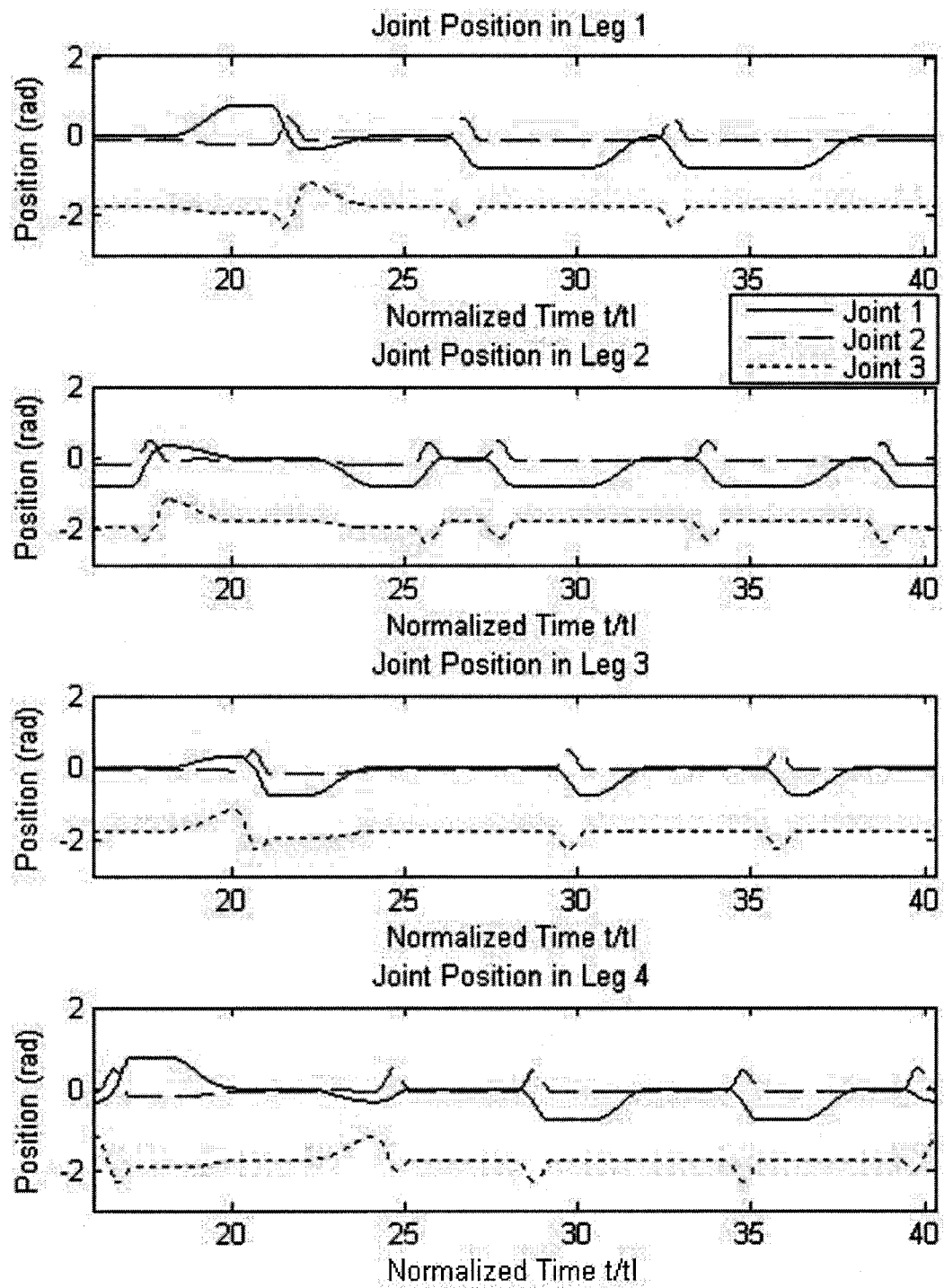


Figure 6.6: Joint Positions for a Height of Travel of 0.4 m Following a Straight Line Path

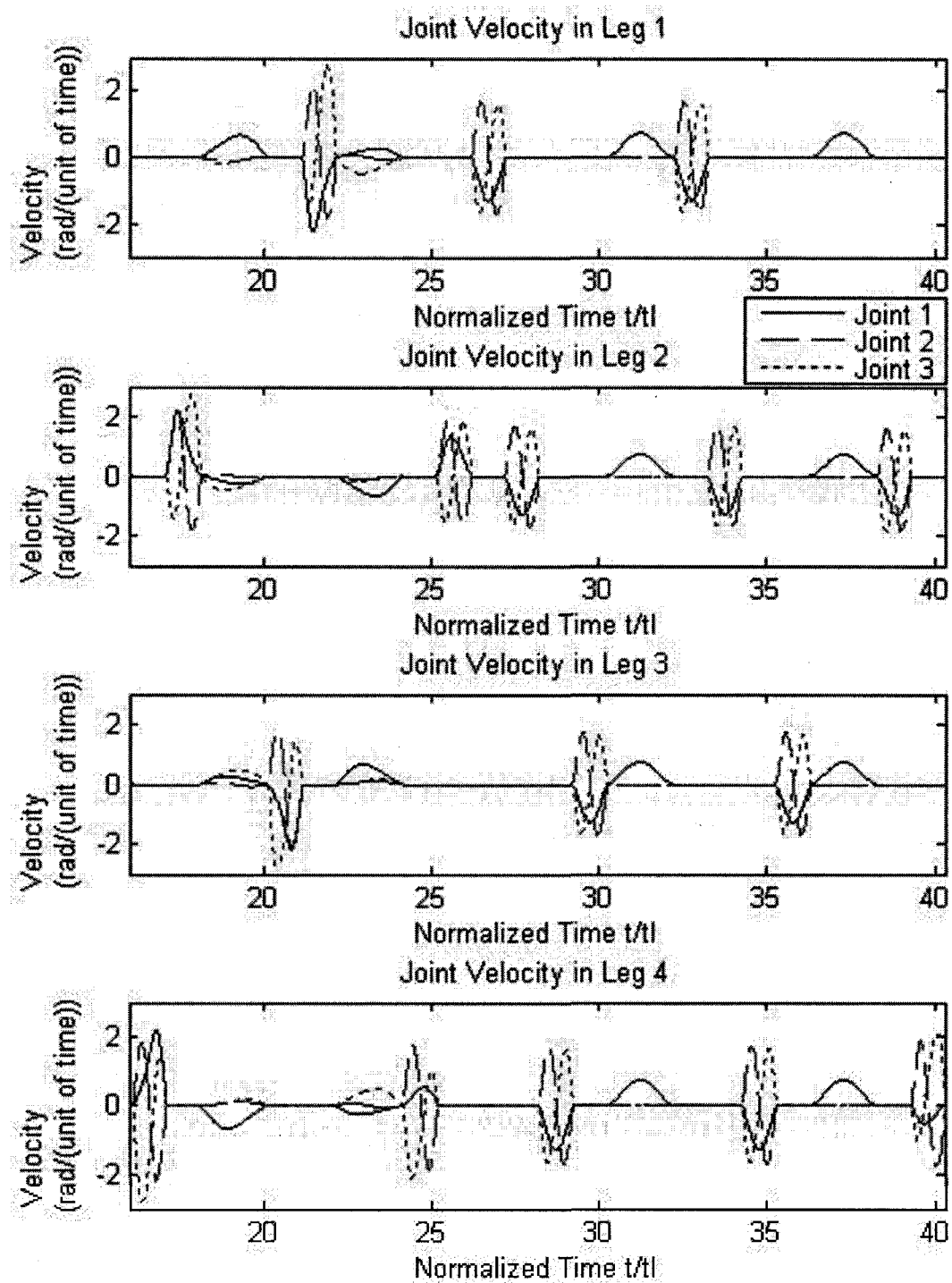


Figure 6.7: Joint Velocities for a Height of Travel of 0.4 m Following a Straight Line Path

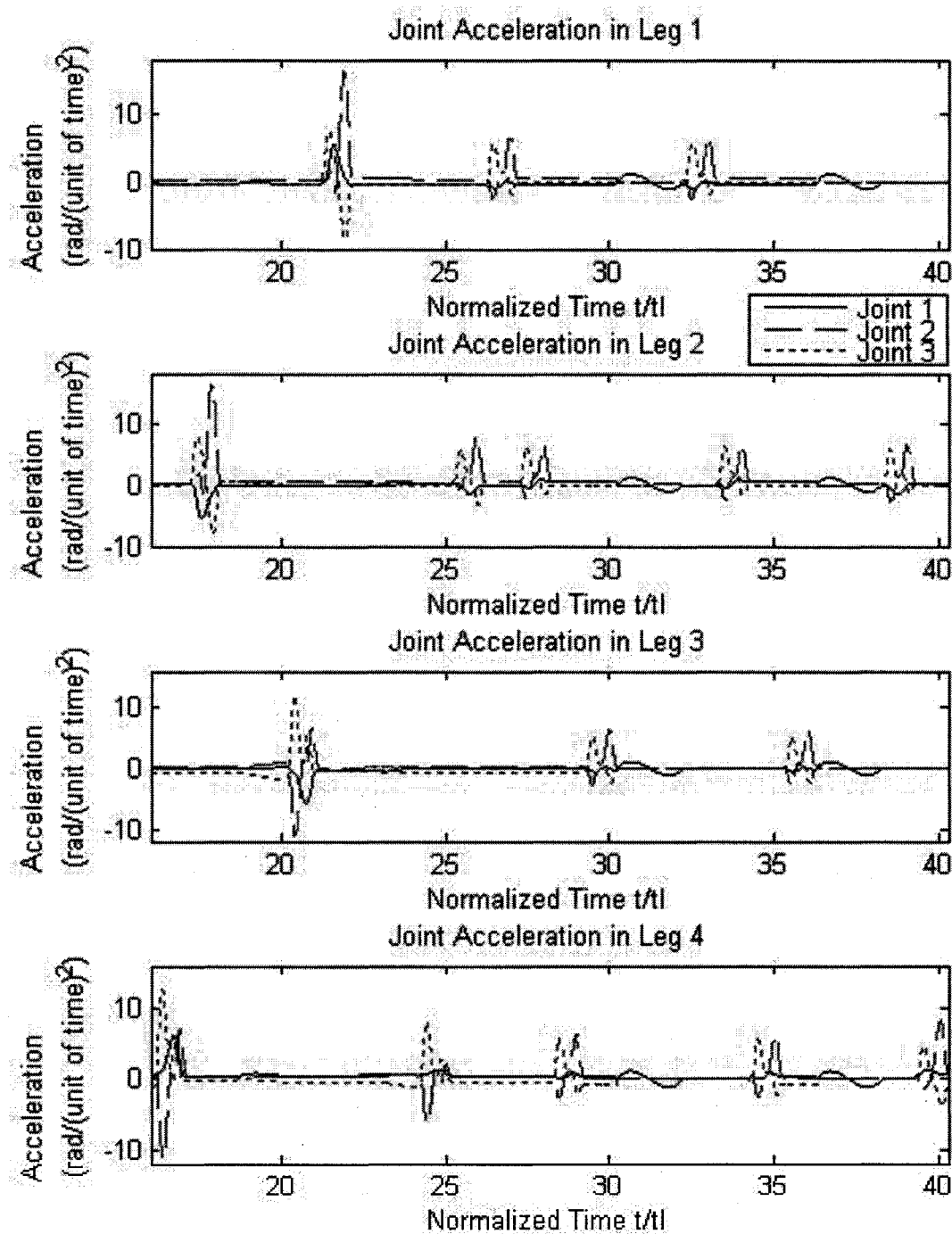


Figure 6.8: Joint Accelerations for a Height of Travel of 0.4 m Following a Straight Line Path

phase of the creeping gait as they are in Figure 6.3. This is due to the increase in the maximum height in the leg trajectory and the decrease in the stride length for the creeping gait that occurs as the height is increased.

Another noticeable difference between traveling at the two different heights can be seen in the accelerations, shown in Figures 6.4 and 6.8. Here the accelerations are in some cases nearly triple for joints 2 and 3 when traveling at a height of 0.4 m vice a height of 0.2 m. Figure 6.9 shows the allowed and desired paths at a height of

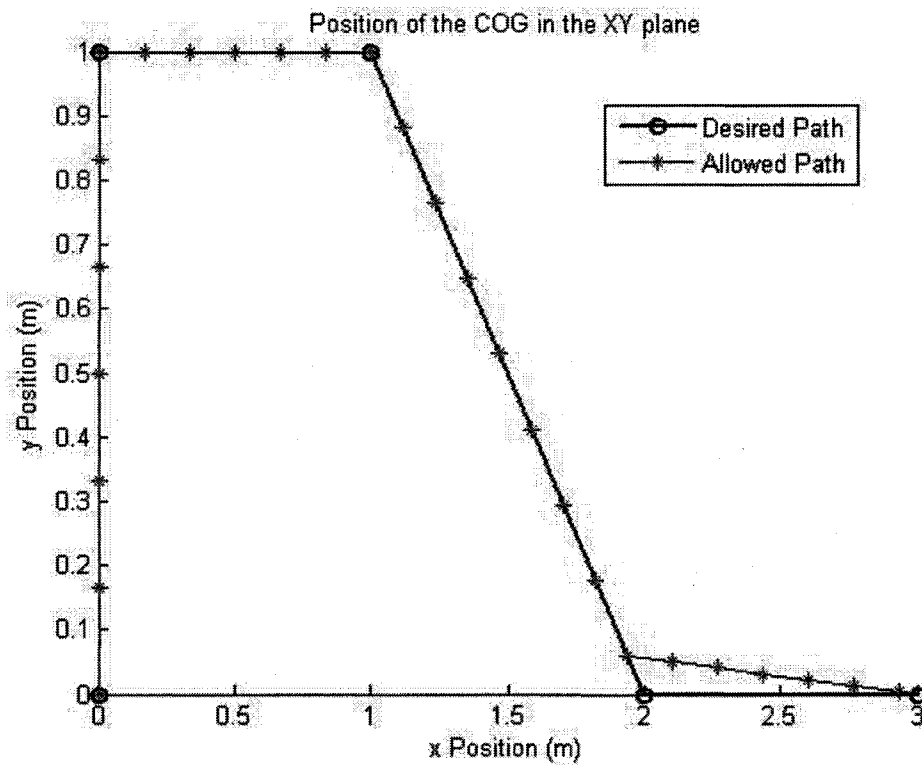


Figure 6.9: Allowed and Desired Straight Line Paths at 0.4 m

0.4 m. At this height, it took a total 140 units of time, to reach the end of the path. The normalized error of the planned trajectory was only 0.04 m. The average speed for the trajectory was 0.031 m/(unit of time).

For a CoG height of travel of 0.6 m, the trajectory planner produced the following time histories for the joint variables for the same section of the path discussed earlier, shown in Figures 6.10, 6.11 and 6.12. Because of large difference in stride length

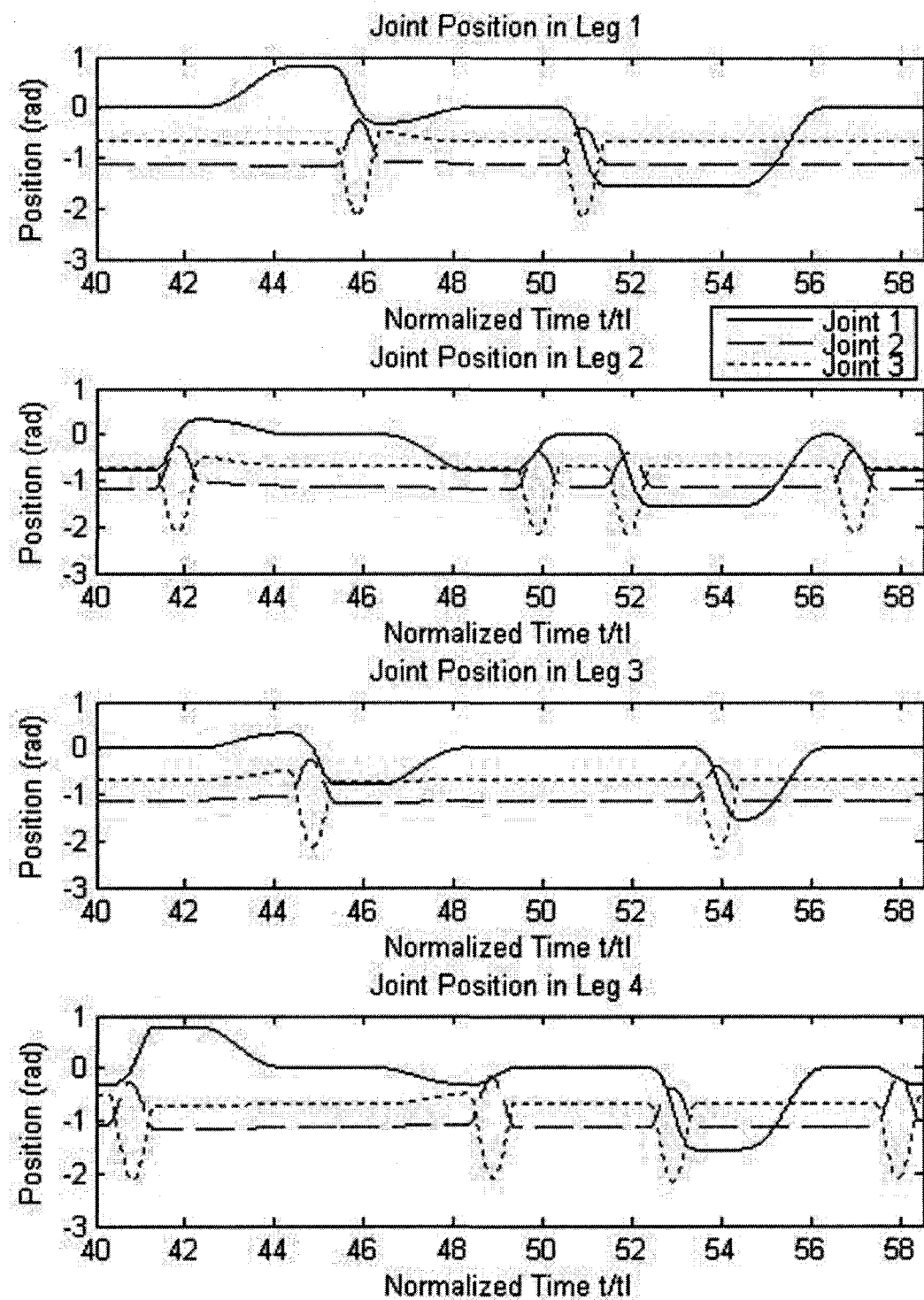


Figure 6.10: Joint Positions for a Height of Travel of 0.6 m Following a Straight Line Path

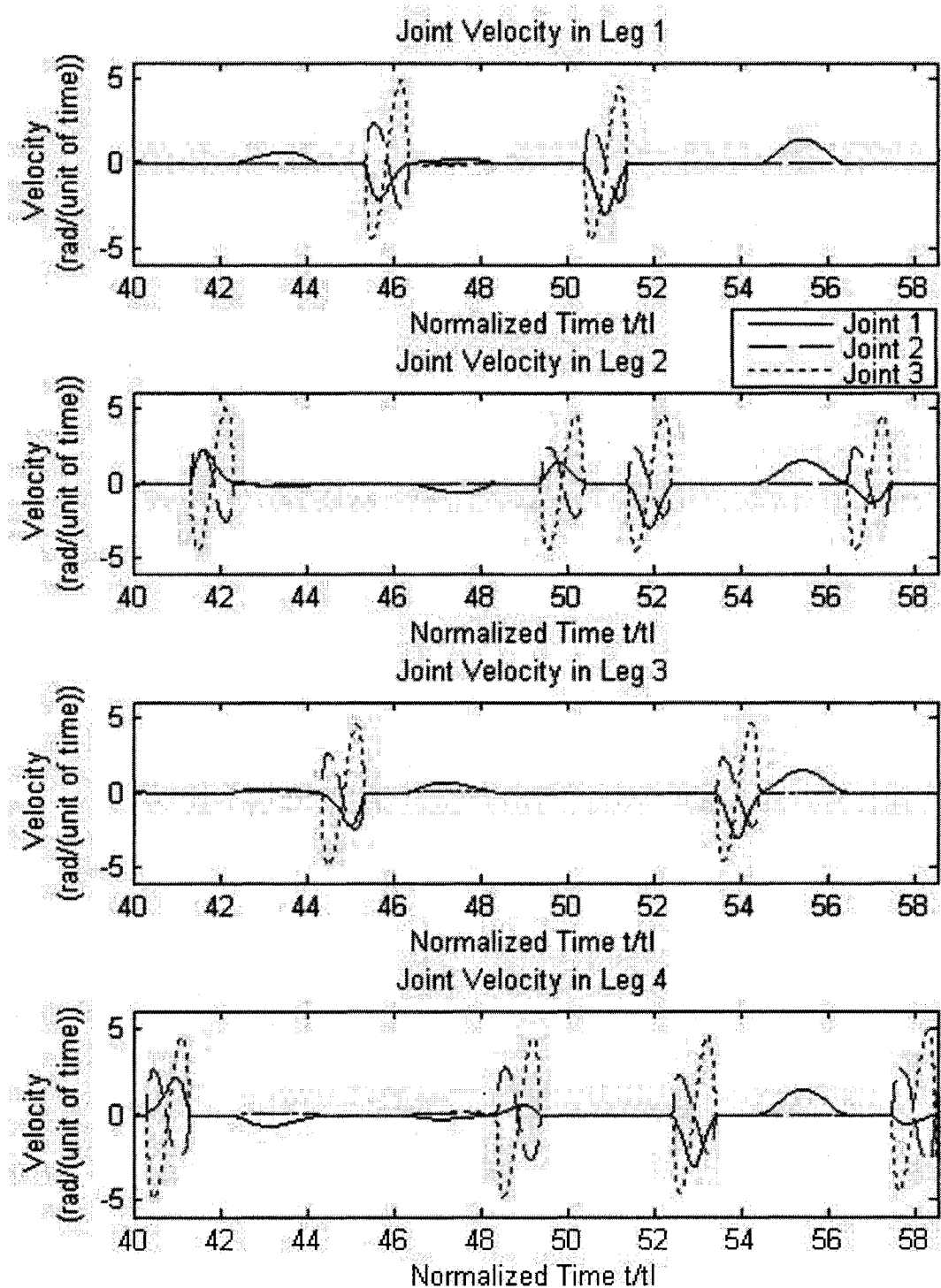


Figure 6.11: Joint Velocities for a Height of Travel of 0.6 m Following a Straight Line Path

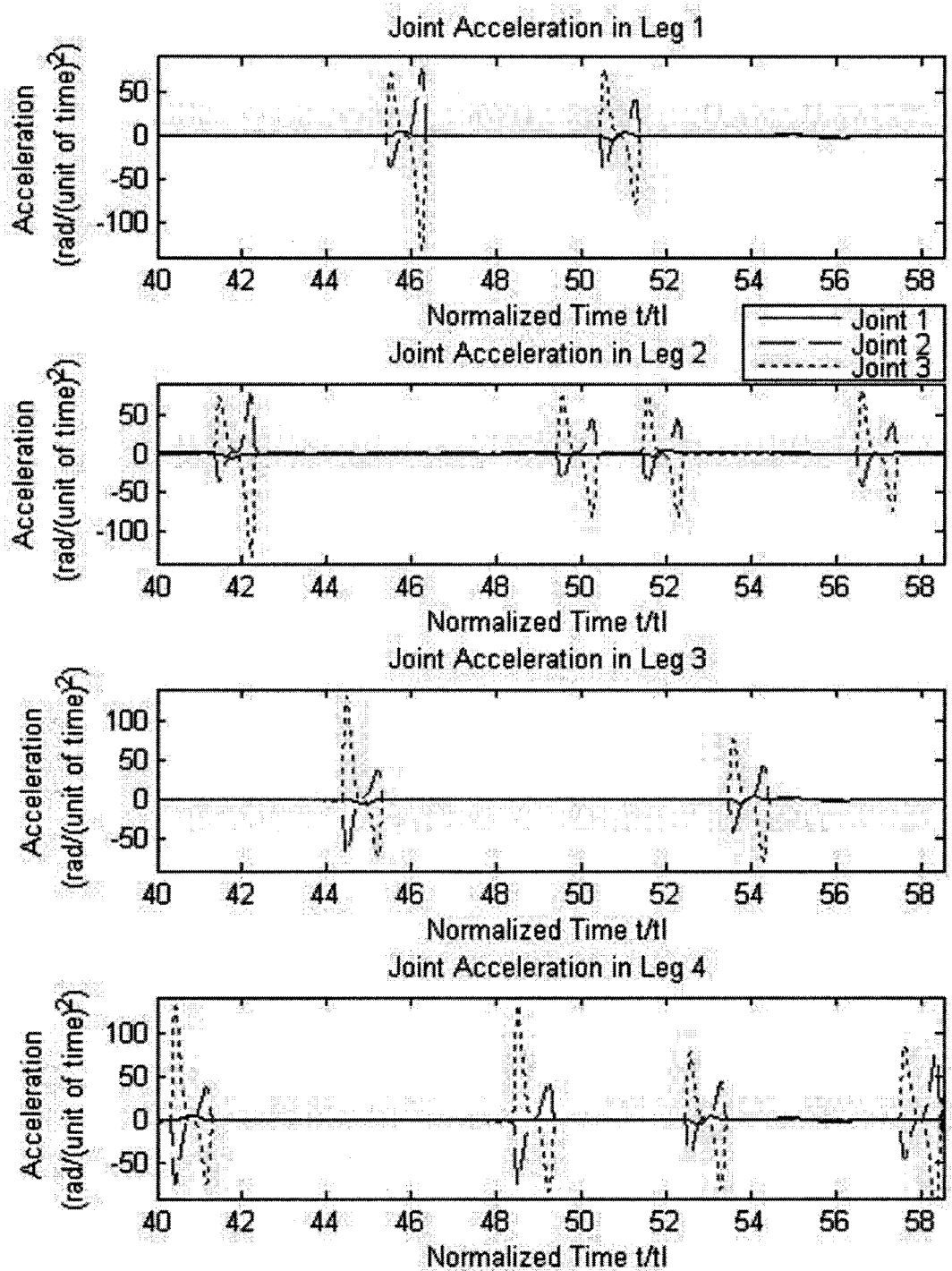


Figure 6.12: Joint Accelerations for a Height of Travel of 0.6 m Following a Straight Line Path

for the creeping gaits at different heights, the same section of the path is this time covered during time periods 40 to 58. Another change can be seen in Figure 6.10 where only one cycle of the spinning gait is carried out and occurs between times 50 to 56. Referring to Figure 6.13, it can be seen that only one cycle of the spinning gait is carried out because in this case the angle of re-orientation is just under $\pi/2$. This, as well as a shortened stride length, is also a factor as to why in Figure 6.11 the velocities for all the joints in the leg transfer phase of the creeping and spinning gaits are quite similar.

When traveling at a height of 0.6 m, the joint accelerations for joints 2 and 3 during the leg transfer phases, shown in Figure 6.12, are significantly larger than when traveling at lower heights. This could become problematic if it is decided to travel at the high range of possible heights of travel for the CoG.

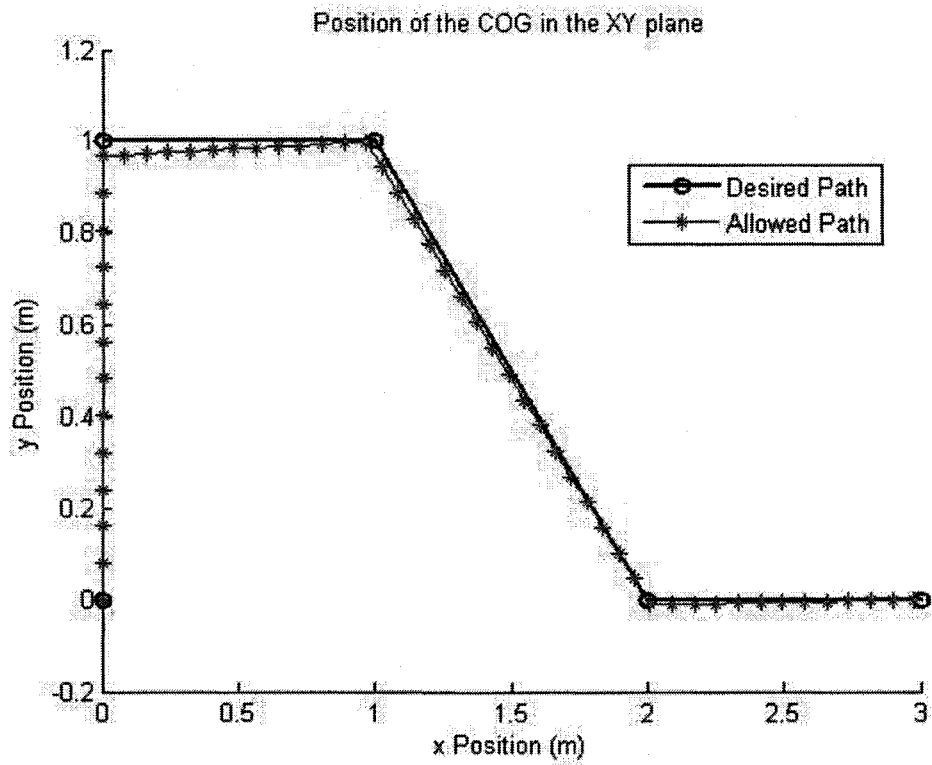


Figure 6.13: Allowed and Desired Straight Line Paths at 0.6 m

Figure 6.13 shows the allowed and desired trajectories at a height of 0.6 m. At

this height, it took a total of 246 units of time, significantly longer than the other heights, to reach the end of the path. The normalized error of the planned trajectory was very close to the normalized error when traveling at a height of 0.4 m and was 0.03 m. The average speed for the trajectory was 0.018 m/(unit of time).

Table 6.1: Performance Values for a Straight Line Path at Different Heights

Parameter	0.2 m	0.4 m	0.6 m
Normalized Time t/t_l	132	140	246
Distance (m)	4.54	4.33	4.36
Average Speed (m/(unit of time))	0.034	0.031	0.018
Normalized Error (m)	0.11	0.04	0.03

The desired path was most closely followed for a height of travel of 0.6 m. With a smaller λ the trajectory planner had the ability to produce an allowed path that followed the desired path more closely, but would require more body movements owing to a slower average speed. It should be noted that the distance to be traveled on each leg of the path will affect the performance of the planned trajectory. If the distance to the waypoint is a multiple of the stride length, the allowed path will follow more closely.

For a CoG height of travel of 0.4 m the planned trajectory had almost the same error as for 0.6 m but the average speed was faster, closer to that for the planned trajectories produced for a height of 0.2 m. Compared to a height of 0.2 m, it was slightly slower, but the allowed path followed the desired path more closely. As discussed earlier, this could simply be a result that the waypoints were closer to being multiples of the stride length at 0.4 m.

From the joint histories produced by the trajectory planner for the straight line path, the different movements required for the different gaits can be identified. As the height of travel of the CoG increased, the velocities and accelerations required for joints 2 and 3 for the leg transfer phases of the spinning gait became more comparable to those required during the leg transfer phase of the creeping gait. This was due to the decrease in the stride length and an increase in the maximum height of the leg trajectories. Another important change that occurred as the height was increased,

that was also a result of the higher maximum leg height, was the increase in velocity and acceleration. This was very significant in the acceleration when traveling at a height of 0.6 m.

6.2 Results of the Trajectory Planner for the Follow of a Circular Path

The circular path has a radius of 1 m. The path is illustrated in Figure 6.14. The distance of the desired path was a total of 6.28 m. The results for the circular path are shown in Table 6.2 at the end of the section. A representative section of the joint

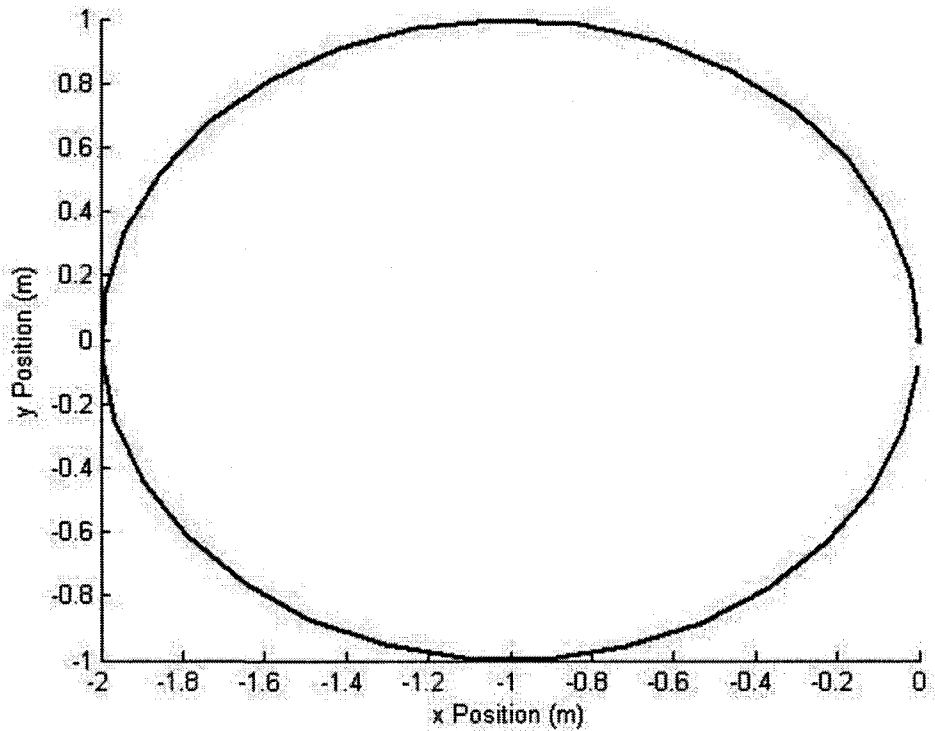


Figure 6.14: Circular Path

variables produced by the trajectory planner to allow a robot to follow the desired path for a height of travel of 0.2 m are shown in Figures 6.15, 6.16 and 6.17. From Figure 6.15, the different movements that occur between time periods 0 and 18 can be identified. During time 0-2 legs 4 and 2 are transferred to position two. Then a cycle of the spinning gait is carried out, times 2 to 8, the transfers of legs 2 and 4 are

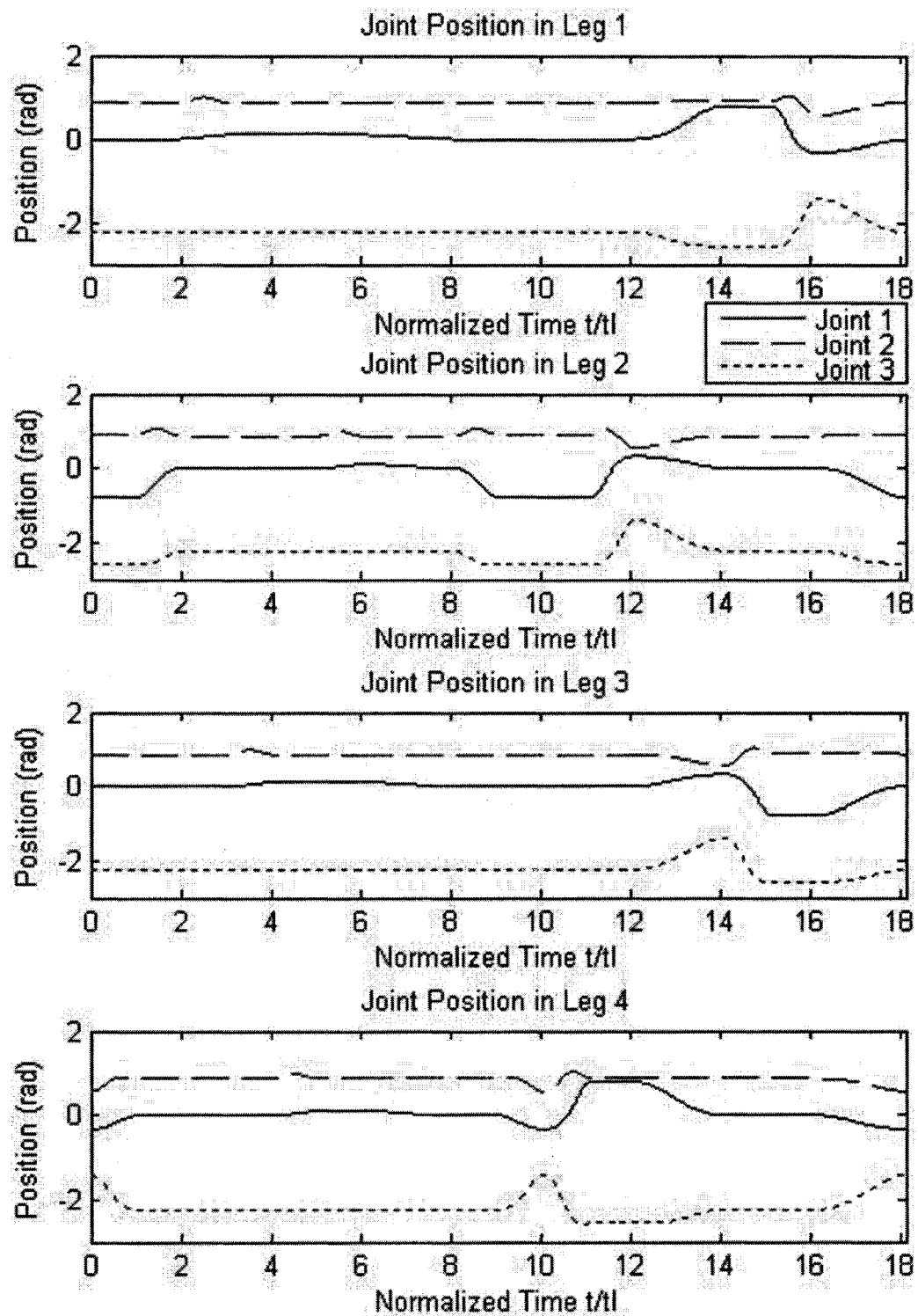


Figure 6.15: Joint Positions for a Height of Travel of 0.2 m Following a Circular Path

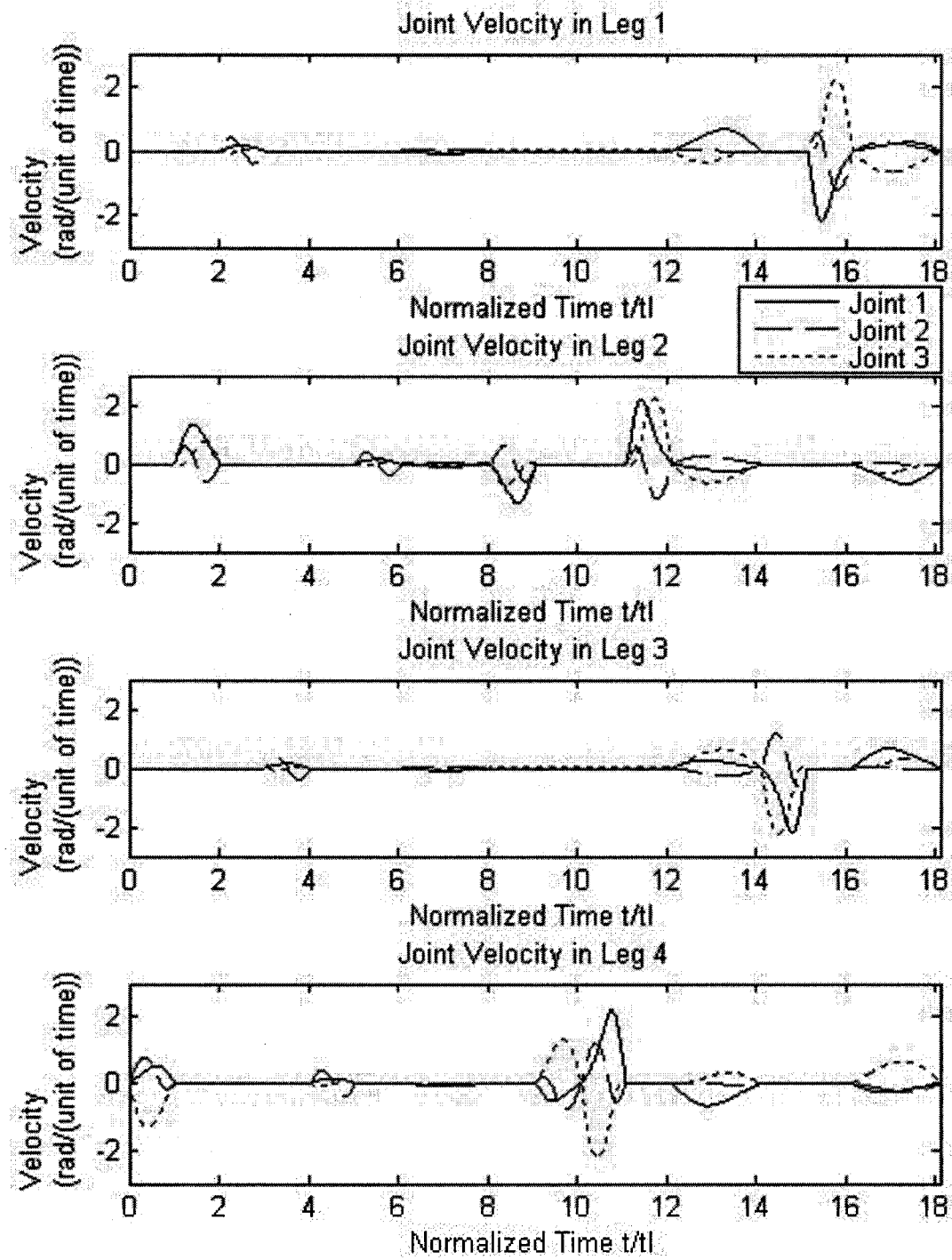


Figure 6.16: Joint Velocities for a Height of Travel of 0.2 m Following a Circular Path

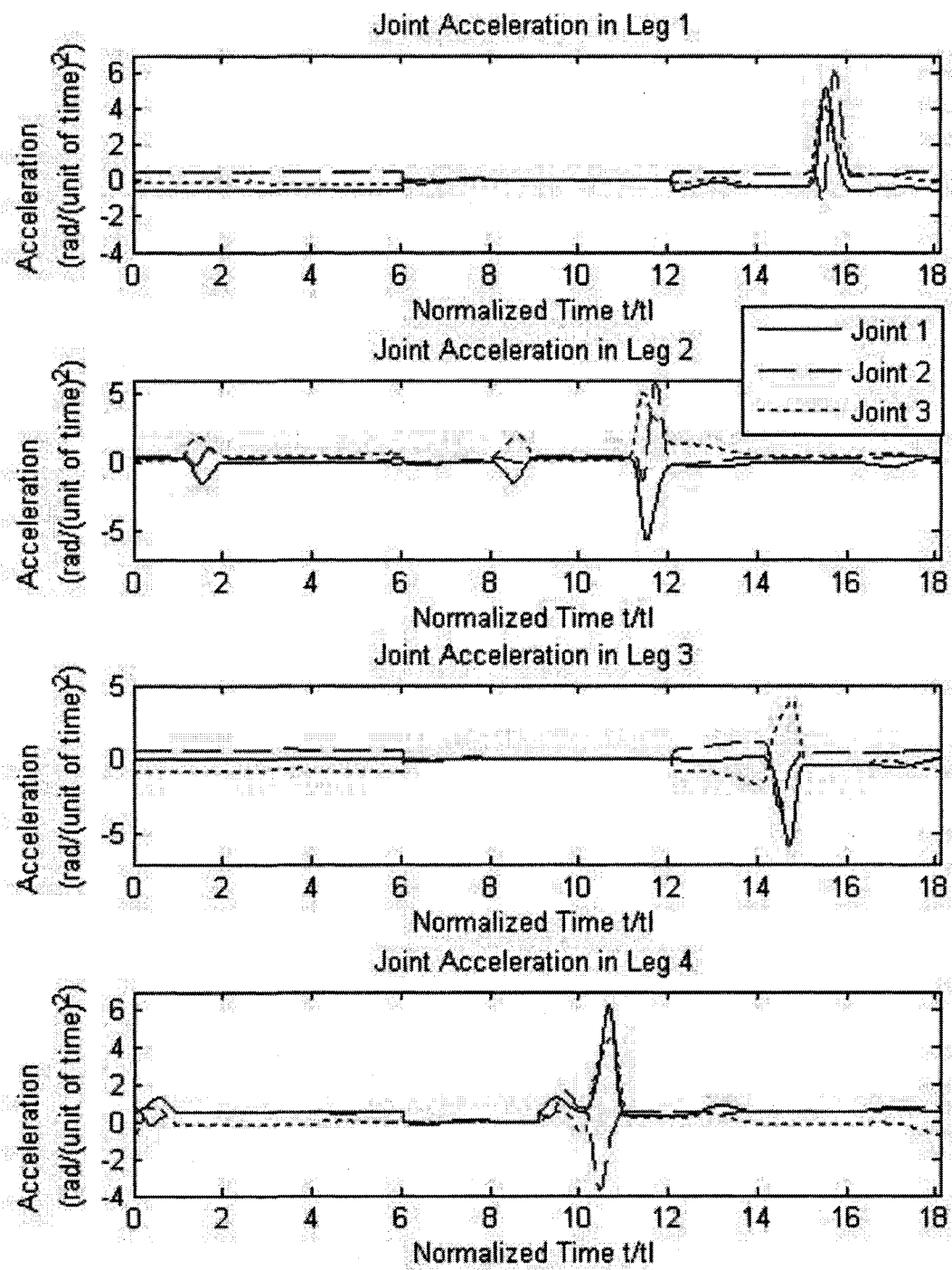


Figure 6.17: Joint Accelerations for a Height of Travel of 0.2 m Following a Circular Path

carried out and then the creeping gait begins at time 10. At time 18, one cycle of the creeping gait is completed. This representative cycle is repeated to complete the trajectory for the follow of the circle. The movements that occur during the spinning gait are not strongly pronounced in Figure 6.15 as only small changes occur, with an angle of re-orientation less than ten degrees. These movements are more noticeable in Figures 6.16 and 6.17. The leg movement pattern for the spinning gait is also easier to see in these figures and is 1-3-4-2, different for that seen with the straight line paths. Again, for a height of travel of 0.2 m, the joint accelerations and velocities are largest in magnitude for the leg transfer phases of the creeping gait. The performance of the trajectory planner for a circular path for a CoG height of travel of 0.2 m, is shown in Figure 6.18. It took a total of 418 units of time, to reach the end of the path, for

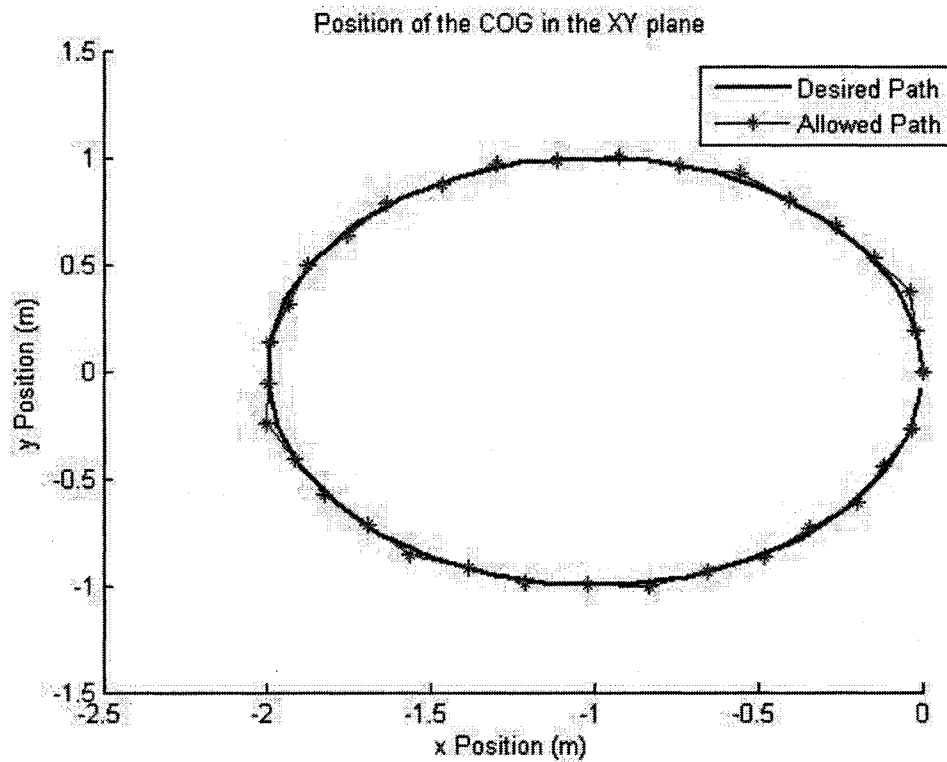


Figure 6.18: Allowed and Desired Circular Paths at 0.2 m

a height of 0.2 m. The normalized error of the planned trajectory was 0.10 m. The average speed for the trajectory was 0.015 m/(unit of time).

Sections of the joint trajectories produced for the trajectory planner for a height of travel of 0.4 m are shown in Figures 6.19, 6.20 and 6.21. As seen with the straight line path, the joint velocities for joints 2 and 3 during the leg transfer phases of the spinning gait are closer to those of that occur during the leg transfer phases of the creeping gait at a higher versus a lower height of CoG travel. As well the required joint accelerations for joints 2 and 3 are also larger at a higher height of travel.

Figure 6.22 shows the allowed and desired paths for a height of 0.4 m. At this height, it took a total 462 units of time, to reach the end of the path. The normalized error of the planned trajectory was 0.09 m. The average speed for the trajectory was 0.014 m/(unit of time).

For a CoG height of travel of 0.6 m, the trajectory planner produced the following time histories for the joint variables for the first 18 units of time for the full trajectory, shown in Figures 6.23, 6.24 and 6.25. Figure 6.23 shows a very distinct change in joint positions during the leg movement phases of the creeping gait, as well as distinct changes of position for joints 2 and 3 during the leg transfer phases of the spinning gait. This translates into increased velocities and accelerations which can clearly be seen in Figures 6.24 and 6.25. Again the accelerations required for joints 2 and 3 in the leg transfer phases are noticeably large. Figure 6.26 shows the allowed and desired circular paths for a height of 0.6 m. At this height, it took a total of 618 units of time to reach the end of the path. The normalized error of the planned trajectory was again low, 0.04 m, and similar to the values of the normalized errors for the straight path. The average speed for the trajectory was 0.010 m/(unit of time).

Table 6.2: Performance Values for a Circular Path at Different Heights

Parameter	0.2 m	0.4 m	0.6 m
Normalized Time t/t_l	418	462	618
Distance (m)	6.06	6.32	6.13
Average Speed (m/(unit of time))	0.014	0.014	0.010
Normalized Error (m)	0.10	0.09	0.04

For the circular path, the same general results were obtained. For a CoG height of 0.6 m the average velocity was slowest, but the normalized error was the smallest.

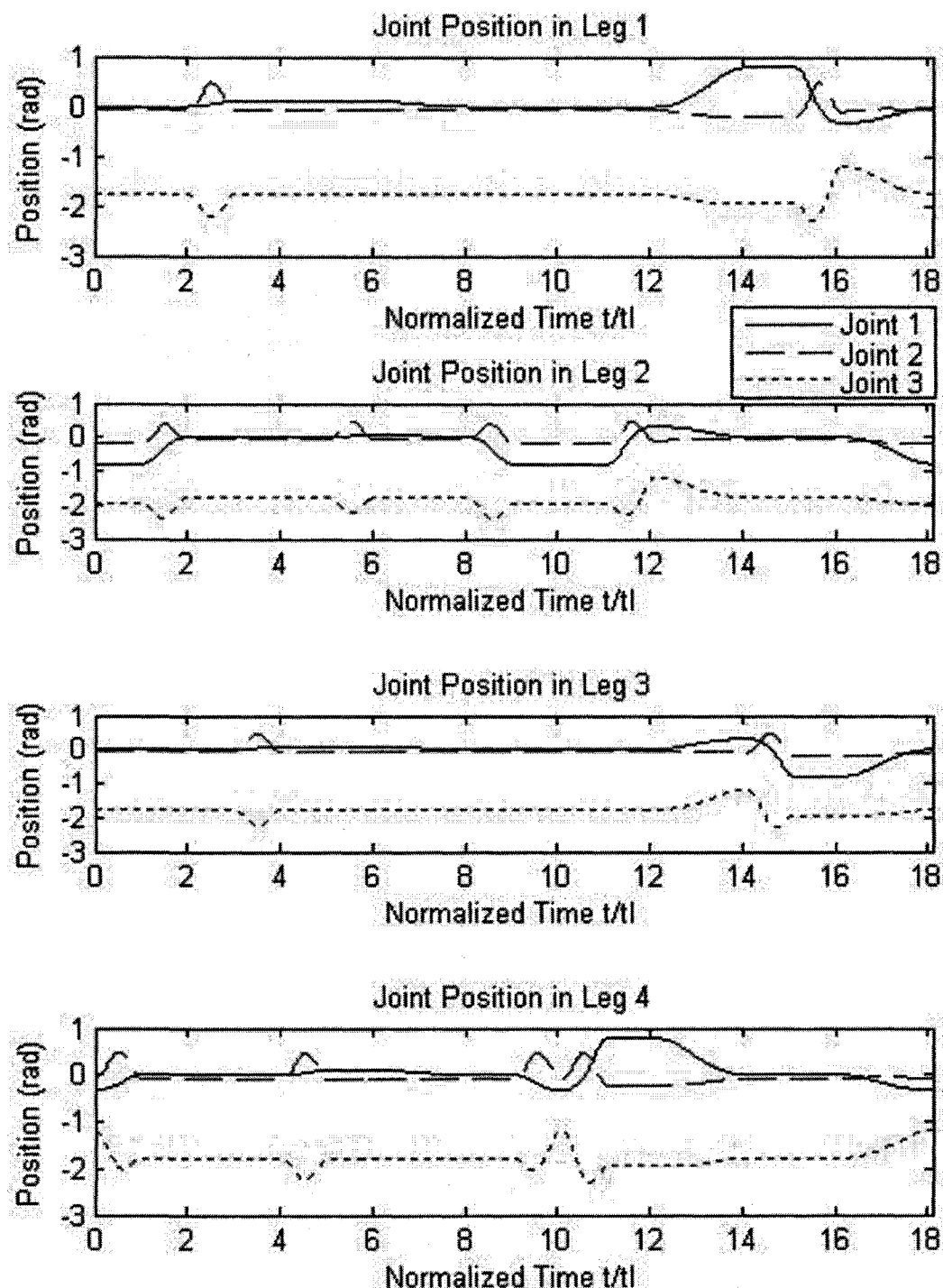


Figure 6.19: Joint Positions for a Height of Travel of 0.4 m Following a Circular Path

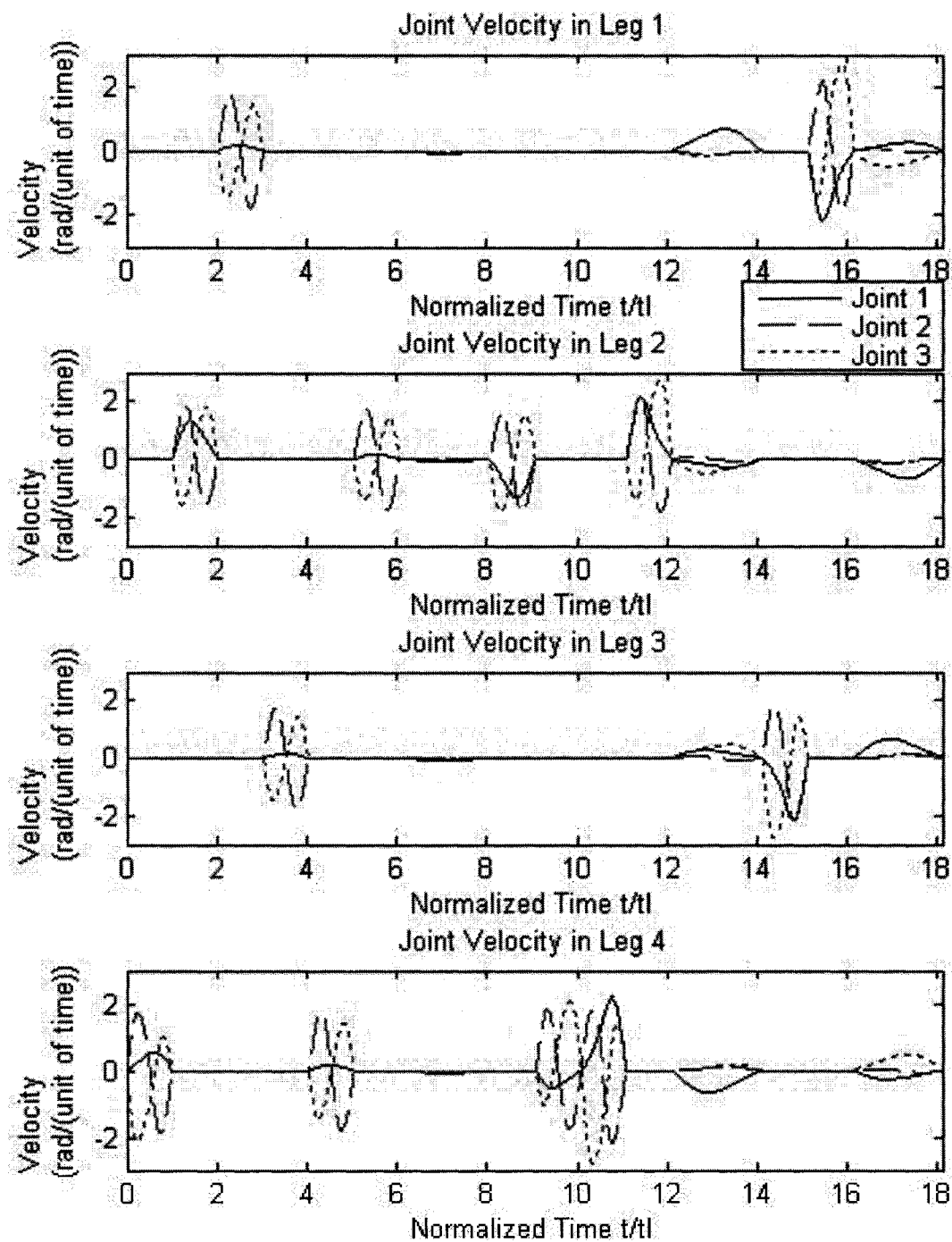


Figure 6.20: Joint Velocities for a Height of Travel of 0.4 m Following a Circular Path

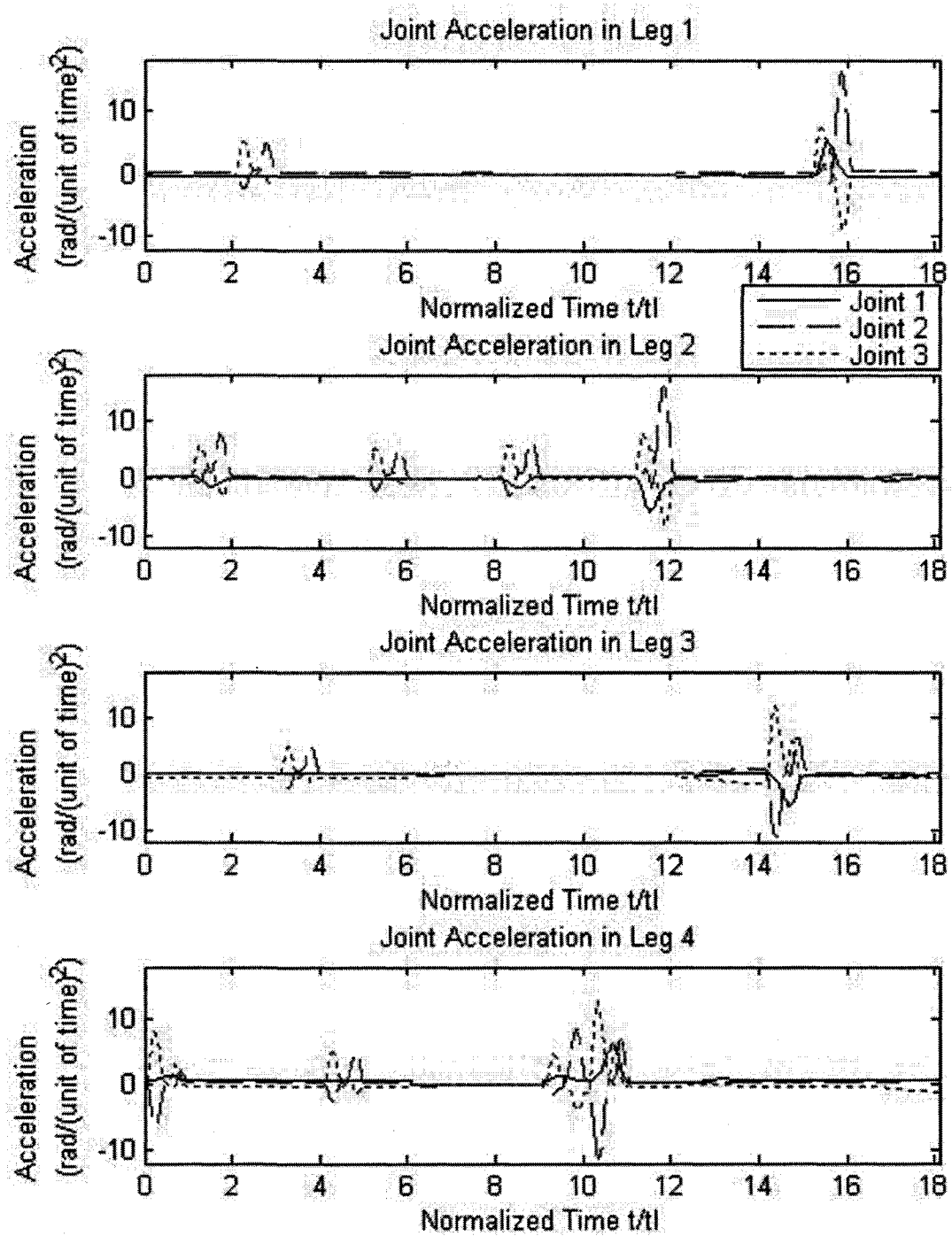


Figure 6.21: Joint Accelerations for a Height of Travel of 0.4 m Following a Circular Path

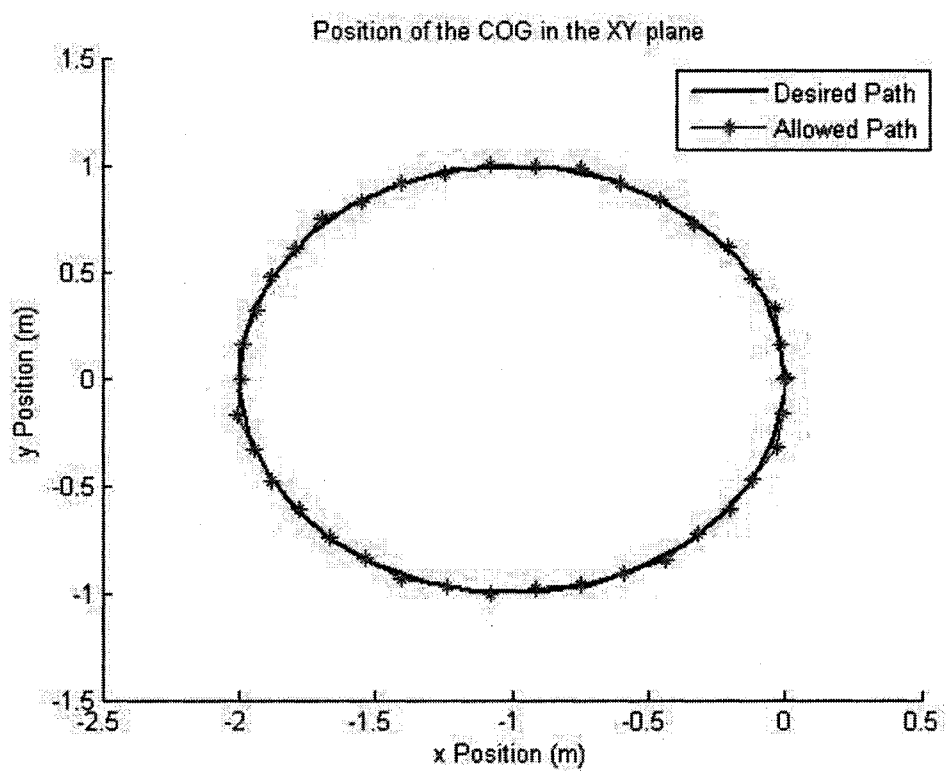


Figure 6.22: Allowed and Desired Circular Paths at 0.4 m

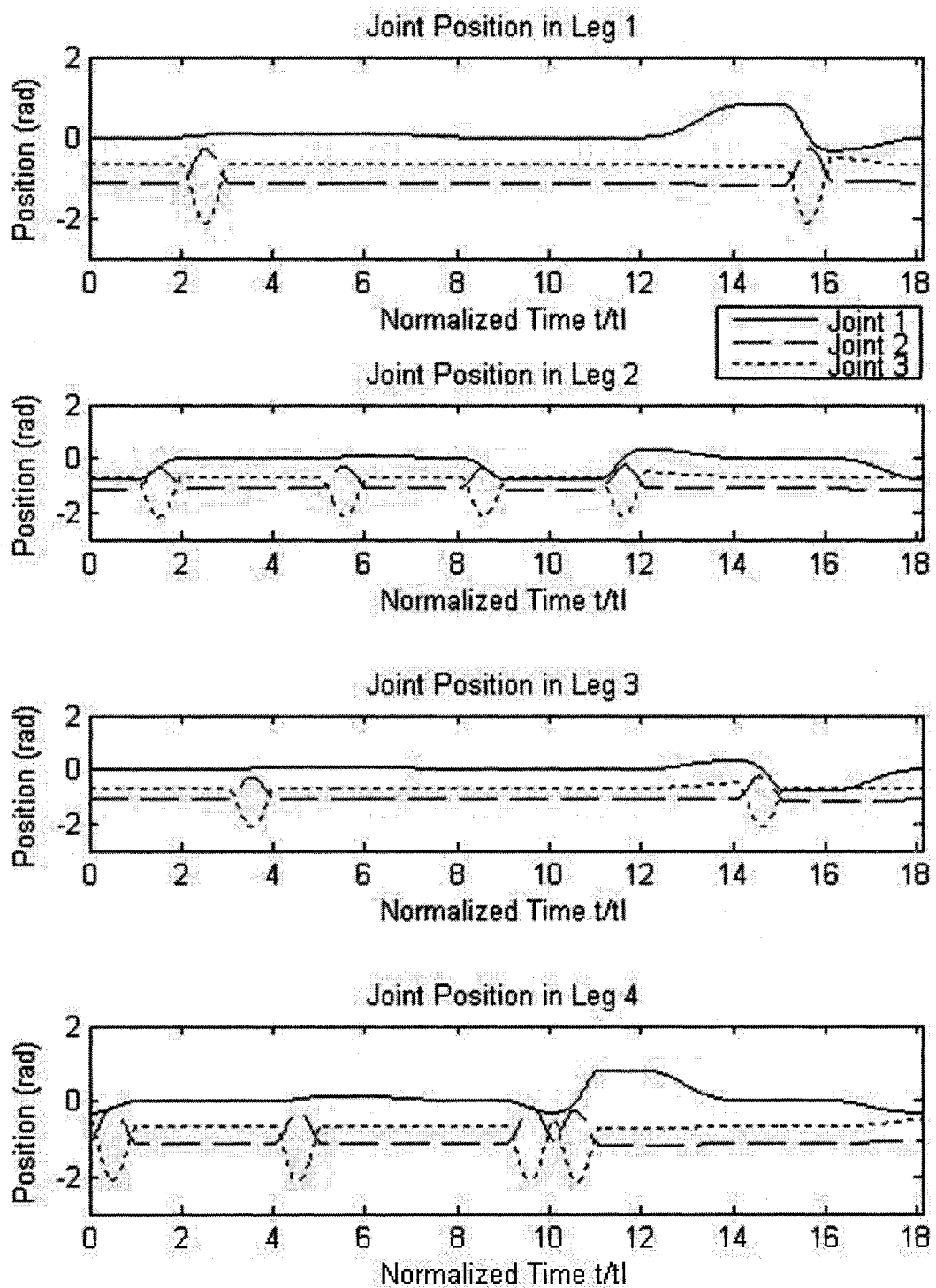


Figure 6.23: Joint Positions for a Height of Travel of 0.6 m Following a Circular Path

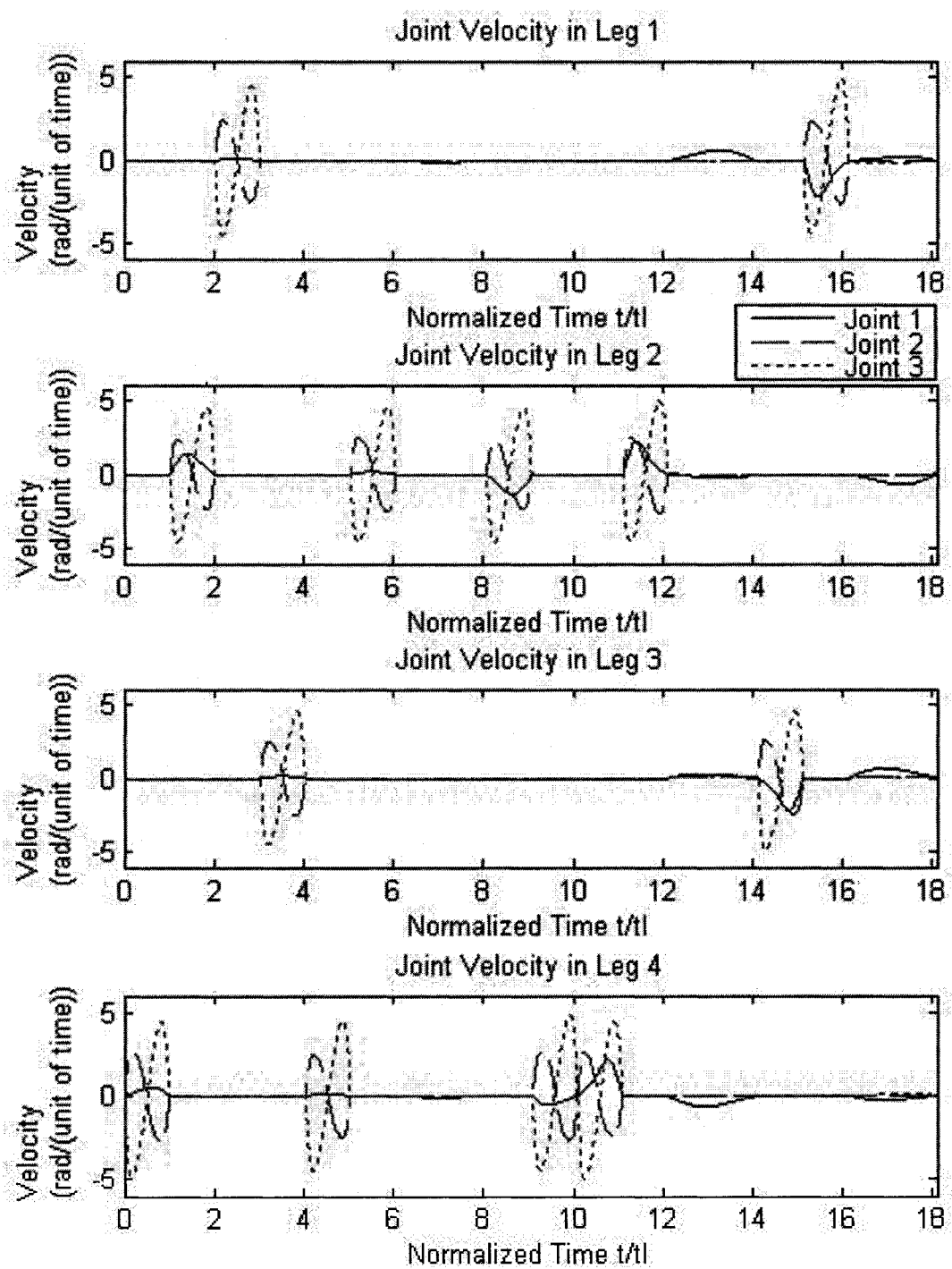


Figure 6.24: Joint Velocities for a Height of Travel of 0.6 m Following a Circular Path

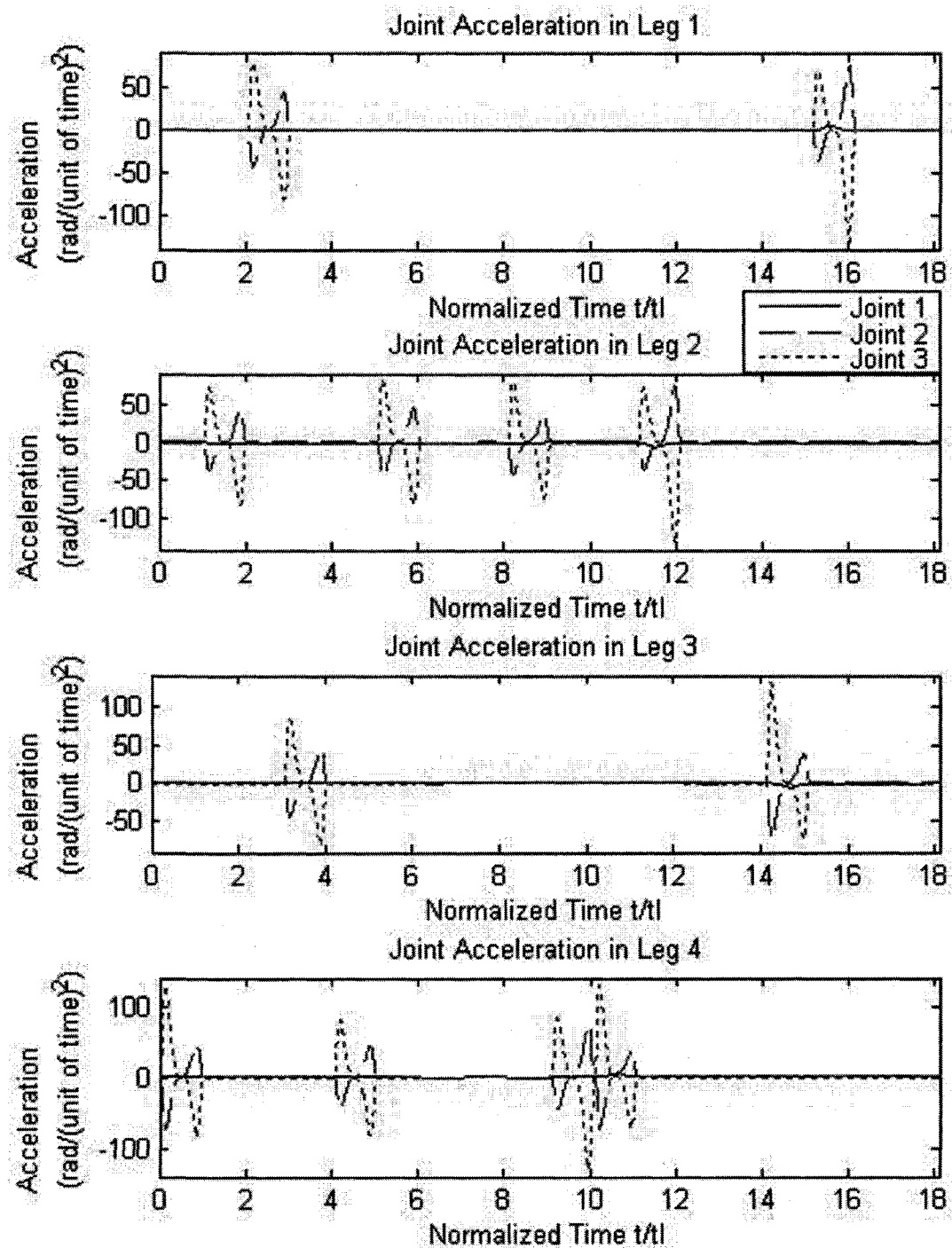


Figure 6.25: Joint Accelerations for a Height of Travel of 0.6 m Following a Circular Path

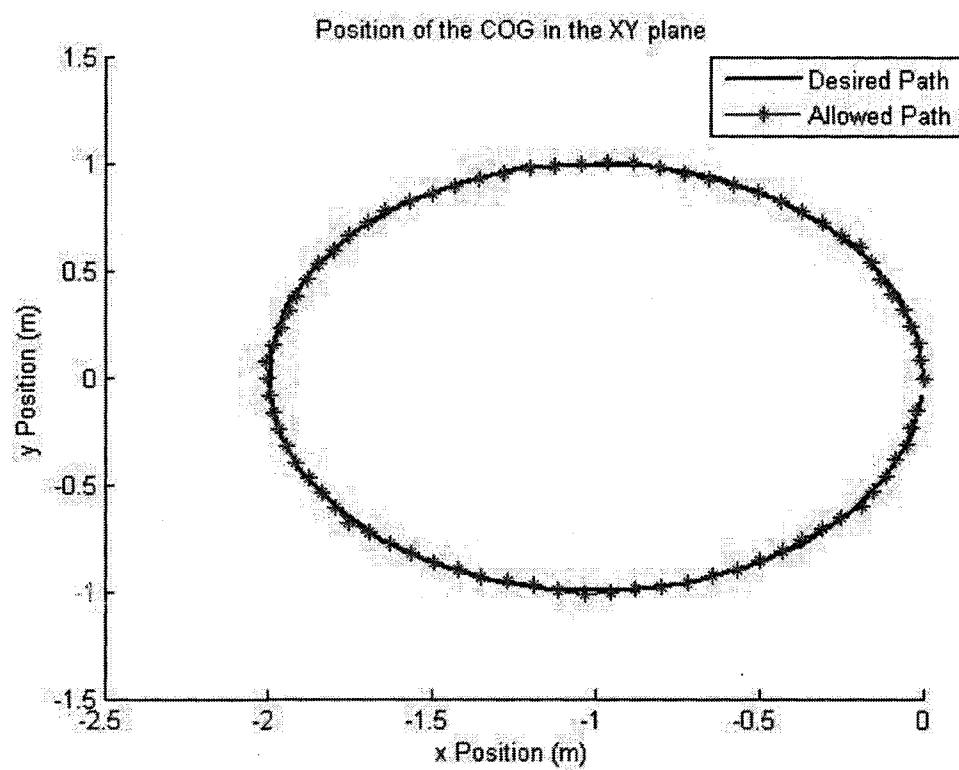


Figure 6.26: Allowed and Desired Circular Paths at 0.6 m

The results for CoG heights of 0.2 m versus 0.4 m were very close.

The joint histories produced by the trajectory planner for the circular path clearly show a repetition of the creeping and spinning gaits at regular intervals. As with the straight line path, an increase in the height of travel of the CoG led to increases in joint positions, velocities and accelerations. The increases in joint accelerations were very large when traveling at a height of 0.6 m.

6.3 Results of the Trajectory Planner when the Accuracy of the Follow is Purposely Reduced

It is important to note that the actual body of the SILO 4 robot is 0.31 m by 0.31 m. This means that normalized errors of 0.04 m or even 0.11 m would still allow the body of the robot over the desired waypoint. This means that depending on the task at hand, the allowed speed of the robot could be improved at the cost of accuracy while still allowing the body of the robot to be over the desired path. To demonstrate this idea the decision process of the trajectory planner was changed so that the plan would only produce joint variables for a forward walk if the waypoint was more than 0.15 m away in the y direction and the spinning gait would only be used to plan for re-orientation only if the distance to waypoint in the x direction was larger than 0.15 m. A trajectory was then planned for the circular path at all three heights. The results for the allowed paths are shown in Table 6.3 and are illustrated in Figures 6.27 to 6.29.

Table 6.3: Performance Values for a Circular Path at Different Heights With Decreased Accuracy

Parameter	0.2 m	0.4 m	0.6 m
Normalized Time t/t_l	252	266	434
Distance (m)	5.68	5.99	6.13
Average Speed (m/(unit of time))	0.023	0.023	0.014
Normalized Error (m)	0.24	0.16	0.17

From the figures it can be seen that the path can still followed relatively well. Tables 6.3 and 6.2 can be compared and it is easily seen that the average speed is increased in all cases, but the ability to closely follow the path decreases significantly

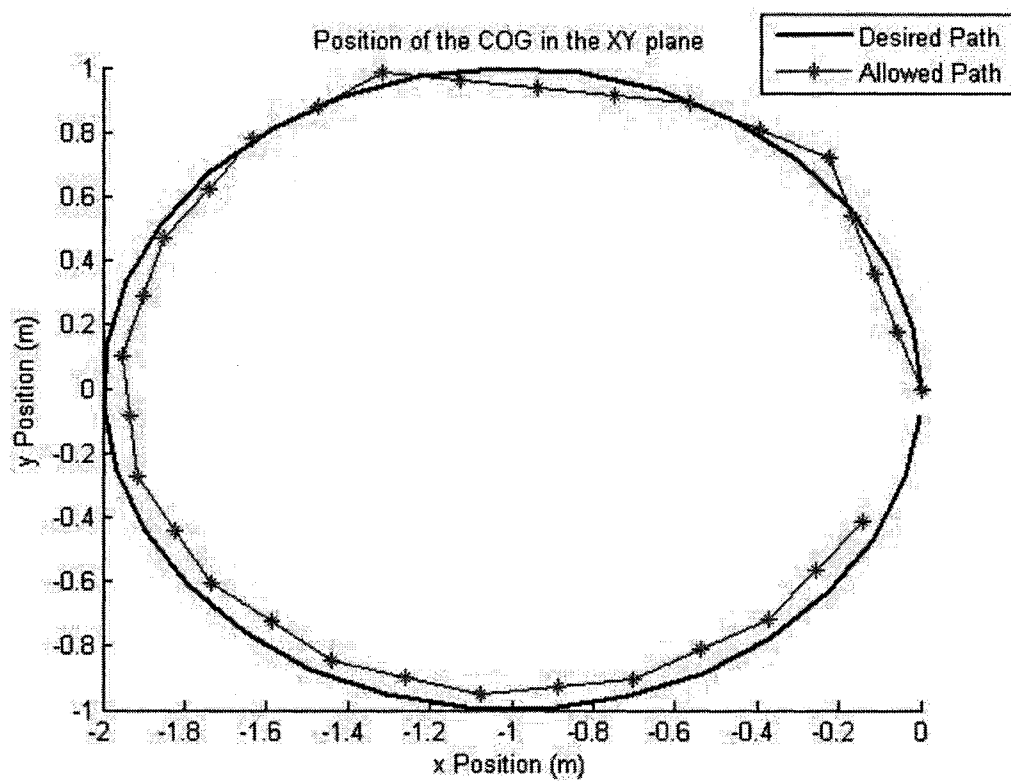


Figure 6.27: Allowed and Desired Circular Paths at 0.2 m With Decreased Accuracy

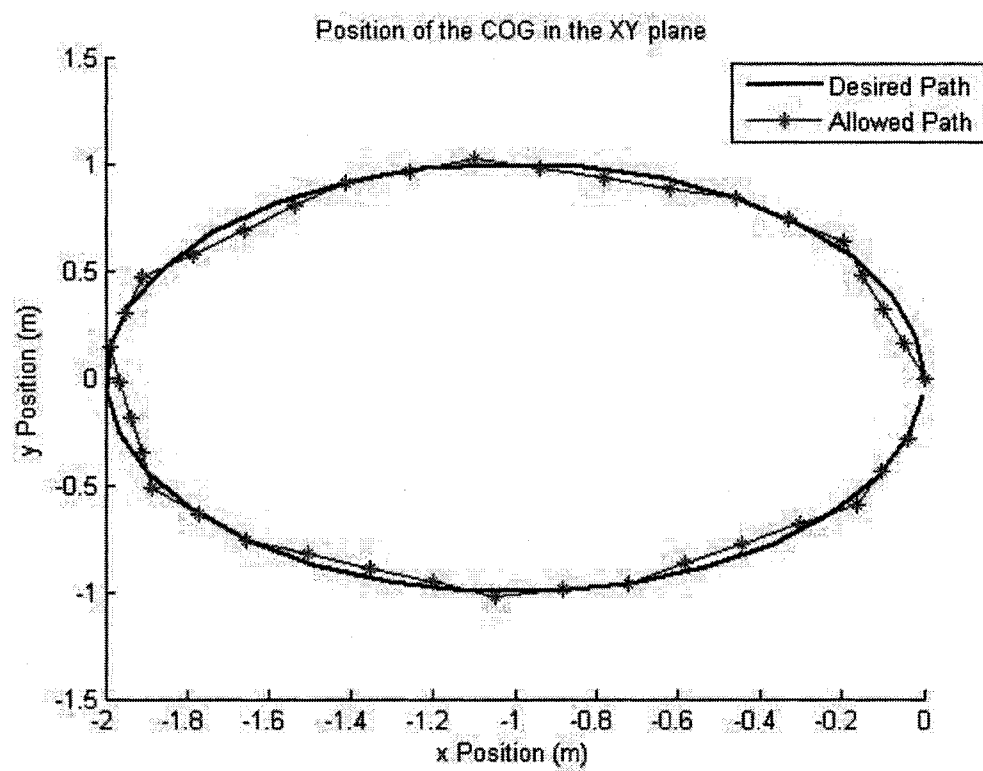


Figure 6.28: Allowed and Desired Circular Paths at 0.4 m With Decreased Accuracy

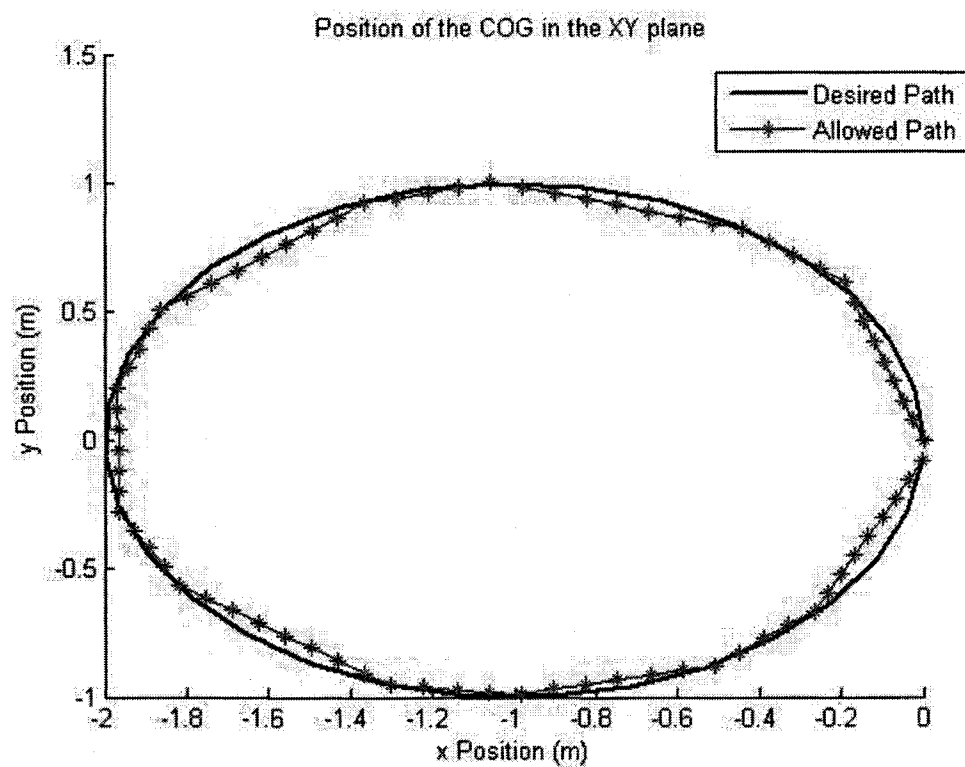


Figure 6.29: Allowed and Desired Circular Paths at 0.6 m With Decreased Accuracy

specifically for a CoG height of 0.6 m. It has been shown that if required the speed can be increased, but at a cost to the accuracy with which the planned trajectory would allow the robot to closely follow the desired path.

6.4 An Example of a Ditch Crossing for a Quadruped Robot

As discussed in the introduction, legged robots have several advantages over wheeled robots specifically when it comes to maneuverability on various terrain. The trajectory planning method described in this thesis was designed for use on fair horizontal terrain. Generally speaking this is the terrain on which wheeled robots have better performance than legged robots. Using the proposed trajectory planner however, a quadruped robot could traverse deep ditches or holes in the ground. Such obstacles would not be traversable for wheeled robots. Figure 6.30 shows the body and feet positions for the robot when traversing a 15 cm wide ditch of possibly infinite depth. The stars represent the footholds, the body positions are outlined and the ditch is represented by a thick horizontal line in the figure.

The figure shows that the CoG a robot can clear the ditch with the footholds located on either side. For the two phase discontinuous creeping gait, the width of ditch that a robot can clear is less than $\lambda/2$ as this is the maximum distance that the body would be shifted during one motion. The example illustrated in Figure 6.30 demonstrates the terrain maneuverability advantage that a legged robot could bring to a collaborative robot team.

6.5 Summary

Changing the height of travel of the CoG affects different aspects of locomotion. The main affect is by the change of the stride length. The closer the CoG is to the ground, the larger the range of possible movement. Closer to the ground, the stride length is also larger. With a larger stride length, a robot has an ability to move faster. As a result of the larger stride length, however, the ability of the trajectory planner to produce a path that would allow a robot to follow certain paths decreases, as the body

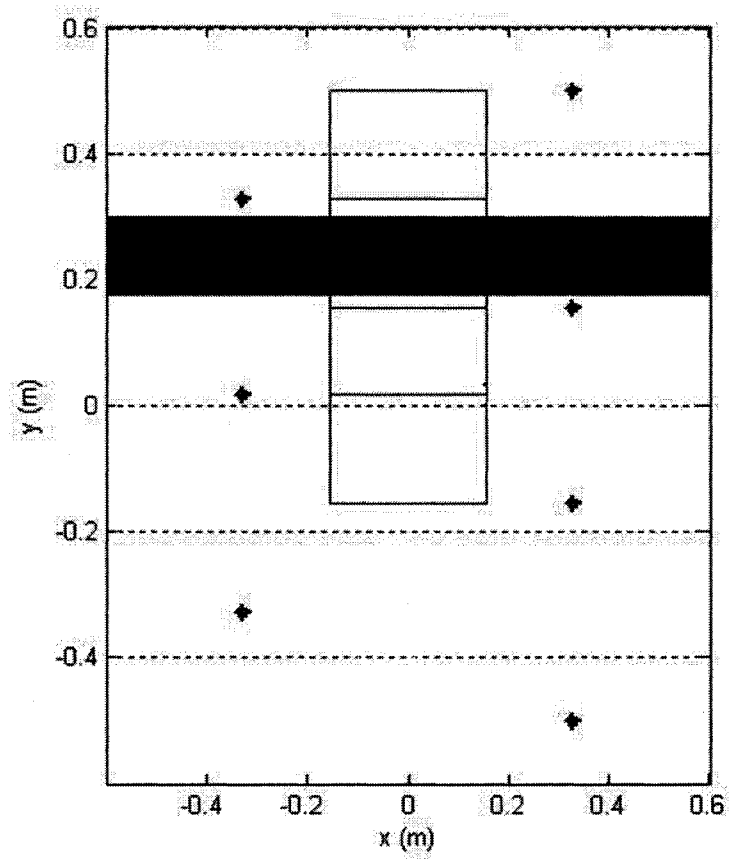


Figure 6.30: Ditch Crossing for a CoG Height of 0.3 m

movements would be larger. As the height of travel of the CoG increases, the possible leg movements become limited. The average possible velocity also becomes smaller, but in most cases the ability of the allowed path to follow a desired path more closely improves. The decision on the height at which a robot should travel is therefore a trade off between speed and accuracy. The requirements for these differ, depending on what is being asked of the robot. In most situations it would be advisable to stay away from the extremes. Selecting a low height of travel would create a plan that would become more prone to making contact with the ground and to overstep waypoints by unacceptable amounts. Too high of a height of travel on the other hand, the slower the possible speed and a possibility of decreased stability may be increased.

Another important consideration when deciding on an appropriate height of travel is the joint histories produced by the trajectory planner. With an increase of height comes an increase in joint velocities and accelerations. The largest increases occur in the required accelerations in joints 2 and 3. At a height of 0.6 m the required accelerations are very large and may become a limiting factor depending on the capabilities of the actuators. At these height it may be required to change the height of the leg trajectory used by the trajectory planner.

The selected gaits create a plan where a robot's CoG is only propelled forward in a straight line. For this reason a straight line path can be followed with a greater speed by the plan produced by the trajectory planner and also has the potential to be followed more closely. This is mainly because in order to follow a curve the planned trajectory must incorporate the spinning gait much more frequently to change its orientation. One cycle of the spinning gait takes 3/4 of a cycle of the creeping gait to complete plus the two transition stages of two time steps each. Several cycles of the spinning gait may be required to change to the desired orientation and the CoG does not advance using this gait.

Using the proposed trajectory planner a plan in the form of joint variables can be produced to allow a quadruped robot to traverse certain terrain not accessible to wheeled robots. A robot can successfully cross a ditch or hole that is less than $\lambda/2$ in width. This ability helps to highlight skills that a legged robot would bring to a

collaborative robot team.

Chapter 7

Conclusions and Recommendations

In this chapter an overview of the trajectory planner developed in this research will be given. Recommendations will also be given for possible areas of improvement. Ideas of possible areas for continuing with the work presented in this thesis will also be discussed.

7.1 Conclusions

The overall goal of this thesis was to design a trajectory planning method that would produce the required joint variables to allow a quadruped robot to move along a two dimensional path, while maintaining static stability. In order to achieve this aim, it was necessary to solve the inverse and direct kinematic problem for the feet of the robot. A plan on how the body and legs should move, detailed by a combination of gaits, was also required. The appropriate gait plan had to ensure that static stability would be obtained with the joint variables that were produced. Leg and body trajectories to provide a means to achieve the different foot and body positions identified in the gait plan were required. The kinematics, gaits, stability measures and trajectories were incorporated together in the trajectory planner which produced the required joint variables to allow a quadruped robot to move along a user defined path.

In order to check stability and to create cartesian trajectories for the legs and body it is necessary to determine the positions of the feet with respect to the projection of the robot's CoG. This is done using the DKP. In order to determine the required joint variables produced by the trajectory planner, the IKP is used. In this thesis the DKP and IKP were solved for a 3 DoF leg with three links and three actuated revolute joints. The problems were solved using the well known Denavit-Hartenberg approach in Chapter 3. This allowed for the development of velocity and acceleration

equations and the representation of the reachable workspace.

Discontinuous gaits, discussed in Chapter 4, were selected as appropriate gaits to meet the aims of this thesis because of their stability properties and their simplicity of implementation. A two phase discontinuous creeping gait was selected to allow for forward movement in a straight line, and a one phase discontinuous spinning gait was selected in order to allow for re-orientation the robot's forward axis. These gaits needed to be joined together by a transition phase that moved the legs into the appropriate start positions for the respective gaits.

In order to assure that the robot maintained static stability during locomotion, a stability measure was implemented. In order to determine if the robot would be stable, the projection of the CoG was checked to see if it would lie in the support polygon formed by the legs in contact with the ground. This stability check was incorporated into the gaits to ensure that the plan they would provide would allow for statically stable locomotion.

Appropriate leg and body trajectories were chosen to be used in conjunction with the selected gaits. The trajectory planner uses the IKP, the DKP, the selected gaits, stability analysis and leg and body trajectories in order to produce the joint variables that can be sent to a robot's actuators and allow it to follow a given path. The plan created by the trajectory planner determines whether the creeping or spinning gait should be used, in which order, and for how many cycles in order to reach the waypoints defined by the path while maintaining static stability.

The trajectory planner created plans for different types of paths to test its performance. Straight line and circular paths were tested. Because of the chosen gaits, the trajectory planner is better suited to create plans that follow straight line paths, but the trajectory planner performed quite well creating plans that would allow for a close follow of curved paths as well. The trajectory planner was also tested for its performance by creating plans for different stride lengths. With a longer stride length, the planned trajectory was faster, but generally less accurate. A shorter stride length led to higher joint velocities and accelerations.

The ability of the trajectory planner to produce a plan that allows for a close path

follow is a function of both the stride length and the distance that is desired to be traveled to a waypoint. With these results, it is clear that the trajectory planning method developed provides planned trajectories, in the form of joint variables, that allow for a quadruped robot to follow multiple user defined paths while maintaining static stability on even horizontal terrain.

7.2 Recommendations and Future Works

The following recommendations are suggestions that may improve or further the work presented in this thesis. It was noted in the results that the ability to allow for a close path follow was a function of the stride length and the distance to the waypoint. In order to improve the ability of the plan created by the trajectory planner to follow a path more closely, an algorithm could be developed to choose the optimum height of travel, which is linked to the stride length. A multiple of the distance to the waypoint would be chosen as the stride length allowing for a planned trajectory that follows the path more closely.

Although the trajectory planner provides a plan to transition between the creeping and spinning gait, the proposed transition does not appear to be an optimal solution. It is recommended that other ways to transition more smoothly between the two gaits be investigated. More optimal means of transition may perhaps mean changes to the feet positions of the gaits.

One of the more important next steps in the validation of the work presented in this thesis is its implementation of the trajectory planner on an actual quadruped robot. Such work would further highlight any strength or weaknesses with the proposed trajectory planning technique. Using the dynamic equations, a control system could be implemented to improve the ability of the robot to achieve the joint variables provided by the trajectory planner. Once successful when implemented on a physical robot moving on flat uneven terrain, the next step would be to adapt the trajectory planner to plan for locomotion on uneven terrain. Such adaptation would allow the robot to climb small stairs. Eventually the robot would be incorporated into a

heterogeneous collaborative robot team in order to search an area, with the ability to search certain regions unreachable to wheeled robots.

References

- [1] J. Estremera, E. Garcia, and P. Gonzalez de Santos. A multi-modal and collaborative human-machine interface for a walking robot. *Journal of Intelligent and Robotic Systems*, Vol.35:397–425, 2002.
- [2] J.A. Galvez, E. Garcia, and P. Gonzalez de Santos. A mathematical model for real-time control of the silo 4 leg. *Proceedings of the 3rd International Conference on Climbing and Walking Robots*, pages 447–460, 2000.
- [3] The silo 4 walking robot. Available: <http://www.iai.csic.es/users/silo4>, 2005.
- [4] E. Muybridge. *Animals in Motion*. Dover Publications: New York, 1957.
- [5] T. Balch and L.E. Parker. *Robot Teams: From Diversity to Polymorphism*. A K Peters: Natick, MA, 2002.
- [6] R.R. Murphy. *Introduction to AI Robotics*. The MIT Press: Cambridge, MA, 2000.
- [7] M.W. Spong and M. Vidyasagar. *Robot Dynamics and Control*. John Wiley and Sons: New York, 1989.
- [8] M.W. Spong, S. Hutchinson, and M. Vidyasagar. *Robot Modelling and Control*. John Wiley and Sons: Hoboken, NJ, 2006.
- [9] R. Manseur. *Robot Modeling and Kinematics*. Da Vinci Engineering Press: Rockland, MA, 2006.
- [10] R. Siegwart and I.R. Nourbakhsh. *Introduction to Autonomous Mobile Robots*. The MIT Press: Cambridge, MA, 2004.
- [11] S. Hirose. Three basic types of locomotion in mobile robots. *Proceeding of the 1991 ICAR. Fifth International Conference on Advanced Robotics*, Vol.1:12–17, 1991.
- [12] M. Buehler, R. Battaglia, A. Cososco, G. Hawker, J. Sarkis, and K. Yamazaki. Scout: A simple quadruped that walks, climbs and runs. *Proceedings of the 1998 IEEE International Conference on Robotics and Automation*, Vol.2:1707–1712, 1998.
- [13] Z. Tang, C. Zhou, and Z. Sun. Trajectory planning for smooth transition of a biped robot. *Proceedings of the 2003 IEEE International Conference on Robotics and Automation*, Vol.2:2455–2460, 2003.

- [14] S.M. Song and K.J. Waldron. *Machines That Walk: The Adaptive Suspension Vehicle*. The MIT Press: Cambridge, MA, 1989.
- [15] R. Linnemann, B. Klaassen, F. Kirchner, and D. Spenneberg. Biomimetic walking scorpion:control and modeling. *Robotics and Autonomous Systems*, Vol.41(no.2):69–76, 2001.
- [16] M.H. Raibert. *Legged Robots That Balance*. The MIT Press; Cambridge, MA, 1986.
- [17] G. Dudek and M. Jenkin. *Computational Principles of Mobile Robots*. Cambridge University Press: New York, 2000.
- [18] R.B. McGhee and A.A. Frank. On the stability properties of quadruped creeping gaits. *Mathematical Biosciences*, Vol.3:331–351, 1968.
- [19] J.J. Craig. *Introduction to Robotics: Mechanisms and Control*. Addison-Wesley Publishing Company: Boston, 1989.
- [20] H.J. Weidemann, F. Pfeiffer, and J. Eltze. A design concept for legged robots derived from the walking stick insect. *Proceedings of the 1993 IEEE/RSJ International Conference on Intelligent Robots and Systems*, Vol.1:545–552, 1993.
- [21] X. Chen, K. Watanabe, and K. Izumi. Study on the control algorithm of the translational crawl for a quadruped robot. *Proceedings of the IEEE SMC '99 Conference on Systems, Man, and Cybernetics*, Vol.6:959–964, 1999.
- [22] J. Estremera, E. Garcia, and P. Gonzalez de Santos. *Quadrupedal Locomotion an Introduction to the Control of Four-Legged Robots*. Springer: New York, 2006.
- [23] S. Hirose, T. Masui, and H. Kikuchi. Titan iii: A quadruped walking vehicle. In *Proceedings of the 2nd ISRR Symposium*, Cambridge, MA, 1984.
- [24] C.M. Angle and R.A. Brooks. Small planetary rovers. *Proceedings of IROS '90 IEEE International Workshop on Intelligent Robots and Systems*, Vol.1:383–388, 1990.
- [25] J.P. Barreto, A. Trigo, P. Menezes, J. Dias, and A.T. de Almeida. Fbd - the free body diagram method. kinematic and dynamic modelling of a six leg robot. In *Proceedings of AMC'98 5th International Workshop on Advanced Motion Control*, Portugal, 1998.
- [26] K. Berns, W. Ilg, M. Deck, and M. Dilmann. The mammalian-like quadrupedal walking machine bisam. *The 5th International Workshop On Advanced Motion Control*, pages 429–433, 1993.
- [27] M. Buehler, U. Saranli, and D.E. Koditschek. Design modeling and preliminary control of a compliant hexapod robot. *Proceedings of the 2000 IEEE International Conference on Robotics and Automation*, Vol.3:2589–2596, 2000.

- [28] E. Celaya and J.M. Porta. A control structure for the locomotion of a legged robot on difficult terrain. *IEEE Robotics and Automation*, Vol.5(no.2):43–51, 1998.
- [29] X. Chen, K. Watanabe, K. Izumi, and K. Kiguchi. A real time kinematics on the translational crawl motion of a quadruped robot. *Journal of Intelligent and Robotic Systems*, Vol.29(no.2):111–131, 2000.
- [30] J. Estremera, E. Garcia, P. Gonzalez de Santos, and J.A Galvez. Silo 4: A true walking robot for the comparative study of walking machine techniques. *IEEE Robotics and Automation Magazine*, Vol.10(no.4):23–32, 2003.
- [31] M.R. Fielding, R. Dunlop, and C.J. Damaren. Hamlet: Force/position controlled hexapod walker- design and systems. *Proceedings of the 2001 IEEE International Conference on Control Applications*, pages 984–989, 2001.
- [32] W.C. Flannigan, G.M. Nelson, and R.D. Quinn. Locomotion controller for a crab-like robot. *Proceedings of the IEEE International Conference on Robotics and Automation*, Vol.1:152–156, 1998.
- [33] B. Gassmann, K.U. Scholl, and K. Berns. Locomotion of lauron iii in rough terrain. *Proceedings of the IEEE/ASME International Conference on Advanced Intelligent Mechatronics*, Vol.2:959–964, 2001.
- [34] Y. Go, X. Yin, and A. Bowling. Navigability of multi-legged robots. *IEEE/AMSE Transactions on Mechatronics*, Vol.11(no.1):1–8, 2006.
- [45] M. Guddat and M. Frik. Control of walking machines with artificial reflexes. In *Advanced Motion of Animals and Machines, the Second International Symposium on Impact and Friction of Solids, Structures and Intelligent Machines*, Montreal, 2000.
- [47] D. Guinea, M.C. Garcia-Alegre, P. Kalata, A. Lacaze, and A. Meystel. Robot learning to walk: An architectural problem for intelligent controllers. *Proceedings of the 1993 IEEE International Symposium on Intelligent Control*, pages 493–498, 1993.
- [46] K.K. Hartikainen, A.J. Halme, H. Lehtinen, and K.O. Koskinen. Mecant i - a six legged walking machine for research purposes in outdoor environment. *Proceedings of the 8th IEEE International Conference on Robotics and Automation*, Vol.1:157–163, 1992.
- [39] F. Iida and P. Pfiefer. Cheap rapid locomotion of a quadruped robot: Self-stabilization of bounding gaits. *Intelligent Autonomous Systems*, Vol.8:642–649, 2004.
- [44] T. Kerscher, J. Albeiz, and K. Berns. Joint control of the six legged robot airbug driven by fluid muscles. *Proceedings of the Third International Workshop on Robot Motion and Control*, pages 27–32, 2002.

- [48] I. Lee and B. Lee. The implementation of the gaits and body structure for a hexapod robot. *Proceedings of the 2001 IEEE International Symposium on Industrial Electronics*, Vol.3:1959–1964, 2001.
- [38] T. Lee and C. Shih. A study of the gait control of a quadruped walking vehicle. *IEEE Journal of Robotics and Automation*, Vol.2(no.2):61–69, 1986.
- [51] W.J. Lee and D.E. Orin. Omnidirectional supervisory control of a multi-legged vehicle using periodic gaits. *IEEE Journal of Robotics and Automation*, Vol.4(no.6):635–642, 1988.
- [49] K.S. Lian. Legged robot. *Proceedings of the IEEE International Conference on Systems, Man and Cybernetics*, pages 1297–1302, 1995.
- [37] J. Muller, M. Schneider, and M. Hiller. Modelling and simulation of the large-scale hydraulically driven alduro. In *Proceedings of the Euromech Colloquim 375*, Munich, 1998.
- [50] K. Nonami and Q. Huang. Humanitarian mine detection six-legged walking robot comet ii with two manipulators. *Proceedings of the 4th International Conference on Climbing and Walking Robots*, pages 989–996, 2001.
- [41] D.K. Pai, R.A. Barman, and S.K. Ralph. Platonic beasts: Spherically symmetric multi-limbed robots. *Autonomous Robots*, Vol.2(no.3):191–201, 1995.
- [40] W. Pengfei, H. Bo, and S. Lining. Walking research on multi-motion mode quadruped bionic robot based on moving zmp. *Proceedings of the IEEE International Conference on Mechatronics and Automation*, Vol.4:1935–1940, 2005.
- [52] G. Ritter, J. Puitti, and E. Sanchez. Leonardo and discipulus simplex: An autonomous, evolvable six-legged walking robot. *Lecture Notes in Computer Science*, Vol.1586:688–696, 1999.
- [43] A. Shkolnik and R. Tedrake. Inverse kinematics for a point-foot quadruped robot with dynamic redundancy resolution. *Proceedings of the International Conference on Climbing and Walking Robots*, pages 4331–4336, 2003.
- [35] M.F. Silva, J.A.T. Machado, and A.M. Lopas. Performance analysis of multi-legged systems. *Proceedings of the Second International Workshop on Robot Motion and Control*, pages 45–50, 2001.
- [42] M. Stelzer, M. Hardt, and O. Von Stryk. Efficient dynamic modeling, numerical optimal control and experimental results for various gaits of a quadruped robot. *CLAWAR International Conference on Climbing and Walking Robots, Catania, Italy*, pages 601–608, 2003.
- [53] M.V. Summer, J. Stiver, and L.H. Davis. Design and control of a dexterous biomimetic multi-limbed walking robot. *Proceedings of the IEEE/ASME International Conference on Advanced Intelligent Mechatronics*, pages 414–419, 2005.

- [36] D. Zhou and K.H. Low. Design of a quadruped walking machine for terrain adaptation. *Proceedings of the First Workshop on Robot Motion and Control*, pages 59–64, 1999.
- [54] T. Zielinska, J. Heng, and G. Steet. Walking machine position and force control. *Proceedings of the First International Workshop on Robot Motion and Control*, pages 141–145, 1999.
- [55] J.E. Bares and D.S. Wettergreen. Dante ii: A technical description, results and lessons learned. *The International Journal of Robotics Research*, Vol.18(no.7):621–649, 1999.
- [56] Desarollo de robots caminantes y escaladores en el iai-csic. Available: <http://webdiis.unizar.es/neira/docs/PGonzalez-CEDI2007.pdf>, 2003.
- [57] M. Hildebrand. Symmetrical gaits of horses. *Science*, Vol.150(no.3697):701–708, 1965.
- [58] R.B. McGhee. Some finite aspects of legged locomotion. *Mathematical Biosciences*, Vol.2:67–84, 1968.
- [59] T.W. Tee, K.H. Low, H.Y. Ng, and F. Young. Mechatronics design and gait implementation of a quadruped legged robot. *Proceedings of the Seventh International Conference on Control Automation, Robotics and Vision*, Vol.2:826–832, 2002.
- [60] K. Inagaki and H. Kobayashi. A gait transition for quadruped walking machine. *Proceedings of the 1993 IEEE/RSJ International Conference on Intelligent Robots and Systems*, Vol.1:525–531, 1993.
- [61] C. Zhang and S.M. Song. Stability analysis of wave-crab gaits of a quadruped. *Journal of Robotic Systems*, Vol.7(no.2):243–276, 1990.
- [62] J. Estremera and P. Gonzalez de Santos. Generating continuous free crab gaits for quadruped robots on irregular terrain. *IEEE Transactions on Robotics*, Vol.21(no.6):1067–1076, 2005.
- [63] M.A. Jimenez and P. Gonzalez de Santos. Terrain-adaptive gait for walking machines. *The International Journal of Robotics Research*, Vol.16(no.3):320–339, 1997.
- [64] P. Gonzalez de Santos and M.A. Jimenez. Path tracking with quadruped walking machines using discontinuous gaits. *Computers and Electrical Engineering*, Vol.21(no.6):383–396, 1995.
- [65] C. Zhang and S.M. Song. Turning gait of a quadrupedal walking machine. *Proceedings of the 1991 IEEE Conference on Robotics and Automation*, Vol.3:2106–2112, 1991.

- [66] S. Hirose, H. Kikuchi, and Y. Umetani. The standard circular gait of a quadruped walking vehicle. *Advanced Robotics*, Vol.1(no.2):143–164, 1987.
- [67] Z. Bien, M.G. Chun, and H.S. Son. An optimal turning gait for a quadruped walking robot. *IEEE/RSJ International Workshop on Intelligent Robots and Systems IROS '91*, Vol.3:1511–1514, 1991.
- [68] M. Lie and M. Peisun. A study of turning gait control for quadruped walking vehicle. *IEEE/RSJ International Workshop on Intelligent Robots and Systems IROS '91*, Vol.3:1524–1527, 1991.
- [69] V. Hugel and P. Blazevic. Towards efficient implementation of quadruped gaits with duty factor of 0.75. *Proceedings of the 1999 IEEE International Conference on Robotics and Automation*, Vol.3:2360–2365, 1999.
- [70] S. MA, T. Tomiyama, and H. Wada. Omni-directional walking of a quadruped robot. *Proceedings of the 2002 IEEE/RSJ International Conference on Intelligent Robots and Systems*, Vol.3:2605–2612, 2002.
- [71] S. Ma, T. Tomiyama, and H. Wada. Omnidirectional static walking of a quadruped robot. *IEEE Transactions on Robotics*, Vol.3:2605–2612, 2005.
- [72] S. Ma, L. Zhang, K. Inoue, and Y. Honda. Omni-directional walking of a quadruped robot with optimal body posture on a slope. *Proceedings of the 2005 IEEE International Conference on Robotics and Automation*, pages 2976–2981, 2005.
- [73] D. Wettergreen and C. Torpe. Gait generation for legged robots. *Proceedings of the 1992 IEEE/RSJ International Conference on Intelligent Robots and Systems*, pages 1413–1420, 1992.
- [74] D.J. Pack and A.C. Kak. A simplified forward gait control for a quadruped walking robot. *Proceedings of the IEEE/RSJ/GI International Conference on Intelligent Robots and Systems*, Vol.2:1011–1018, 1994.
- [75] C. Chevallereau, A. Formal'sky, and B. Perrin. Control of a walking robot with feet following a reference trajectory derived from ballistic motion. *Proceedings of the 1997 IEEE International Conference on Robotics and Automation*, Vol.2:1094–1099, 1997.
- [76] A. Muraro, C. Chevallereau, and Y. Auostin. Optimal trajectories for a quadruped robot with trot, amble and curvet gaits for two energetic criteria. *Multibody System Dynamics*, Vol.9(no.1):39–62, 2003.
- [77] R.B. McGhee and G.I. Iswandhi. Adaptive locomotion of a multilegged robot over rough terrain. *IEEE Transactions on Systems, Man and Cybernetics*, Vol.9:176–182, 1979.

- [78] H. Igarashi, T. Machida, F. Harashima, and M. Kakikura. Free gait for quadruped robots with posture control. *Proceedings of the 9th IEEE Workshop on Advanced Motion Control*, pages 433–438, 2006.
- [79] P.K. Pal and K. Jayarajan. A free gait for generalized motion. *IEEE Transactions on Robotics and Automation*, Vol.6(no.5):597–600, 1990.
- [80] P.K. Pal and K. Jayarajan. Generation of a free gait-a graph search approach. *IEEE Transactions on Robotics and Automation*, Vol.7(no.3):299–305, 1991.
- [81] R.A. Brooks. A robot that walks; emergent behaviours from a carefully evolved network. *Proceedings of the 1989 IEEE International Conference on Robotics and Automation*, Vol.2:692–696, 1989.
- [82] Y. Ding and E. Scarf. Deadlock avoidance for a quadruped with free gait. *Proceedings of the 1994 IEEE International Conference on Robotics and Automation*, Vol.1:143–148, 1994.
- [83] D. Katic and M. Vukobratovic. Survey of intelligent control techniques for humanoid robots. *Journal of Intelligent and Robotic Systems*, Vol.37(no.2):117–141, 2003.
- [84] H. Hemami, F. Weimer, and S.H. Koozekanani. Some aspects of the inverted pendulum problem for modeling of locomotion systems. *IEEE Transactions on Automatic Control*, Vol.18(no.6):658–661, 1973.
- [85] B.S. Choi and S.M. Song. Fully automated obstacle-crossing gaits for walking machines. *IEEE Transactions on Systems, Man, and Cybernetics*, Vol.18(no.6):952–964, 1988.
- [86] J. Estremera, E. Garcia, and P. Gonzalez de Santos. A classification of stability margins for walking robots. In *Proceedings of the 5th International Conference on Climbing and Walking Robots*, Paris, 2002.
- [87] X. Chen, K. Watanabe, and K. Izumi. A new method on judgement of static stability for the quadruped robot. *Proceedings of the IEEE SMC '99 Conference on Systems, Man, and Cybernetics 1999*, Vol.6:953–958, 1999.
- [88] D.A. Messuri and C.A. Klein. Automatic body regulation for maintaining stability of a legged vehicle during rough-terrain locomotion. *IEEE Journal of Robotics and Automation*, Vol.1(no.3):132–141, 1985.
- [89] H. Igarashi and M. Kakikura. Adaptive gait for a quadruped robot on 3d path planning. *Transactions of the Institute of Electrical Engineers of Japan*, Vol.123(no.10):1813–1821, 2003.
- [90] Y. Sakakibara, K. Kan, and Y. Hosoda. Foot trajectory for a quadruped walking machine. *Proceedings of the 1990 IEEE International Conference on Intelligent Robots and Systems*, Vol.1:315–322, 1990.

- [91] M.F Silva, J.A.T. Machado, A.M. Lopes, and J.K. Tar. Gait selection for quadruped and hexapod walking systems. *Proceedings of the Second IEEE International Conference on Computational Cybernetics*, pages 217–222, 2004.
- [92] A. Ude, C.G. Atkeson, and M. Riley. Planning of joint trajectories for humanoid robots using b-spline wavelets. *Proceedings of the 2000 IEEE International Conference on Robotics and Automation*, Vol.3:2223–2228, 2000.
- [93] D. Lee, D. Kwon, S. Yeong, and Y. Hong. Teleoperation of a quadruped walking robot using an aperiodic gait that converges to a periodic gait. *Proceedings of the 1999 IEEE/RSJ International Conference on Intelligent Robots and Systems*, pages 1639–1644, 1999.
- [94] X. Chen, K. Watanabe, K. Izumi, and K. Kiguchi. Translational crawl and path tracking of a quadruped robot. *Journal of Robotic Systems*, Vol.19(no.12):569–584, 2002.
- [95] M. Arsenault. Me 591 robot mechanics. Course Notes, 2007.
- [96] M.R. Spiegel. *Schaum's Outline Series: Mathematical Handbook*. McGraw Hill: New York, 1968.
- [97] R.H Cannon. *Dynamics of Physical Systems*. Dover: New York, 1967.
- [98] W.A Wells. *Schaum's Outlines: Lagrangian Dynamics*. McGraw Hill: New York, 1967.
- [99] D. Schaum. *Schaum's Outline Series: College Physics*. McGraw Hill: New York, 1961.

Appendix A

Dynamics of an Insect Type Leg

Dynamic Equations are often used in control system design. The dynamic equations are developed here for a leg using Lagrangian dynamics. The joint variables provided by the trajectory planner are also used with the direct dynamic equations to determine the required torques for leg movements. These torques can be combined with the torques required to support the body in order to size the motors.

A.1 Developing the Dynamic Equations

The dynamics of a mechanism express the relationship between the motion of the mechanism and the forces involved [2]. The dynamic equations usually take the form of second order differential equations. These equations link the joint variables to the torque required by each actuator. Using these equations, a control system can be created in order to improve the performance of the robot. The inputted torques will produce actual joint variables which can be compared to the desired joint variables produced by the trajectory planner.

Lagrange's equations were developed around 1780 by the Italian/French mathematician, Joseph-Louis Lagrange. They make up a method that is based on energy balance relations that stem from the Law of Conservation of energy [97]. Lagrange's approach takes both conservative and non conservative forces into account. Another benefit of this approach is that unlike the development using Newton's equations of motion, vectors are not used in the Lagrangian formulation. In some cases, this can simplify the development of the equations of motion. Lagrange's equations are shown in Equation A.1 described by [97] :

$$\frac{d}{dt} \left(\frac{\delta T}{\delta \dot{q}_i} \right) - \frac{\delta T}{\delta q_i} + \frac{\delta U}{\delta q_i} = W_i \quad (\text{A.1})$$

Where q_i represents the generalized coordinates, in the case of the leg θ_1 , θ_2 , and θ_3 . It is important to note that in the Lagrangian method, the generalized coordinates

are assumed to be independent of each other. T represents the total kinetic energy of the system. U represents the total potential energy of the system, which in the case of the robot leg is made up only of gravity terms. W_i represents the generalized external forces acting on link i , the joint torques. In this development, friction is assumed to be zero, this is clearly untrue as any real system has some amount of friction.

The leg consists of three actuated joints and three links. Relevant constants are shown in Table A.1. The centre of mass, (CM), of the links is not necessarily at the midpoint of the link.

Table A.1: Dynamic Constants of the Leg [2]

Parameter	Link 1	Link 2	Link 3
Mass (kg)	1.22	1.26	0.63
Position of the CM (m)	0.0478	0.1306	0.1555
Moment of Inertia (kgm^2)	0.0184	0.0225	0.0108

A.1.1 Determining the Kinetic Energy

Essentially, kinetic energy describes the energy of motion. It is the work required to go from one velocity to another [98]. It is a scalar quantity. For link $i = 1, 2, 3$ the kinetic energy can be expressed as:

$$T_i = \frac{1}{2}I_{cm_i}\dot{\theta}_i^2 + \frac{1}{2}m_i\nu_{cm_i}^2 \quad (\text{A.2})$$

The total kinetic energy for the system includes the energy from both translational and rotational velocities. Determining the kinetic energy resulting from the rotational motion is relatively straight forward. In order to determine the kinetic energy from the translational motion of each link, the velocity, ν_{cm_i} is required. First the position of the centre of mass of each link, with respect to the hip, must be determined. This is done by referring to the DH parameters defined in Chapter 3.

$$p_{cm_1} = c_{cm_1} = \begin{bmatrix} L_{cm_1} \cos \theta_1 \\ L_{cm_1} \sin \theta_1 \\ 0 \end{bmatrix} \quad (\text{A.3})$$

$$p_{cm_2} = c_1 + Q_{2 \rightarrow 1} c_{cm_2} = \begin{bmatrix} L_1 \cos\theta_1 + L_{cm_2} \cos\theta_1 \cos\theta_2 \\ L_1 \sin\theta_1 + L_{cm_2} \sin\theta_1 \cos\theta_2 \\ L_{cm_2} \sin\theta_2 \end{bmatrix} \quad (A.4)$$

$$p_{cm_3} = c_1 + Q_{2 \rightarrow 1} c_2 + Q_{2 \rightarrow 1} Q_{3 \rightarrow 2} c_{cm_3} = \begin{bmatrix} \cos\theta_1 (L_1 + L_2 \cos\theta_2 + L_{cm_3} \cos(\theta_2 + \theta_3)) \\ \sin\theta_1 (L_1 + L_2 \cos\theta_2 + L_{cm_3} \cos(\theta_2 + \theta_3)) \\ L_2 \sin\theta_2 + L_{cm_3} \sin(\theta_2 + \theta_3) \end{bmatrix} \quad (A.5)$$

Next the translational velocity of the centre of mass of each link is determined by taking the derivative of the position.

$$\nu_{cm_1} = \begin{bmatrix} -\dot{\theta}_1 L_{cm_1} \sin\theta_1 \\ \dot{\theta}_1 L_{cm_1} \cos\theta_1 \\ 0 \end{bmatrix} \quad (A.6)$$

$$\nu_{cm_2} = \begin{bmatrix} -\dot{\theta}_1 L_1 \sin\theta_1 - \dot{\theta}_1 L_{cm_2} \sin\theta_1 \cos\theta_2 - \dot{\theta}_2 L_{cm_2} \cos\theta_1 \sin\theta_2 \\ \dot{\theta}_1 L_1 \cos\theta_1 + \dot{\theta}_1 L_{cm_2} \cos\theta_1 \cos\theta_2 - \dot{\theta}_2 L_{cm_2} \sin\theta_1 \sin\theta_2 \\ \dot{\theta}_2 L_{cm_2} \cos\theta_2 \end{bmatrix} \quad (A.7)$$

$$\nu_{cm_3} = \begin{bmatrix} (-\dot{\theta}_1 L_1 \sin\theta_1 - \dot{\theta}_1 L_2 \sin\theta_1 \cos\theta_2 - \dot{\theta}_2 L_2 \cos\theta_1 \sin\theta_2) \\ -\dot{\theta}_1 L_{cm_3} \sin\theta_1 \cos(\theta_2 + \theta_3) - (\dot{\theta}_2 + \dot{\theta}_3) L_{cm_3} \cos\theta_1 \sin(\theta_2 + \theta_3) \\ (\dot{\theta}_1 L_1 \cos\theta_1 + \dot{\theta}_1 L_2 \cos\theta_1 \cos\theta_2 - \dot{\theta}_2 L_2 \sin\theta_1 \sin\theta_2) \\ + \dot{\theta}_1 L_{cm_3} \cos\theta_1 \cos(\theta_2 + \theta_3) - (\dot{\theta}_2 + \dot{\theta}_3) L_{cm_3} \sin\theta_1 \sin(\theta_2 + \theta_3) \\ \dot{\theta}_2 L_2 \cos\theta_2 + (\dot{\theta}_2 + \dot{\theta}_3) L_{cm_3} \cos(\theta_2 + \theta_3) \end{bmatrix} \quad (A.8)$$

The velocities can now be inputted into Equation A.2 to arrive at an expression for the kinetic energy in terms of the joint variables. The total kinetic energy of the system is obtained by adding the kinetic energies of the individual links.

A.1.2 Determining the Potential Energy

Potential energy refers to the work that must be done to change the position of an object [99]. The change of potential energy is determined by the difference in energy from an arbitrary point. Potential energy is generally described by Equation A.9:

$$U_i = m_i g h_i \quad (A.9)$$

Where g represents the gravity term, 9.8 m/s^2 , and h_i is the position, on the z axis, of the body's centre of mass from the arbitrary point. In order to simplify the development, the arbitrary point will be chosen to be at the hip. As with the kinetic energy, the total potential energy is the sum of the potential energy of each link.

As the origin was chosen to be at the hip, which can only rotate about the z axis, the force of gravity on link one is a constant and equal to zero. The derivation of the potential energy of a leg is therefore similar to that of the double pendulum. A planar view of the leg is shown in Figure A.1.

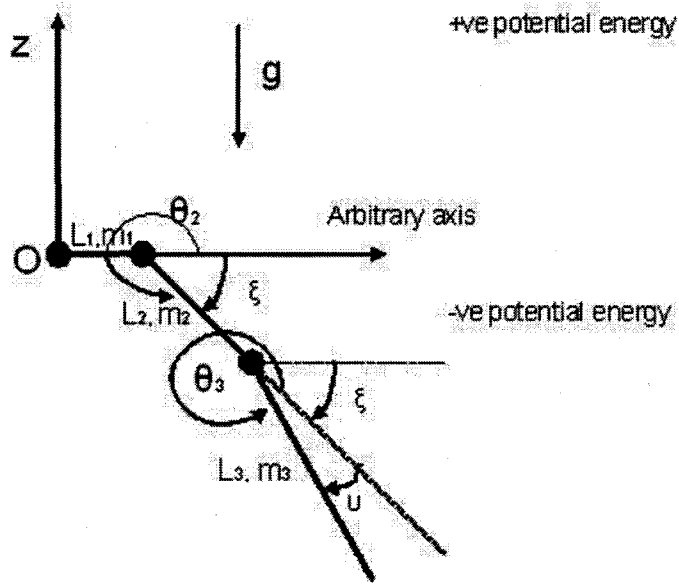


Figure A.1: Planar View of a Leg

Where:

$$\xi = 2\pi - \theta_2 \quad (\text{A.10})$$

$$\eta = 2\pi - \theta_3 \quad (\text{A.11})$$

Using Equation A.9, the potential energy can be determined for the system as:

$$U = -m_2gL_{cm2}\sin\xi - m_3g(L_2\sin\xi + L_{cm3}\sin(\xi + \eta)) \quad (\text{A.12})$$

Equations A.10 and A.11 can be substituted into Equation A.12 which can then be simplified [96], to give:

$$U = m_2gL_{cm2}\sin\theta_2 + m_3gL_2\sin\theta_2 + m_3gL_{cm3}\sin\theta_2\cos\theta_3 + m_3gL_{cm3}\sin\theta_3\cos\theta_2 \quad (\text{A.13})$$

A.1.3 The Dynamic Equations

Once the kinetic and potential energies have been determined, Equation A.1 can be applied. The various acceleration, velocity and position terms are then grouped

together to give an equation in the following form:

$$[M] \begin{bmatrix} \ddot{\theta}_1 \\ \ddot{\theta}_2 \\ \ddot{\theta}_3 \end{bmatrix} + [H] + [G] = \begin{bmatrix} \tau_1 \\ \tau_2 \\ \tau_3 \end{bmatrix} \quad (\text{A.14})$$

M represents the mass matrix. H represents the coriolis and centrifugal forces, these terms arise as the reference frames of the links are in rotation. The centrifugal and coriolis terms are generally small when compared to the other terms and for this reason are sometimes omitted. G represents the effect of the gravitational forces. The matrices are defined as follows:

$$\begin{aligned} M_{11} = & ((2m_2L_1L_{cm_2} + 2m_3L_1L_2)\cos\theta_2 + m_3L_2L_{cm_3}\cos\theta_3 + 2m_3L_1L_{cm_3}\cos(\theta_2 + \theta_3) \\ & + m_3L_2L_{cm_3}\cos(\theta_3 + 2\theta_2) + (\frac{1}{2}m_3L_2^2 + \frac{1}{2}m_2L_{cm_2}^2)\cos 2\theta_2 \\ & + (\frac{1}{2}m_3L_{cm_3})^2\cos(2\theta_2 + 2\theta_3) + m_2L_1^2 + m_3L_1^2 + \frac{1}{2}m_3L_{cm_3}^2 + \frac{1}{2}m_3L_2^2 + m_1L_1^2 \\ & + J_1 + \frac{1}{2}m_2L_{cm_2}^2) \end{aligned} \quad (\text{A.15})$$

$$M_{12} = 0 \quad (\text{A.16})$$

$$M_{13} = 0 \quad (\text{A.17})$$

$$M_{21} = 0 \quad (\text{A.18})$$

$$M_{22} = 2m_3L_2L_{cm_3}\cos\theta_3 + m_3L_2^2 + m_3L_{cm_3}^2 + J_2 + m_2L_{cm_2}^2 + 2m_3L_2 \quad (\text{A.19})$$

$$M_{23} = m_3L_2L_{cm_3}\cos\theta_3 + m_3L_{cm_3}^2 \quad (\text{A.20})$$

$$M_{31} = 0 \quad (\text{A.21})$$

$$M_{32} = m_2L_2L_{cm_3}\cos\theta_3 + m_3L_{cm_3}^2 \quad (\text{A.22})$$

$$M_{33} = J_3 + m_3L_{cm_3}^2 \quad (\text{A.23})$$

$$G_1 = 0 \quad (\text{A.24})$$

$$G_2 = (m_2gL_{cm_2} + m_3gL_2)\cos\theta_2 + m_3gL_{cm_3}\cos(\theta_2 + \theta_3) \quad (\text{A.25})$$

$$G_3 = m_3gL_{cm_3}\cos(\theta_2 + \theta_3) \quad (\text{A.26})$$

$$\begin{aligned}
H_1 = & (\dot{\theta}_1 \dot{\theta}_2 ((-m_3 L_2^2 - m_2 L_{cm_2}^2) \sin 2\theta_2 - (2m_2 L_1 L_{cm_2} + 2m_3 L_1 L_2) \sin \theta_2 \\
& - 2m_3 L_1 L_{cm_3} \sin(\theta_2 + \theta_3) - m_3 L_{cm_3}^2 \sin(2\theta_2 + 2\theta_3) - 2m_3 L_2 L_{cm_3} \sin(\theta_3 + 2\theta_2)) \\
& + \dot{\theta}_1 \dot{\theta}_3 (-4m_3 L_1 L_{cm_3} \sin(\theta_2 + \theta_3) - m_3 L_{cm_3}^2 \sin(2\theta_2 + 2\theta_3) \\
& - m_3 L_2 L_{cm_3} \sin(\theta_3 + 2\theta_2) - m_3 L_2 L_{cm_3} \sin \theta_3))
\end{aligned} \tag{A.27}$$

$$\begin{aligned}
H_2 = & (\dot{\theta}_1^2 (\frac{1}{2} m_3 L_{cm_3}^2 \sin(2\theta_2 + 2\theta_3) + (\frac{1}{2} m_3 L_2^2 + \frac{1}{2} m_2 L_{cm_2}^2) \sin 2\theta_2 \\
& + m_3 L_2 L_{cm_3} \sin(\theta_3 + 2\theta_2) + (m_2 L_{cm_2} L_1 + m_3 L_1 L_2) \sin \theta_2 \\
& + m_3 L_1 L_{cm_3} \sin(\theta_2 + \theta_3)) - \dot{\theta}_2 \dot{\theta}_3 2m_3 L_2 L_{cm_3} \sin \theta_3 - \dot{\theta}_3^2 m_3 L_2 L_{cm_3} \sin \theta_3)
\end{aligned} \tag{A.28}$$

$$\begin{aligned}
H_3 = & (\dot{\theta}_2^2 m_3 L_2 L_{cm_3} \sin \theta_3 + \dot{\theta}_1^2 (\frac{1}{2} m_3 L_{cm_3}^2 \sin(2\theta_2 + 2\theta_3) \\
& + \frac{1}{2} m_3 L_{cm_3} L_2 \sin(2\theta_2 + \theta_3) + \frac{1}{2} m_3 L_{cm_3} L_2 \sin \theta_3 + m_3 L_1 L_{cm_3} \sin(\theta_2 + \theta_3)))
\end{aligned} \tag{A.29}$$

Using Langrange's equation, the equations of motion were successfully developed. In order to apply Langrange's equation, it was first necessary to develop expressions for the kinematic and potential energies of each link in the leg. Like terms were grouped together and the final equations were written in terms of a mass matrix, a matrix containing the coriolis and centrifugal terms and a matrix containing the gravitational terms. With this, the required torque can be determined in terms of the joint variables.

A.2 Sizing the Motors

In the previous section the inverse dynamics were used to test the validity of the proposed model. The direct dynamics given in Equation A.14 can be used in order to select the appropriate motors to actuate the joints. There are two main factors to be considered when selecting the motors: the torque and the angular velocity of the joint, [36]. The angular velocity is produced by the trajectory planner with use of the inverse kinematic equations. The torque requirement can be determined by using the direct dynamics and the outputs of the trajectory planner: joint positions, velocities and accelerations. There are required torques to move the joints as well as

torque requirements to support the body which are not taken into account with the dynamic equations that treat each leg separately.

A.2.1 Moving the Joints

In order to determine the torque required to move a joint to the desired position, a position, velocity and acceleration are used in the direct dynamic model. The output is the required joint torque for the motion.

For example, the required torques to move the joints in order to complete one cycle of the creeping gait, when traveling at a height of 0.4 m and with a leg transfer phase of one unit of time and a support phase of two units of time, are shown in Figure A.2. The leg transfer phases can be clearly seen in the figure.

A.2.2 Supporting the Body

The dynamic equations that were developed address the legs separately and do not take into account the weight of the body that the legs must support during locomotion. The torque required to support the body depends on how many legs are on the ground and where they are placed. First the case where all four legs are in contact with the ground will be considered. In this case a 3x4 matrix, Equation A.30, can be used to define the foot positions relative to the body [22].

$$A = \begin{bmatrix} x_1 & x_2 & x_3 & x_4 \\ y_1 & y_2 & y_3 & y_4 \\ 1 & 1 & 1 & 1 \end{bmatrix} \quad (\text{A.30})$$

The vertical ground reaction force for each leg can then be found using Equation A.31:

$$F = A^T (AA^T)^{-1} W \quad (\text{A.31})$$

Where W is given by Equation A.32.

$$W = \begin{bmatrix} 0 \\ 0 \\ -m_b g \end{bmatrix} \quad (\text{A.32})$$

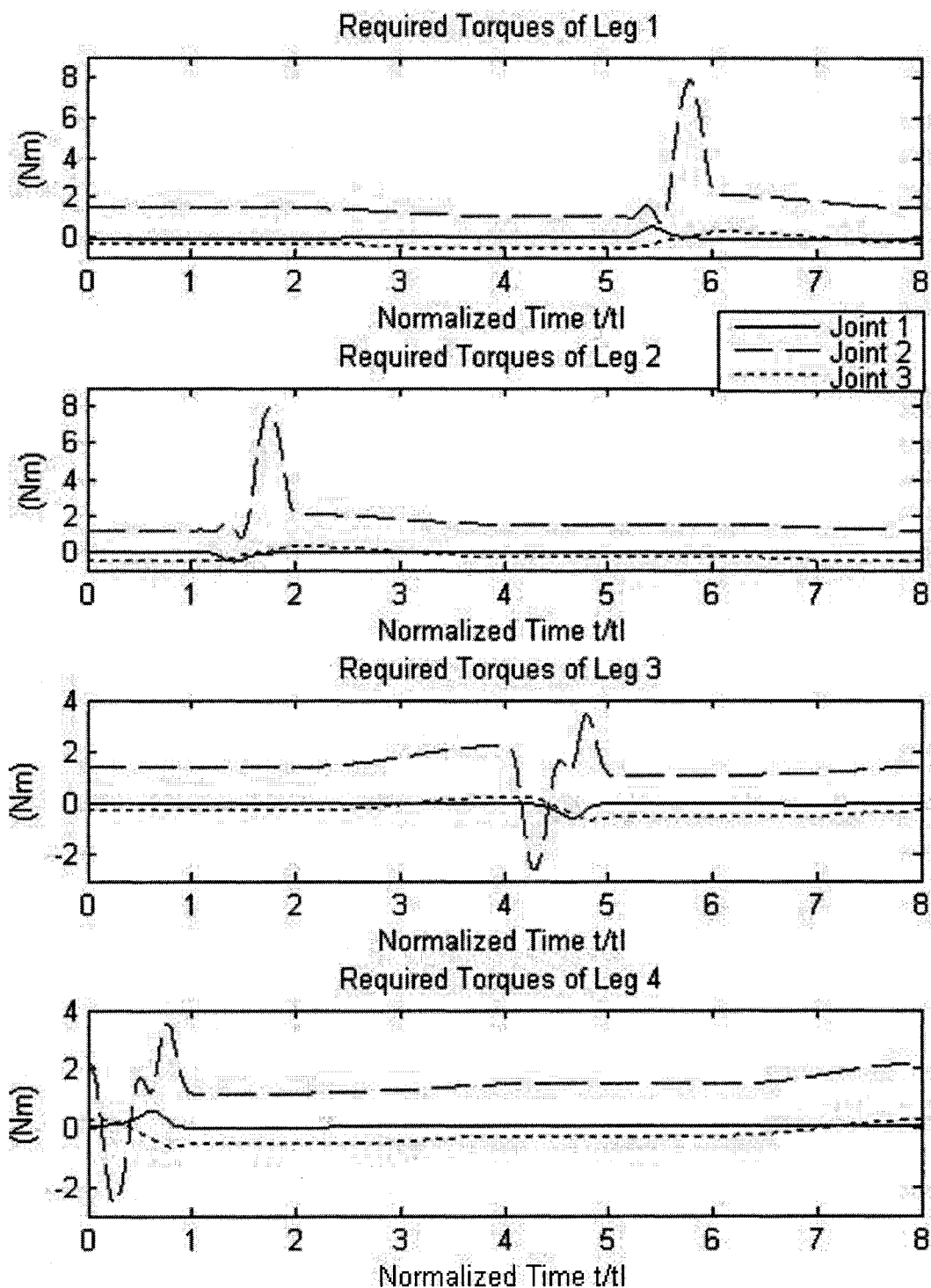


Figure A.2: Torque Requirements to Move the Legs during one Cycle of the Creeping Gait

m_b is the mass of the body, which is 30 kg for the SILO 4 robot [1]. When only three legs are in contact with the ground the same process is used, but A becomes a 3x3 matrix and Equation A.33 is used to find F instead of Equation A.31.

$$F = A^{-1}W \quad (\text{A.33})$$

The force that the foot must exert on the ground is given by $-F$. The joint torques required in order to provide that force is defined by Equation A.34 [22].

$$\tau_i = J^T(-F_i) \quad (\text{A.34})$$

Where i represents a given leg and J is the Jacobian matrix defined in Chapter 3. The joint torques that are required to support the body for one cycle of the creeping gait at a height of travel of 0.4 m are shown in Figure A.3. From Figure A.3 it can be seen that no extra torque is required in the leg transfer phase as the leg is no longer supporting the body. During a leg transfer phase the torque requirement remains constant. This is not the case during the support phase as the legs change their position with respect to the robot's CoG.

A.2.3 Motor Torques and Angular Velocities

The torques required for leg movement and to support the body can be added together to give the total required joint torques. Gear ratios, μ , and gear efficiencies, η , must be taken into account to obtain the required motor torques. The motor torque can be obtained using Equation A.35, [36].

$$\tau_m = \frac{\tau_j}{\mu\eta} \quad (\text{A.35})$$

When considering the maximum angular velocity, the gear ratios and efficiencies must also be taken into account. This is shown in Equation A.36, [36].

$$\omega_m = \mu\omega_i \quad (\text{A.36})$$

With values for τ_m and ω_m the appropriate motor can then be selected.

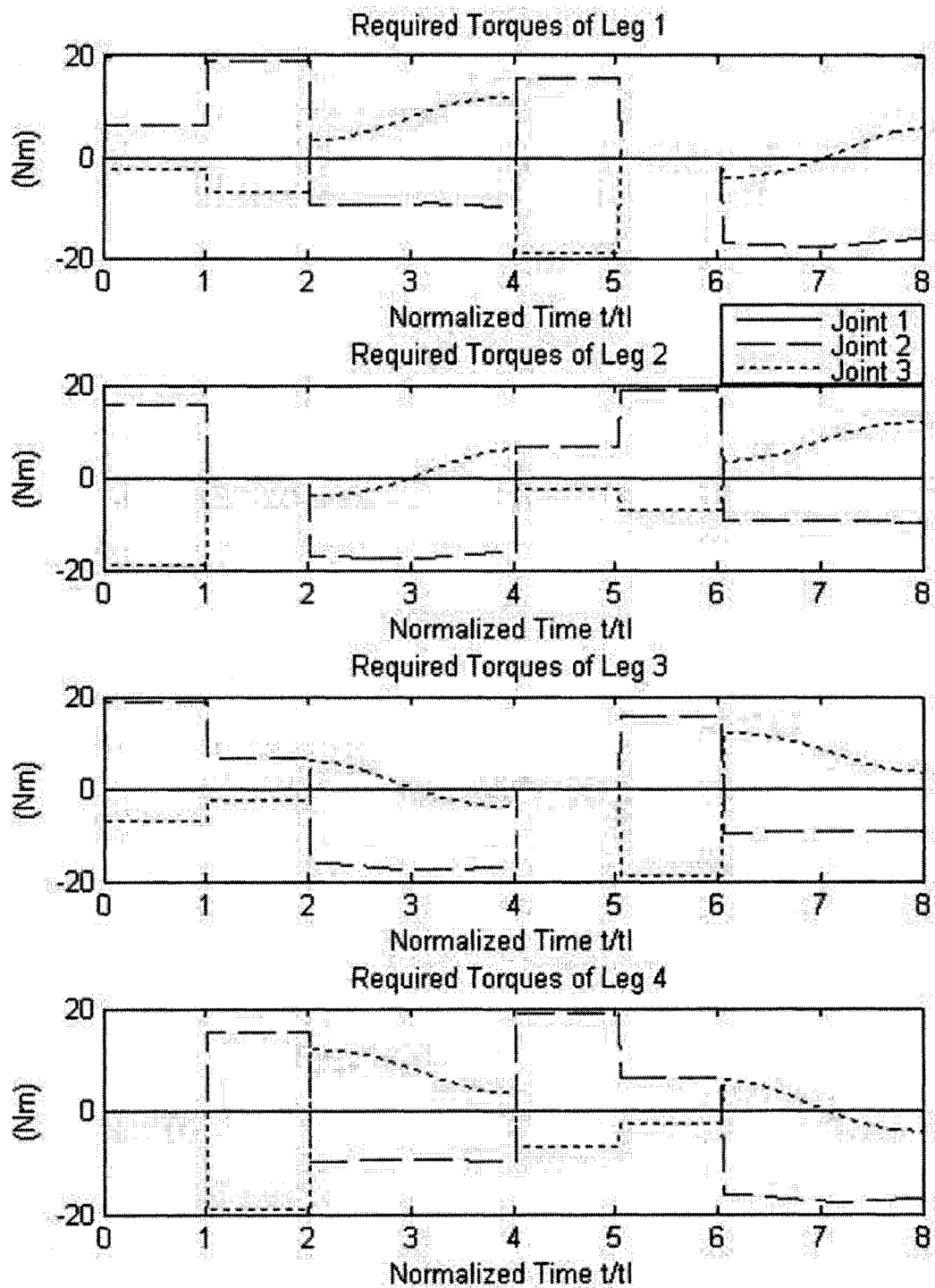


Figure A.3: Torque Requirements to Support the Body for one Cycle of the Creeping Gait